STUDY OF SULFATE ATTACK RESISTANCE OF CARBONATED LOW-LIME CALCIUM SILICATE SYSTEMS

by

Raikhan Tokpatayeva

A Dissertation

Submitted to the Faculty of Purdue University

In Partial Fulfillment of the Requirements for the degree of

Doctor of Philosophy

Lyles School of Civil Engineering

West Lafayette, Indiana

December 2020

THE PURDUE UNIVERSITY GRADUATE SCHOOL
STATEMENT OF COMMITTEE APPROVAL

Dr. Jan Olek, Chair

School of Civil Engineering

Dr. Terry West

Department of Earth, Atmospheric and Planetary Sciences

Dr. Luna Lu

School of Civil Engineering

Dr. Jitendra Jain

Solidia Technologies

Approved by:

Dr. Dulcy M. Abraham

Dedicated to my Grandma and Grandpa – Galiya Tokpatayeva and Abdildabek Tokpatayev

ACKNOWLEDGMENTS

TABLE OF CONTENTS

LIST OF TABLES

LIST OF FIGURES

ABSTRACT

The increasing awareness of the impact of cement production on the greenhouse gasses emissions (directly, in the form of carbon dioxide released during decomposition of calcium carbonate in the cement kiln as well as indirectly, through the combustion of fossil fuels) stimulates innovations in development of materials with reduced carbon footprint. One of such new materials, Solidia Cemen™, is a low-lime calcium silica binder that can be produced from the same raw ingredients, and using the same kiln, as ordinary portland cement but at lower temperature (thus requiring less fuel) and at reduced calcium:silica ratio (thus requiring less calcium carbonate). While this low-lime binder is non-hydraulic (and thus it will not harden as a result of chemical reaction with water) it solidifies by the process of carbonation, therefore further reducing carbon footprint. However, in order to determine to what extent such material can serve as a replacement for concrete based on the ordinary portland cement (OPC), a comparative study of durability of these carbonated low-lime calcium silicate systems (CCS) is needed.

One of the durability issues facing OPC concrete exposed to sulfate-rich environment (e.g., certain types of soils, sea water, drainage or ground water, etc.) is the potential for an external sulfate attack which can lead to leaching of components from the hydration products, softening of the CSH gel, formation of new reaction products, precipitation and growth of expansive crystallo-hydrates of sulfate salts in free space of the matrix. When continuing over prolonged periods of time, all of these processes ultimately contribute to disintegration of the hydrated cement paste.

Despite sizeable amount of previous work on the carbonation of calcium silicates, little data can be found in the literature regarding the potential performance issues associated with the CCS based cementitious systems. Therefore, a specific motivation for the work presented in this thesis was to contribute to the body of knowledge on the sulfate resistance of the CCS materials. The specific topics explored as a part of the work leading to this dissertation included: chemical interactions and kinetics of reactions between CCS and sulfates, the role of chemical and mineralogical composition of calcium silicates, response of the CCS system with respect to the type of the sulfates, verification of the possibility of thaumasite sulfate attack (TSA) in CCS systems, and compositional alterations and damage processes in the CCS matrix resulting from the sulfate attack.

The scope of the study included evaluation of four different types of CCS materials, three different types of sulfate solutions and two different exposure temperatures. The main findings from the study indicate that CCS binder type systems are much more resistant to sulfate attack than the based system. However, some matrix alterations were, nevertheless, observed in the CCS-based systems, with the degree of these changes strongly depending on the type of sulfate solution. Specifically, while sodium sulfate did not cause any observable changes, magnesium and aluminum sulfates cased formation of gypsum as a result of decalcifications of calcium carbonates. It was also found that CCS materials that formed stable, crystalline phases were more resistant to sulfate attack.

1.   INTRODUCTION

1.1   Motivation and Objectives

Due to environmental issues associated with production of traditional construction materials, including energy consumption, green gas emissions and depletion of non-renewable natural resources, studies on development of materials with reduced energy requirements and lower carbon footprint are on the rise. One group of such materials (e.g., Solidia cement™) consists of low-lime calcium silicates that can be produced from the same raw materials as ordinary portland cement but at lower clinkering temperature (hence energy savings) and utilizes lower amount of limestone (hence reduced levels of CO_2 emissions). In addition, rather than hydrating and developing strength as a result of reaction with water, these materials solidify by carbonation, i.e., by reacting with CO_2, thus providing additional environmental benefits. However, in order to determine to what extent the carbonated low-lime calcium silicate systems (CCS) can be considered as viable alternative to the ordinary portland cement (OPC), various aspects of their performance should be evaluated, including mechanical and durability characteristics.

One of the durability issues associated with concrete elements exposed to sulfate-rich environment (sulfated soil, sea water, drainage, or ground water, etc.,) is the external sulfate attack which might cause significant damage to entire concrete structure. As a result of continuous exposure to sulfates, such processes as leaching/dissolution of the matrix forming phases, softening of the CSH gel, formation of new products of chemical reactions, precipitation and growth of expansive crystal-hydrates of sulfate salts in free space of the matrix are all contributing the concrete disintegration. Due to predominantly chemical nature of the sulfate attack, it is important to focus on the mineralogical and chemical composition of the CCS system, especially when attempting to camporee the response of these materials with the response of the OPC systems. In other words, revealing the key features in CCS microstructural composition, and how these features make this microstructure different (stronger or weaker) from hydrated OPC system with respect to sulfate resistance represents an important research problem. This gives rise to the need for the study of behavior of the CCS materials exposed the sulfate-rich media in order to understand the process of their interaction with sulfates, to determine the compositional alterations, if any, and to evaluate possible consequences resulting from these interactions with respect to the

damage of the structure. These considerations provided motivation for the research work presented in this PhD thesis. Despite sizeable amount of work on the carbonation of calcium silicates, little can be found in the literature regarding the potential performance issues associated with the CCS systems. Therefore, another more specific motivation of this work was to contribute to the basic knowledge on the sulfate resistance of the CCS materials by considering the influence of the specific compositions of the low-lime calcium silicates, types of sulfate solutions and temperature of exposure.

Considering all of the above, the general focus of the research work presented here was on investigation of microstructural and chemical changes taking place in CCS pastes and mortars subjected to sulfates. The general objectives are divided into several goals which aim to address the following points:

- To understand the nature of chemical interactions between CCS and sulfates and the kinetics of these interactions;
- To understand the role of the type of calcium silicate;
- To evaluate the response of the CCS system with respect to the type of the sulfate;
- To assess (in addition to the conventional sulfate attack) the potential for thaumasite sulfate attack (TSA) in CCS systems;

To characterize any compositional alterations and damage processes in the CCS matrix resulting from the sulfate attack.

1.2 Outline of the Research Work and Hypotheses

To accommodate the above-stated goals, the work plan has been divided into three phases, each consisting of specific tasks. The details of activities associated with each of the phases are provided within the specific chapters as listed below:

- Phase I: The study of length changes of mortar specimens subjected to modified sulfate resistance test (ASTM C1012). During this part of the study, the expansion of the CSC and OPC mortar specimens were monitored while they were exposed to three types of soak solutions: sodium sulfate, magnesium sulfate and deionized water. Once the test was terminated, the material collected from the specimens was investigated using several analytical techniques. The details of all experiments, along with the analysis of the results

17

are presented in Chapter 2. The importance of this part of the work lies in the fact that it shed light on some characteristics of the CCS materials that influence their sulfate resistance and which are different from those governing the behavior of hydrated OPC system exposed to the same kind of environment. In doing so, the results of this phase of the work contributed to formulation of hypotheses for subsequent investigations.

- Phase II: Experimental study on exposure of CCS paste samples to sulfate solutions at room temperature. The main focus of this part of the study was on evaluation of the effect of mineralogical composition of CCS pastes on their chemical interactions with sulfates containing various types of cations. This details of this part of the work are provided in Chapter 3.

- Phase III: This part of the work was dedicated to the evaluation of the possibility of occurrence of the thaumasite sulfate attack (TSA) in the CCS paste systems exposed to sulfate solutions at low temperature. The results and discussion of the work are presented in Chapter 4.

- General Summary and Conclusions are given in Chapter 5.

- The prospective directions of future work are described in Chapter 6.

The hypotheses of the research work presented in this thesis, formulated on the basis of relevant literature sources and the results of Phase I of the study are following:

- The sulfate resistance of the CCS depends on the type of sulfates. They are likely to be susceptible to magnesium sulfate ($MgSO_4$) attack, but not sodium sulfate attack.

- The relative inertness of CCSs exposed to sodium sulfate is mainly due to the absence of calcium hydroxide in the matrix of CCS.

- Chemical interactions between magnesium sulfate and CCSs will result in decalcification of the matrix and formation of gypsum.

- Unlike in case of hydrated OPC, the gypsum formed in CCS matrix will not serve as an internal source of sulfates capable of initiating the secondary sulfate attack.

- CCSs containing highly crystalline (more stable) calcium carbonate phases will be more sulfate resistant.

2.   PHASE I: STUDY OF SULFATE RESISTANCE OF THE CCS SYSTEM ON THE BASIS OF THE MORTAR BAR TEST

This part of the research work was completed in the frame of the preliminary investigations. The results of the work were published in the proceedings of the 6th International Conference on Durability of Concrete Structures (University of Leeds, UK, 2018).

Abstract

Presented here work summarizes the results of sulfate resistance study of carbonated mortar specimens made with Solidia Cement™ (SC) and tested for expansion according to ASTM C1012 specification while exposed to three types of soak solutions: sodium sulfate, magnesium sulfate and deionized water. A control set of ordinary portland cement (OPC) mortars was also evaluated. Besides the length change measurements, visual observations of changes in the appearance of specimens were conducted after various lengths of exposure. In addition, microstructural characterization of the specimens was conducted using scanning electron microscopy (SEM), X-ray diffraction (XRD) and thermo-gravimetric analysis (TGA) techniques. Finally, changes in the concentration of the chemical species present in the soak solutions in contact with the SC specimens were evaluated using both, the ion chromatography (IC) and the inductively coupled plasma optical emission spectrometry (ICP-OES).

As expected, the OPC mortar specimens started deteriorating early and reached the critical (i.e. 0.1%) level of expansion in about 4 months in case of sodium sulfate solution and in about 6 months in case of magnesium sulfate solution. With respect to the SC mortar specimens, those exposed to magnesium sulfate solution showed higher expansion than those exposed to sodium sulfate solution. However, after 18 months of exposure to both types of sulfate solutions the maximum expansion levels of specimens were still only about 33% of the critical value.

The SEM examination of SC mortar bars indicated that the matrix of the specimens exposed to magnesium sulfate solution showed evidence of formation of gypsum and magnesium-silica compounds. Magnesium and sulfate ions seem to have altered the morphology of the carbonation-generated silica phase and produced gypsum deposits in the air-voids, within the matrix and at the

paste – aggregate interfaces. The formation of gypsum in those specimens was confirmed by the results of thermal and XRD analyses. Finally, the ionic analysis of the magnesium sulfate soak solution indicated consumption of sulfate ions whereas the concentration of the sulfates in sodium sulfate soak solution did not change during the exposure period.

2.1   Introduction

The carbonation reactions have been used in the past to increase the rate of strength development of hydraulic calcium silicates (i.e., $3CaO \cdot SiO_2$ (C_3S) and β-$2CaO \cdot SiO_2$ (β-C_2S)) (Young et al., 1971, Goto et al., 1995) and to explore the potential for using non-hydraulic calcium silicates (e.g., γ-$2CaO \cdot SiO_2$ (γ-C_2S) and $CaSiO_3$ (CS)) as carbon dioxide (CO_2) activated binders (Bukowski and Berger, 1979). More recently, long-term sequestration of CO_2 by carbonation of naturally occurring calcium silicates emerged as a promising technology to curb raising levels of carbon dioxide is the Earth's atmosphere (Huijgen and Comans, 2005). The Solidia Cement™ (SC), developed by Solidia Technologies Inc., illustrates the case of implementation of carbonated calcium silicate as a binding medium in concrete. SC is a low-lime calcium silicate-based cement which can be produced in the conventional cement kiln and which requires lower clinkering temperature (~1200°C) compared to the clinkering temperature of the OPC (~1450°C).

The response of the OPC system to sulfate solutions has been widely studied and the basic mechanisms are reasonably well established. As an example, according to Taylor (1997), the monosulfate present in the matrix located in the interior of the hydrated OPC specimens exposed to sodium sulfate solution gets replaced by microcrystals of ettringite thoroughly intermixed with calcium silicate hydrate (C-S-H). Closer to the surface, the formation of gypsum (both in the form of veins parallel to the surface as well as microcrystals intermixed with C-S-H) was also observed (Santhanam et al. (2002), Bonen and Cohen (1992)). The same authors also reported that the matrix of OPC exposed to magnesium sulfate solution will experience higher degree of decalcification than that observed in the case of exposure to sodium sulfate solution. In addition, the surface of the OPC specimens exposed to magnesium sulfate solution will typically develop a thin coat of composite material consisting of an outside layer of brucite ($Mg(OH)_2$) and underlying layer of gypsum. In addition, in cases of a very severe attack involving magnesium sulfate solution,

formation of the non-binding magnesium silicate hydrate was also observed.

Despite sizeable amount of work on CO_2 sequestration in the calcium silicate systems, little can be found in the literature regarding the potential performance issues associated with the carbonated calcium silicate systems exposed to sulfate containing environment. In contrast, sulfate durability has been studied for other silicate systems alternative to OPC such as slag cements and geopolymers (e.g., Słomka-Słupik et al. (2016), Duda (1987), Bakharev (2005)).

Due to previously mentioned lack of data on the sulfate durability of carbonated low-lime silicate systems, the objective of the presented work was to investigate the expansion potential of such materials upon exposure to sulfate-bearing solutions and to compare it to the behavior of the OPC system exposed to the same solutions. In addition, microstructural and chemical changes resulting from sulfate exposure were also evaluated.

2.2   Materials and Methods

2.2.1   Materials

The mortar specimens (25mm x25mm x285 mm prisms) were prepared using both, SC (Solidia Cement™, also labeled as cement #3 in Chapter 3) and OPC (Type I) cements and the ASTM C778-13 graded standard sand (Ottawa sand). The SC mortar bars were prepared using the w/c=0.30 and cement to sand ratio of 1:2.75 by mass. After casting, the SC mortar bars were immediately carbonated for 24 hours at 65°C in the environmental chamber. The carbonation was achieved by continuously purging the chamber with high purity CO2 gas supplied at the pressure of 1 atm. The OPC mortar samples were prepared according to ASTM C109-12. After demolding, the OPC specimens were cured in saturated lime water at 23°C for 28 days. No such treatment was provided to the SC mortar bars since these do not require any post curing.

The chemical compositions of both, OPC and SC are given in Table 2.1. The main mineral phases present in SC cement (determined by XRD) include rankinite, pseudowollastonite and larnite/belite (reactive phases), and melilites and feldspars (inert phases). The XRD patterns of SC cement before and after carbonation are presented in Results section. The 0.35M sulfate solutions used in the experiment were prepared using analytical grade chemical reagents (anhydrous sodium sulfate and anhydrous magnesium sulfate).

Table 2.1. Chemical compositions of Type I OPC and SC

OPC (Type I)										
Component	CaO	SiO$_2$	Fe$_2$O$_3$	Al$_2$O$_3$	MgO	SO$_3$	Total alkalis	C$_3$S	C$_2$S	C$_3$A	C$_4$AF
Wt, %	64.0	19.6	2.9	5.2	2.6	3.3	0.7	63.4	8.4	9.0	8.7
Solidia Cement™										
Component	CaO	SiO$_2$	Fe$_2$O$_3$	Al$_2$O$_3$	MgO	SO$_3$	Na$_2$O	K$_2$O	TiO$_2$	SrO	P$_2$O$_5$
Wt., %	43.6	44.0	1.79	5.13	1.15	0.16	0.33	1.94	0.22	0.12	0.06

2.2.2 Methods

Experimental setup for length change measurements

The sulfate exposure experiment was performed according to the ASTM C1012-13. All mortar bars were exposed to 0.35M solutions of sodium sulfate and magnesium sulfate with solid-to-solution volume ratio as 1:4 at 23°C. Mortar bars soaked in de-ionized water were used as reference specimens. The measurements of change in the length and the mass of the bars were recorded at different time intervals (1, 2, 3, 4, 8, 11, 13, 15 weeks and 4, 6, 9, 12, 15 and 18 months). In addition, changes in the chemical composition of the soak solutions were evaluated after 8, 16 and 32 weeks of exposure. Before starting the soaking process, all SC mortar bars were pre-saturated in de-ionized water for 48 hours. Length change measurements were performed after previously outlined period of exposure using the length comparator equipped with digital gauge with the resolution of 0.0025 mm. The percentage of the length change was calculated according to ASTM C1012. In addition, once the specimens were removed from the soak solutions for length and mass measurements, they were also photographed to document changes in their physical appearance.

Post-exposure analysis of the mortar bar specimens

The sulfate expansion test was terminated for OPC mortar bars immersed in sodium and magnesium sulfate solutions at 9 months and 12 months, respectively. The SC mortar bars underwent the full 18-month testing perioid. After completion of the sulfate resistance test both, the SC and OPC mortar bars (1 bar/per each solution) were dried at 50°C in vacuum oven and used to prepare the test specimens for XRD, TGA and SEM analyses.

XRD analysis

For XRD analysis, SC cement, pulverized small pieces of SC paste, SC and OPC mortar samples (removed from several locations) were used. Before being mounted in the XRD sample holder, ground samples were sieved using the No. 200 (75 μm) sieve. The XRD patterns were collected using Siemens D500 diffractometer (30 mA, 50 kV) at 0.02°/sec scanning rate (in 10-80° 2θ range). The analysis of the pattern was performed using the Jade 9 software.

Thermal analysis

The SC and OPC powders utilized for XRD analysis were subsequently subjected to thermogravimetric analysis (TGA). The TGA analysis was performed using TA Instruments Q50 Thermogravimetric analyzer with the nitrogen gas atmosphere (the flow rate of 50 mL/min) in the temperature range from 20°C to 1000°C at the heating rate of 10°C/min.

SEM analysis

The specimens for SEM observation were prepared by cutting the bar at two locations (~ 15 mm apart) in the direction perpendicular to the longitudinal axis (see Fig.2.1). This resulted in the 20 mm thick specimen with the 25mm x 25mm area that was used for conducting the SEM analysis. Once cut out of the beam, the cube specimens were vacuum impregnated with epoxy and dried at ~60°C. After the epoxy hardened, the surface of the specimens was ground using Hillquist 45, 30 and 15 μm mesh flat diamond laps. Lapped samples were subsequently polished on Buehler micro clothes lubricated with diamond pastes with mesh sizes of 9, 6, 3, 1 and 0.25 μm. The polished surfaces were coated with Pd for 30 s in Hummer 6.2 Sputter Coating machine. The SEM analysis was performed using the ASPEX Personal SEM equipped with the energy dispersive x-ray (EDX) analyzer and operated in the backscattered and secondary electron modes. The accelerating voltage used in the examination was 15 keV.

Surface used for SEM analysis
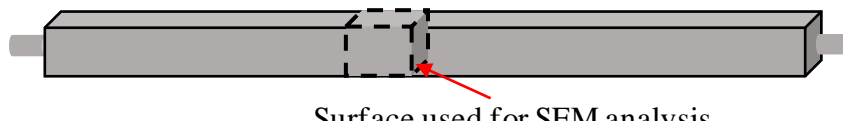
Figure 2.1. Location of SEM specimen

Chemical analysis of the soak solutions of SC specimens

The soak solutions (de-ionized water, magnesium sulfate and sodium sulfate solutions) that remained in contact with SC mortar bars during the testing period were collected at various intervals during the exposure cycle and analyzed to monitor the changes in concentration of Na^+, Mg^{2+}, Ca^{2+}, SO_4^{2-} and Si species. The solutions were filtered and analyzed using Ion Chromatographer (IC) (DIONEX ICS-900) and Inductively Coupled Plasma – Optical Emission Spectrometer (ICP-OES) (Perkin Elmer OPTIMA 8300). The ion concentration results reported here represent an average of two samples per each solution.

2.3   Results and Discussion

2.3.1   Length change and visual observation results

As it can be seen from Fig.2.2, the appearance of the SC mortar bars did not change during the entire (i.e., 18 months) exposure period. However, the mortar bars made from the OPC and exposed to the sodium sulfate solution developed severe bending, which ultimately led to two of them becoming completely broken after 9 months of exposure. On the other hand, in case of the OPC mortar bars exposed to magnesium sulfate solution such symptoms as exfoliation, formation of brucite deposits (white precipitates) and slight bending were observed (right part of Fig. 2.3). The SC mortar specimens exposed to magnesium sulfate solution (left side of Figure 2.3) initially developed hairline cracks along the length of the bars which, over time, spread toward the end corners of the bars. The summary of visual observations of the conditions of the bars is presented in Table 2.2.

Figure 2.2. Appearance of the mortar bars exposed to sodium sulfate (SS): left – SC mortar bars after 18 months of exposure; right – OPC mortar bars after ~9 months of exposure
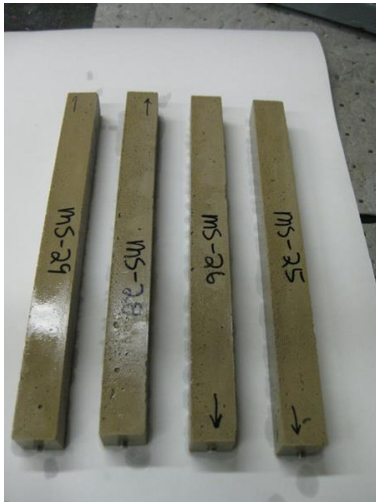
Figure 2.3. Appearance of the mortar bars exposed to magnesium sulfate (MS): left – SC mortar bars after 18 months of exposure; right – OPC mortar bars after ~9 months of exposure

Table 2.2. Summary of visual observations of the condition of mortar bars exposed to sulfate solutions

Solution	OPC mortar	SC mortar
Sodium sulfate (SS)	✓ 3 of the bars cracked and broke (test have been terminated after 6 months) ✓ Cracks appeared mostly near the corners, along the edges and along sides close to the finished surface. ✓ A network of cracks developed along the long sides of the bars near the end of the test	✓ No visible changes
Magnesium sulfate (MS)	✓ All bars bent and cracked after 12 months of exposure ✓ The surfaces of the bars were covered with white deposits. ✓ Edges became blunt due to crumbling of sand particles.	✓ Fine horizontal cracks started to propagate along the length of the bar in the region close to the finished surface ✓ Cracks started to propagate along the ends and corners of the bars after about 14-15 months of exposure (See Fig.2.4).

a)   b)

c)

Figure 2.4. Cracks on the surface of SC mortar bar exposed to magnesium sulfate (MS) solution (0.35M): a) – longitudinal cracks on the top of the vertical face in the region close to the finished surface; b) – crack at the end face of the bar near the steel stud; c) – side view of the crack on a vertical face near the end of the bar

Figures 2.5 (a, b) and 6 (a, b) show the values of length change measurements for all SC and OPC mortar bars exposed to, respectively, the sodium sulfate (SS) and magnesium sulfate (MS) solutions. In general, regardless of the type of the sulfate solution used, the maximum expansion of the SC mortar bars after 72 weeks (~18 months) of exposure was very low (~0.03%). That maximum expansion was observed in the bars immersed in magnesium sulfate solution. The maximum expansion limit (at 180 days or ~26 weeks) for moderate sulfate exposure specified in the ACI 201.2R-16 is 0.1%. According to that, the SC bars can be definitely considered to be resistant to the distress caused by the sulfate sources external to the concrete.

However, as it can be seen in Figures 2.5 (b) and 2.6 (b), the OPC mortar bars expanded beyond the critical level (0.1%) after, respectively, 4 months of exposure to sodium sulfate solution and 6 months of exposure to magnesium sulfate solution. In fact, the test involving the OPC specimens had to be terminated due to severe cracking and disintegration of the bars. Also, it is worthwhile to point out the 2-stage expansion trend of the OPC mortar specimens exposed to sodium sulfate characterized by relatively moderate initial expansion (stage 1 – up to 16 weeks of exposure) and rapid acceleration of the expansion (stage 2 – after 16 weeks of exposure). This phenomenon was previously described by Santhanam et al. (2002). These authors suggested that the sudden acceleration of expansion observed during stage two can be the result of increased rate of formation of gypsum and ettringite. The expansion of SC mortar bars exposed to both magnesium sulfate and sodium sulfate solutions stabilized after 48 and 32 weeks of exposure respectively. However, the SC mortar bars exposed to magnesium sulfate experienced a higher total length change (~0.03%) as compared to the total length change of ~0.015% observed for the SC mortars exposed to sodium sulfate.

Fig. 2.7 presents the detailed comparison of average length change values of the SC mortar bars immersed in de-ionized water, sodium sulfate and magnesium sulfate solutions. As one can observe from the graph, the SC specimens exposed to magnesium sulfate solution behaved differently than those exposed to de-ionized water and sodium solution. Specifically, after approximately 36 weeks of exposure the expansions of specimens exposed to deionized water and sodium sulfate solutions stabilized at about 0.015%. However, the SC mortars exposed to magnesium sulfate solution continued to expand, reaching a steady level of expansion (~0.03%) only after about 48 weeks of exposure. Even though (as it has been mentioned above) all SC mortar specimens passed the maximum length change (expansion) criterion, the bars exposed to

magnesium sulfate expanded significantly more compared to those exposed to sodium sulfate solution. This observation suggests that magnesium sulfate solution may have some chemical effect that changes the structure of the specimens. The microstructure of the SC mortar specimens after sulfate exposure provided some confirmation of this observation. The results of the microstructural study are presented and discussed in the following paragraphs.

a) SC mortar bars   a) OPC mortar bars
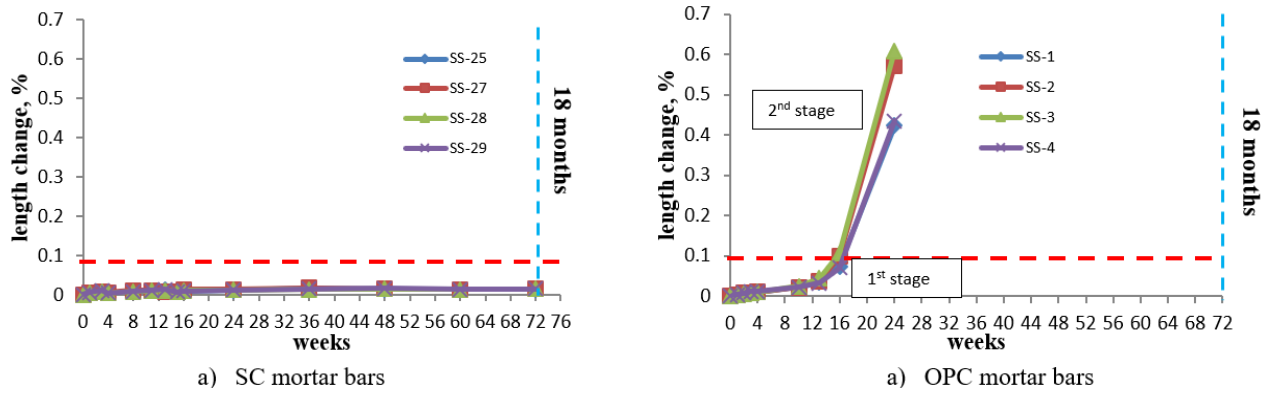
Figure 2.5. Length change results for the SC mortar specimens exposed to sodium sulfate (SS) solution (Note: the horizontal dashed line represents the 0.1% maximum expansion limit (at 180 days or ~26 weeks) for moderate sulfate exposure as per ACI 201.2R-16)

a) SC mortar bars   a) OPC mortar bars
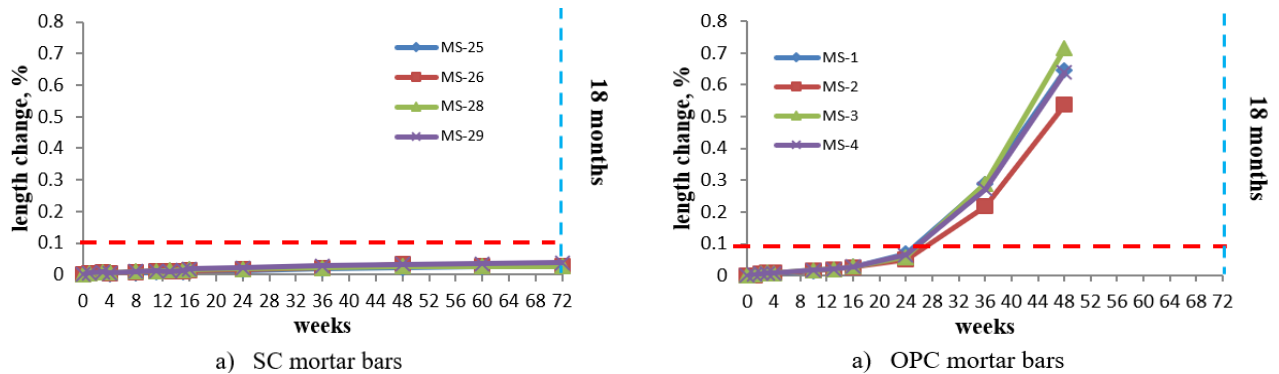
Figure 2.6. Length change results for the OPC mortar specimens exposed to magnesium sulfate (MS) solution (Note: the horizontal dashed line represents the 0.1% maximum expansion limit (at 180 days or ~26 weeks) for moderate sulfate exposure as per exposure as per ACI 201.2R-16)
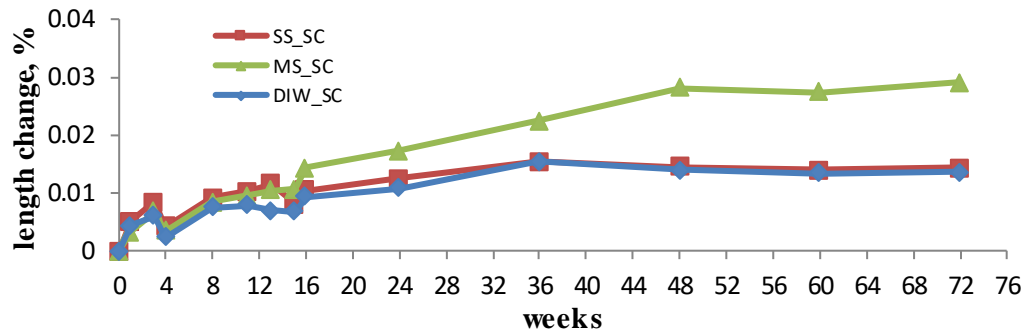
Figure 2.7. Length change measurement results for SC mortar bars (a) and OPC mortar bars (b) (key: DIW – de-ionized water, MS – magnesium sulfate, SS – sodium sulfate)

2.3.2 Results of SEM analysis

The SEM analysis of the SC and OPC mortar specimens was used to evaluate the changes in the microstructure and examine the morphology of any new phases that might have formed as the result of the exposure of the matrix to sulfate solutions. In general, the microstructure of carbonated SC system consists of calcium carbonate, hydrated silica gel, unreacted cement grains and micro-/nano-pores (see Fig. 2.8). Calcium carbonate phases (calcite, vaterite and aragonite) are the main space-filling and binding components. In addition, the microstructure also contains an "intermediate phases" composed of calcium carbonate with traces of silica and Ca-modified silica. That phase can be described as "low-silica carbonate phase". The formation of this type of intermediate phase might be due to multi-mineral nature of the SC cement. The layer of hydrated silica gel tends to deposit around the contours of un-carbonated grains of cement. As mentioned earlier, the SC contains non-reactive particles which act as an inert filler.

Fig. 2.9 contains SEM images of the microstructure of both, the SC mortar bars (images (a) and (c)) and the OPC mortar bars (images (b) and (d)) exposed to either sodium sulfate (images (a) and (b)) or magnesium sulfate (images (c) and (d)) solutions. As it can be seen by comparing images shown in Fig. 2.9 (a) and (b), the sodium sulfate solution does not appear to have any significant negative effects on the microstructure of the carbonated SC system. The only observable change is the increase in porosity of the very near surface (about 1 mm deep) region of

the specimen which might be due to dissolution and leaching of certain species (see section on soak solution analysis near the end of the paper). In contrast, the matrix of the OPC specimen exposed the same sodium sulfate solution is severely cracked. However, the microstructure of the SC mortar specimens exposed to magnesium sulfate looks deteriorated (Fig. 2.9 (c)) and the degree of deterioration appears to be similar to that observed in the matrix of OPC specimens exposed to the same solution (see Fig.2.9 (d)). It should be noted, however, that despite the observed microstructural changes the observed length changes of SC bars in the MS solution were very low.

a)   b)
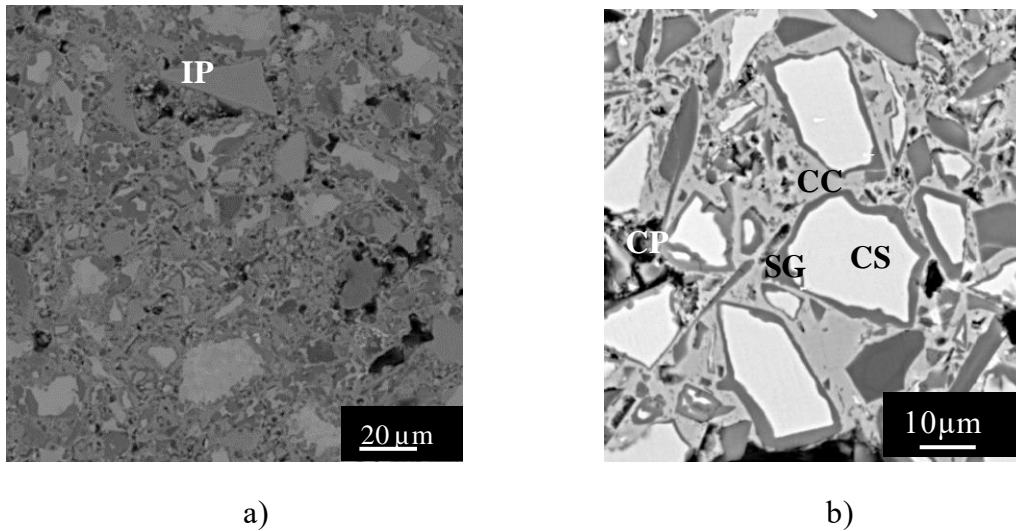
Figure 2.8. SEM micrograph of SC paste matrix (key: CS – calcium silicate, SG – silica gel, CC – calcium carbonate, CP – capillary pore, IP – inert phase)

a) SC-SS

b) OPC-SS

c) SC-MS

d) OPC-MS
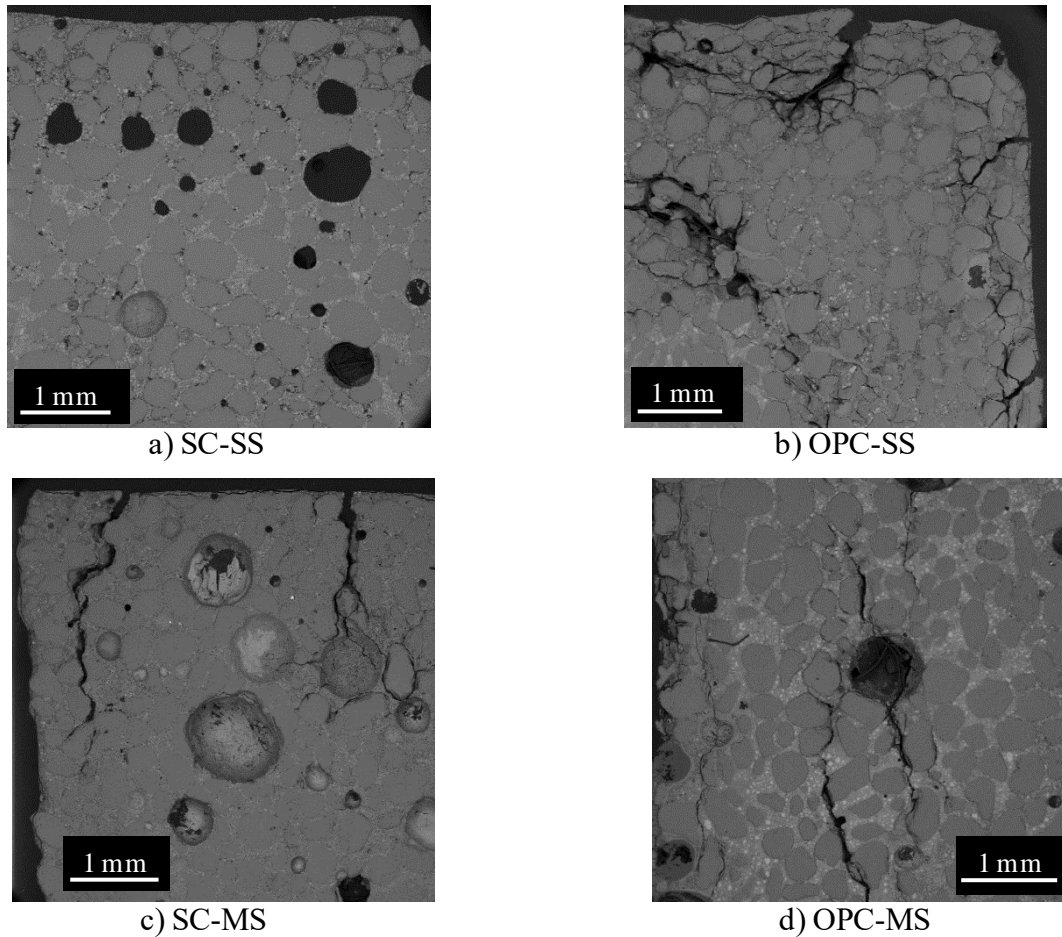
Figure 2.9. Comparison of the microstructure of the mortar matrices after exposure to sodium sulfate solution (a – SC and b – OPC) and magnesium sulfate solution (c – SC and d – OPC)

Fig.2.10 compares SEM images taken at the low (~18X) magnification from the matrices of the SC mortar bars exposed to three different solutions: the deionized water, the sodium sulfate solution and the magnesium sulfate solution. It can be observed that the top 1 mm of the specimen exposed to the sodium sulfate solution (Fig. 2.10 (b)) appears to be more porous than the same region of the specimen exposed to deionized water. While the top region of the specimen exposed to the magnesium sulfate solution (Fig. 2.10 (c)) does not display any signs of increased porosity, it does contain a series of microcracks extending to the depth of about 2 mm from the surface of the bar. No cracks were observed in the microstructure of specimens exposed to the deionized water and to the sodium sulfate solution. When examined at higher magnification (~100X) the microstructure of mortar bar specimens exposed to magnesium sulfate solution displays several

other alterations described below. First, the deposits of gypsum were observed in several locations within the matrix. Specifically, the gypsum crystals were found in the air-voids (see Fig. 2.11), at the aggregate – matrix interface (see Fig. 2.12) and in other random locations within the bulk of the matrix. The somewhat preferential deposition of gypsum at paste-aggregate interface might be the result of the availability of free space at this location (the interface regions tend to be more porous).

a)   b)   c)
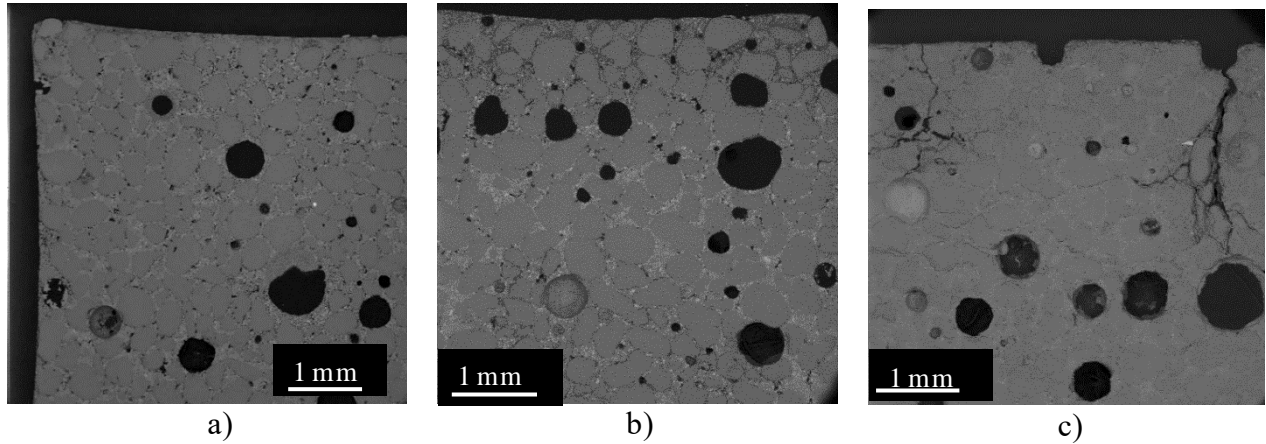
Figure 2.10. The SEM micrographs of the matrix of the SC mortar bars matrix collected at low magnification (18X): after exposure to a) deionized water, b) sodium sulfate solution, and c) magnesium sulfate solution

a)   b)
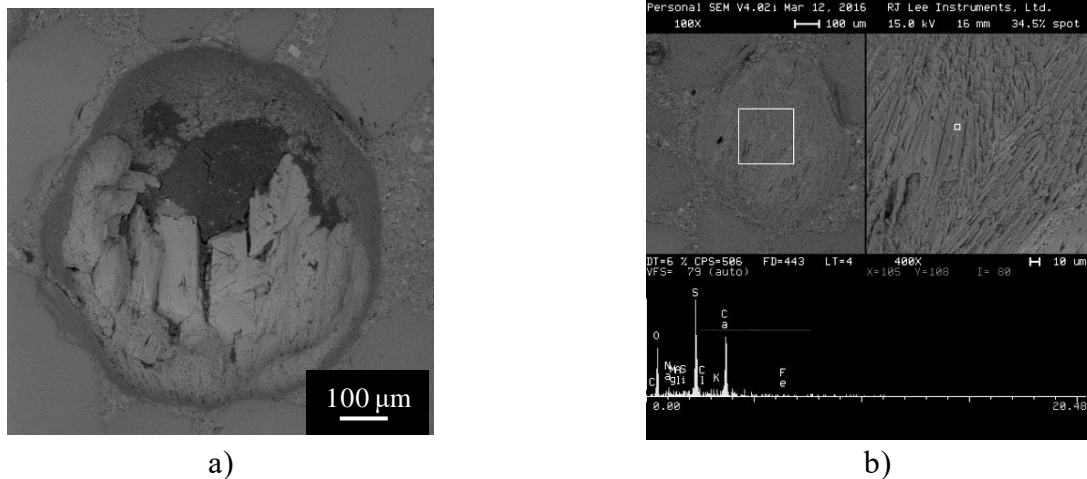
Figure 2.11. Higher magnification (~100X) SEM micrographs of the microstructure of the SC mortar bar matrix exposed to magnesium sulfate solution showing; (a) the air void partially filled with gypsum and (b) the air void completely filled with gypsum (composition confirmed by EDX spectrum)
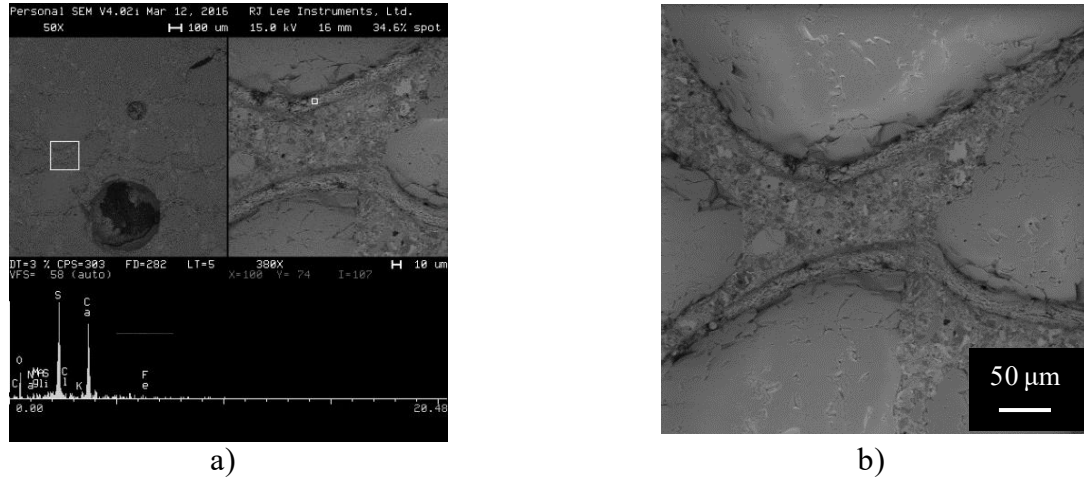
Figure 2.12. The SEM images of the microstructure of the SC mortar bar matrix exposed to magnesium sulfate solution showing: (a) the deposits of gypsum at the interface between the matrix and the aggregate and (b) the close-up of the interfacial zone with the veins of gypsum surrounding the aggregate particles

Other alteration of the matrix observed in the SC mortar bars exposed to magnesium sulfate solutions involved decalcification (Fig. 2.13 (a)) and infusion of silica gel with the Mg^{2+} ions (Fig. 2.13 (b)). More specifically, the magnesium ions were found both, within the silica gel as well as in the non-carbonated cement particles (where it was substituting for Ca^{2+}). As demonstrated in Fig. 2.13 (b), one can see Mg-Si-O signal originating from the silica rim of the carbonated calcium silicate particle. This might be interpreted as a formation of magnesium-silicate hydrate type gel, similar to that observed to form in the hydrated OPC system exposed to magnesium containing solutions. However, there is a significant difference in morphology of the affected regions in the SC and the OPC systems as can be seen by comparing the images shown in Fig. 2.14 (a) and (b). Specifically, the replacement of the Ca^{2+} ion by Mg^{2+} in the matrix of the SC does not seem to have any visible damaging effects. On the other hand, the formation of magnesium-silicate-hydrate (MSH) type of product in the matrix of the OPC mortar bar resulted in cracking.
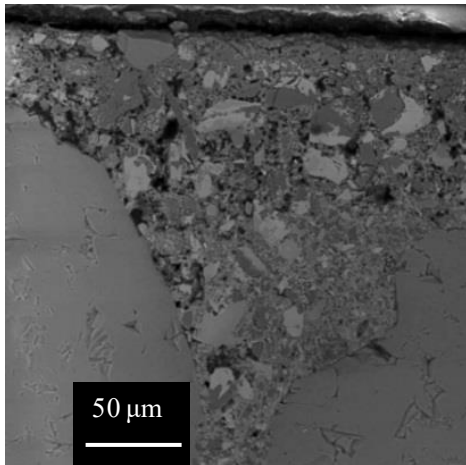
a)
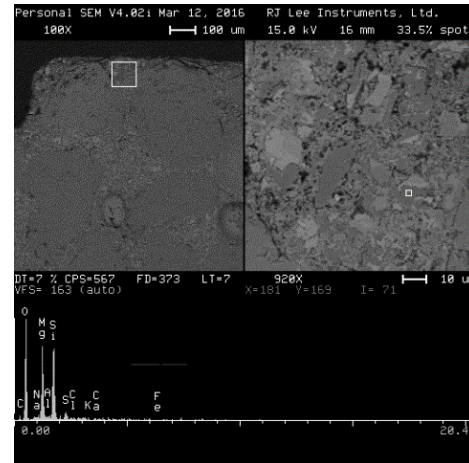
b)

Figure 2.13. The SEM images of matrix of the SC mortar bar specimen exposed to magnesium sulfate solution; (a) the decalcified (porous) zone located close to the outer surface of the specimen and (b) the EDX signal indicating the presence of the Mg2+ inclusions in the silicate rim of partially reacted cement particle
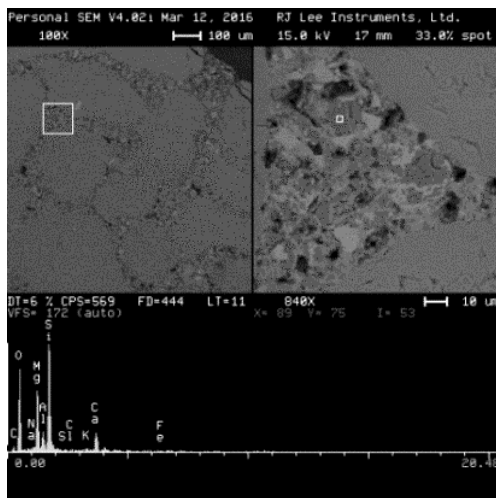
a)
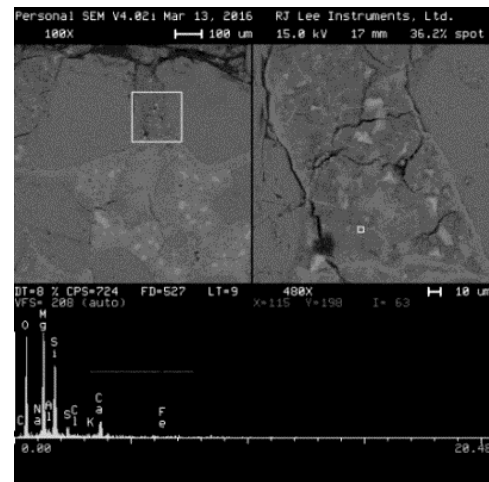
b)

Figure 2.14. Comparison of the effects of the formation of the MSH-type phase in: (a) the SC and (b) the OPC mortar samples exposed to magnesium sulfate solution

2.3.3 XRD analysis results

As seen in Fig. 2.15 (lower trace) the main reactive crystalline phases present in SC cement before carbonation include rankinite, pseudo-wollastonite and larnite/belite. The main non-reactive phases include gehlenite (melilite family) and feldspars. After carbonation, peaks of calcium carbonate minerals appear as well as the peak intensity of the reactive phases decrease (see Fig. 2.15 upper trace). Fig.2.16 shows the XRD pattern of SC mortar specimens exposed to de-ionized water, sodium sulfate and magnesium sulfate solutions. The results of the XRD analysis did not show any significant differences in the mineralogy of the specimens immersed in de-ionized water and sodium sulfate solution (other than decrease in the height of the calcite peaks in specimens exposed to SS). This might be attributed to the dissolution of calcite phase which was evidenced by SEM results as an appearance of less dense area close to the surface of the specimen.

On the other hand, the XRD pattern of the specimen exposed to magnesium sulfate revealed the peaks of gypsum, in agreement with SEM results. In addition to that, one can notice that the intensities of the peaks for calcite were significantly lower than those observed in the specimen exposed to the de-ionized water. The slightly acidic pH level of the magnesium sulfate solution (~5-6) may accelerate the dissolution of the calcite phase compared to other soak solutions used in this study. Thus, the affected calcite phase may be the source of calcium ions for the formation of gypsum. Moreover, it is also interesting to note that the vaterite peaks appeared to be more pronounced in the specimens exposed to both types of sulfate solutions. In the specimens exposed to de-ionized water, any initially presented vaterite (also, amorphous calcium carbonate, if any) might have been converted into calcite. This may explain relatively higher intensity calcite peaks observed in these specimens. The studies conducted in biomineralization area (and mimicking of the synthesis of the less stable calcium carbonate polymorphs) suggests that the presence of organic macromolecules (e.g., proteins, polysaccharides, etc.) and different ionic species (e.g., ammonia, phosphates, sulfates, silica, etc.) during the precipitation event may extend the time of phase transformation and/or help to keep those phases unchanged (Kirboga and Oner (2013), Popescu et al. (2014) and Fiori et al. (2009)). Magnesium ion is believed to act as a preservation agent for amorphous calcium carbonate phase and vaterite according to research work done by Ma and Feng (2015) and Lowenstam and Abbot (1975). Lastly, as it can be seen from Fig. 2.16 (b),

carbonated system exposed to sulfate did not contain any AFt/AFm phases (most likely because alumina present in this cement is incorporated in non-reactive gehlenite.
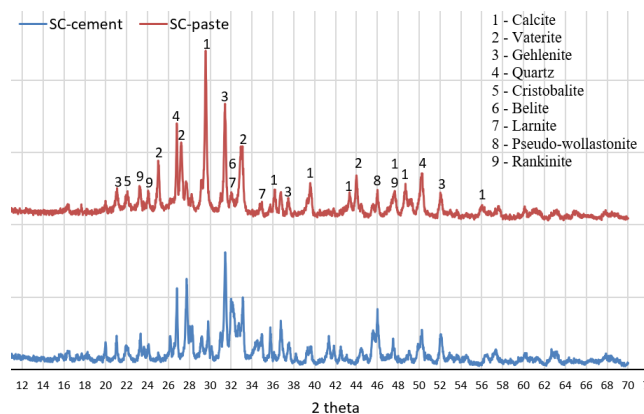
Figure 2.15. The XRD patterns of SC cement (lower trace) and carbonated SC paste (upper trace)

a)

b)
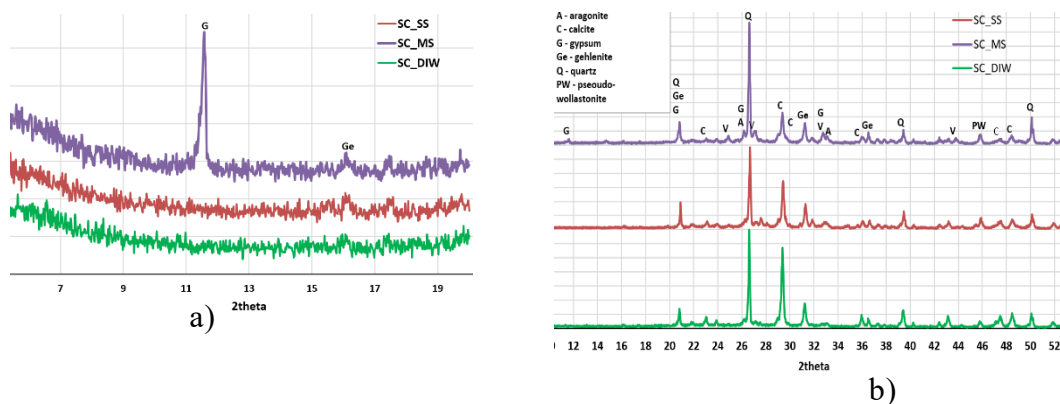
Figure 2.16. Fig. 2.16 The XRD patterns of SC mortar bar specimens after 18-month exposure to the de-ionized water, sodium sulfate and magnesium sulfate solutions; key: SC – Solidia cement, DIW – de-ionized water, SS – sodium sulfate, MS – magnesium sulfate); (a) – 5°-20° 2 theta range, (b) –10°-54° 2 theta range

2.3.4 Results of thermal analysis

The results of the thermogravimetric analysis (TGA) of the SC mortar specimens are given as a first derivative of weight change thermogram in Fig. 3.16. According to the curves, there is a reduction in the quantity of highly crystalline calcium carbonate (present in the temperature range of 650°-900°C) in mortar bars exposed to both sodium and magnesium sulfate solutions compared

to the same mortars immersed in de-ionized water. This reduction is manifested by the shift of the TGA curve in the direction of lower temperature range and the appearance of the humps in between ~520°-650°C (encircled by the black dashed line in Fig. 2.17). The value of this reduction was estimated to be in the range of 30-35% (compared to the DIW (reference) sample). As mentioned above, the decomposition humps observed in the temperature range of ~520°-650°C might be attributed to the decomposition of less crystalline types of calcium carbonate and calcium bearing silica phases. In addition, the total amount of mass loss in the range of ~525°-900°C is lowest in case of the specimen exposed to magnesium sulfate solution. This implies that part of the calcium bearing phases was consumed during gypsum formation. The weight loss at the temperature of about 70°-150°C, visible in the curve of SC bars exposed to the magnesium sulfate, is attributed mainly to the dehydration of gypsum.
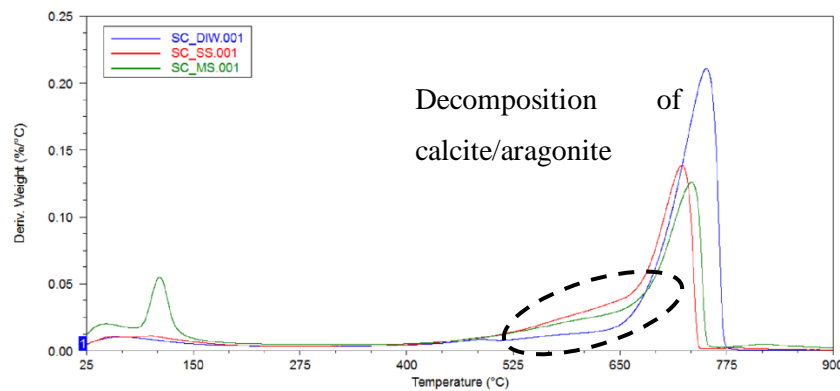
Figure 2.17. The TGA curves of SC mortar samples: first derivative of weight (%) vs. temperature (key: DIW – de-ionized water, SS – sodium sulfate, MS – magnesium sulfate)

2.3.5   Results of chemical analysis of the soak solutions

The analysis of all soak solutions involved monitoring the levels of sulfate ions that could potentially be removed from the soak solution and incorporated (bound) within the matrix of the SC mortar specimens as well as the levels of Ca^{2+} ions and the dissolved silica which can migrate into the solution as the result of leaching. The pH values of the freshly prepared (i.e., not yet in contact with the mortar bars) sulfate solutions were in the range of ~5-6 for magnesium sulfate and

~7-8 for sodium sulfate solutions. When the solutions came in contact with the SC mortar bars, the pH values increased to the range of about 8.5-8.7 for magnesium sulfate solution and up to about 10 for sodium sulfate solution. Changes in sulfate concentration within first 8 months of exposure (normalized with respect to the initial concentration in the fresh solutions) are plotted in Fig.2.18. The analysis of trends presented in Fig. 2.17 reveals that relative concentrations of the SO_4^{2-} ions, in the magnesium sulfate solution in contact with the SC mortar specimens decreased by about 20% compared the original concentration. These results can indicate that the sulfate ions were likely incorporated into the microstructure in the form of gypsum.

The graphs shown in Fig. 2.19 illustrate how the type of sulfate solution influences the amount of calcium and silica that can be leached out from the carbonated SC system. As seen in Fig. 2.19, the highest amount of calcium leached out of SC specimens exposed to magnesium sulfate solution. This can be explained by higher dissolving potential of the magnesium sulfate solution.
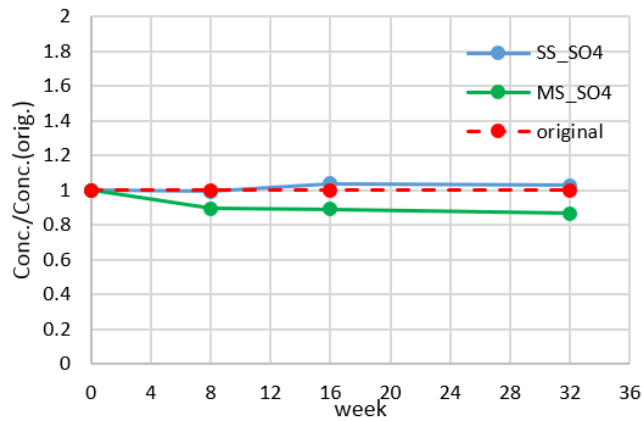
Figure 2.18. Changes in the concentration of sulfate ions (SO42-) in sulfate solutions in contact with the SC mortar bars (normalized with respect to e concentration of SO42- in the original solution). (key: SS – sodium sulfate, MS – magnesium sulfate)
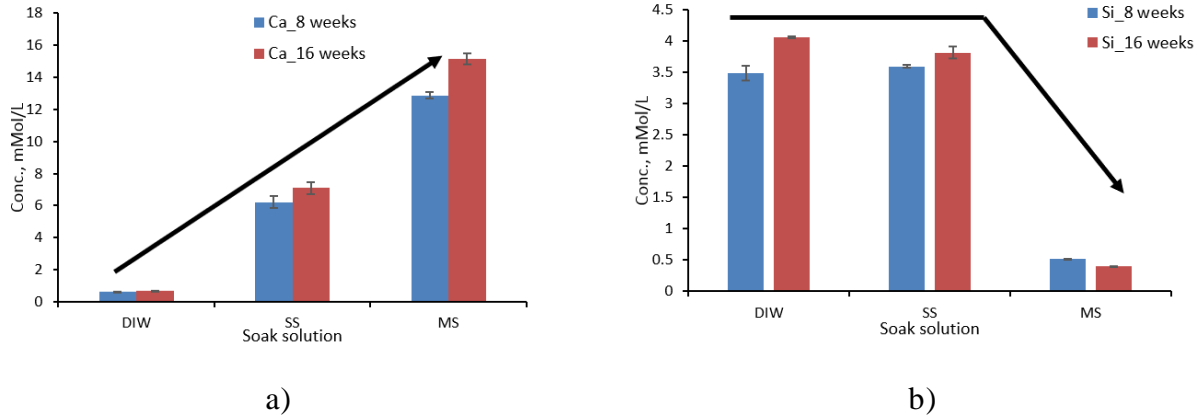
Figure 2.19. Levels of calcium ions (Ca2+) (a) and silicon species (Si) in various soak solutions in contact with the SC mortar bars for a period of 8 and 16 weeks (key: DIW – de-ionized water, SS – sodium sulfate, MS – magnesium sulfate)

As for leaching of silica from the carbonated SC system after exposure to sulfate solutions, the amount present in the magnesium sulfate solutions was significantly (~8 times) lower compared to reference condition (i.e., the SC bars immersed in de-ionized water). This may indicate the presence of some chemical reactions which result in binding of silica in the microstructure.

2.4   Conclusions

This chapter contains the summary of the results of the 18-month long sulfate resistance tests performed on both, the carbonated SC and hydrated OPC mortar specimens according to modified ASTM C1012 standard. In general, the study indicated that the SC mortars are not negatively affected by the exposure to the sodium and magnesium sulfate solutions (i.e., this type of matrix was determined to be durable under sulfate exposure). When compared to the OPC system, the carbonated SC system has its own advantageous peculiarities, which help it to withstand the sulfate attack.

The following points briefly highlight the main findings of this study:

- At the end of the test period (i.e., 18 months) the SC mortar bar specimens did not reach the critical level of expansion (in fact their maximum expansion was only about 33% of the value of 0.1%). On the other hand, the OPC mortar bars not only exceeded the threshold value of expansion, but they also started to disintegrate after about 5-6 months of exposure.

- The results of multiple post-exposure tests (chemical analysis of soak solutions as well as the XRD, TGA and SEM analyses of solid phases) indicates importance of the cation present in sulfate solution. To be exact, there is a chemical interaction between the SC mortar matrix and the magnesium sulfate solution. This reaction resulted in partial decalcification of the SC matrix, in the reduction of more crystalline forms of calcium carbonate (calcite/aragonite), formation of gypsum, and incorporation of Mg^{2+} ions into the structure of silica. However, as mentioned earlier, this reaction did not seem to cause substantial expansion or have other destructive effect on the matrix.

- There were not significant effects of sodium sulfate solution on the microstructure of the SC mortar specimens with the exception of the slight increase in porosity of the thin (about 1 mm) near-surface region of the specimen and possible formation of less crystalline polymorphs of calcium carbonate (exposure to magnesium sulfate led to similar changes).

- The absence of calcium hydroxide and reactive calcium aluminates in the SC matrixes may be considered as one of the big advantages of this system with respect to its durability when exposed to external sulfate attack.

3. PHASE II: ROOM TEMPERATURE SULFATE EXPOSURE EXPERIMENTS PERFORMED ON DIFFERENT CCS PASTES

3.1 Introduction

In the study of the hydrated OPC system, the sulfate attack related questions are well comprehensively addressed. That level of comprehensiveness includes:

- Identification of the individual "participants" in chemical interaction with the sulfates (portlandite, calcium silica hydrate gel (CSH), calcium aluminates);

- Description of each particular reactions and reaction products

e.g. $Ca(OH)_2 + Na_2SO_4 (aq.) + 2H_2O \rightarrow CaSO_4 \cdot 2H_2O + 2Na^+ + 2OH^-$

- destruction mechanisms (e.g., expansion due to crystal growth or decomposition of CSH gel and formation of Magnesium Silica Hydrate (MSH) gel);

- prediction of the type of "attack" scenario expected depending a cation of a sulfate;

- development of the ways of improving the sulfate resistance (e.g., cut off on calcium aluminates, reduction of calcium hydroxide amount by means of pozzolanic reaction);

- attempts on correlation of the expansion level with the amount of expansive products of sulfate attack (e.g. ettringite, gypsum);

- consequently, attempts on constructing predictive models.

The ongoing investigations of the behavior of the alternative systems hydrated OPC in sulfate-rich environment actively takes place. However, the explanation of all the findings in that area mostly can rely on those fundamental research outcomes and postulates developed for OPC system. Therefore, the conventional hydrated OPC matrix can be considered as a reference point and spectrum of "worst case scenarios".

In the frame of this presented study, also one of the alternative systems – carbonated low-lime calcium silicates (CCS) are investigated. Even though the composition (cements by themselves, binding phases) of the CCS matrix is quite different (may be even radically) from the OPC one, the interpretation of the outcomes of the sulfate exposure experiment is based on the knowledge accumulated during the study of OPC system.

Particularly, this part of the whole research work aims at addressing the sulfate resistance of CCS matrix by implementing purely chemical approach, e.g., from the perspective of interactions

of the substances in aqueous medium wherein with the variation of the types of CS cements and sulfates.

Begin a new chapter here. Each chapter must begin on a new page. If you are pasting in previously published articles, you will need to reformat the articles to match the guidelines that are set in this template. You will also want to use the heading styles above even though you may have previously applied styles in the original document. The styles above will ensure you meet the Graduate School requirements.

3.2   Description of the Analytical Methods

3.2.1   Thermal analysis

The thermal analysis of the powdered samples was conducted by using thermo-gravimetrical analysis (TGA) and differential scanning calorimeter (DSC) techniques. For both techniques, high purity nitrogen gas atmosphere was implemented.

TGA was carried out in Q50 (TA Instruments) apparatus. The powdered sample, in the amount of 15-20 mg, was placed in an open platinum pan and it was heated in nitrogen atmosphere (60 mL/min) at a rate of 10°C/min rate up to 900°C.

The thermographs were analyzed using Thermal Analysis (TA Instruments) software.

3.2.2   X-Ray Diffraction analysis

For the XRD analysis the powdered samples were mounted in the aluminum holder as shown in Fig. 3.1. The diffractograms were collected using Siemens D500 diffractometer with CuKα radiation operated at 50 kV and 30 mA. The samples were scanned in the 2θ range of 5-60° at scanning rate of 0.02° 2θ/sec. The peak identification and Rietveld analysis were carried out using Jade 9 and Profex software packages. The visualization of the crystal structures was achieved using VESTA software.
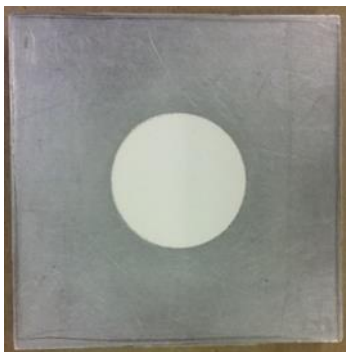
Figure 3.1. XRD sample mounted in aluminum holder

3.2.3 Fourier Transport Infrared (FT-IR) analysis

FT-IR spectra of the powder samples were acquired in the range of $600 – 3000\ cm^{-1}$ on a Perkin Elmer Frontier FT-IR Spectrometer. For every spectrum, the average of total 10 scans were recorded with a resolution of $4\ cm^{-1}$.

3.2.4 Scanning Electron Microscopy (SEM) analysis

The samples for (SEM) analysis were prepared by attaching them to the metal holder with adhesive carbon tape. Once mounted, they were coated with palladium (Pd). The SEM imaging was performed using ASPEX Personal SEM operating at 15 keV and equipped with energy dispersive X-ray Spectrometer (EDX).

3.2.5 Soak solution analysis

Soak solutions were first filtered by using $0.2\ \mu m$ cellulose acetate filter to separate solids from the soak solutions and then analyzed by using inductively coupled plasma - atomic emission spectroscopy (ICP-AES) and Ion Chromatography (IC) techniques.

ICP-AES analysis was conducted using Thermo Scientific iCAP 7000 spectrometer. Before testing, the machine readings were calibrated by using the standard solutions from VWR Chemicals BDH®. The concentrations of the standard solutions are given in Table 3.1. The test samples were prepared by diluting the original solutions with de-ionized water followed by addition of concentrated nitric acid (2% by volume).

Table 3.1. Concentrations of the standard solutions for the ICP-AES analysis, ppm

Ca	Si	Na	Mg	Al
0.5	0.5	1	1	1
1	1	5	5	5
2	2	10	10	10
5	5	20	20	20
10	10	50	50	50
20	20	100	100	100

The samples for the IC analysis were prepared by diluting the original solutions with de-ionized water. The IC analysis was conducted using the DIONEX ICS-900 machine equipped with the anion exchange Ion Pac AS23 column. The sodium carbonate/sodium bicarbonate (4.5 mM/0.8 mM respectively) was used as the eluent solution. As a regenerant solution, 72 mN solution of sulfuric acid was used. Calibration curve was developed using standard solutions of sulfate ions with concentrations of 1, 5, 10, 20, 50 and 100 ppm.

3.3   Characterization of the Materials

3.3.1   Characterization of cements

In this study, four different low-lime calcium silicate cements were used. The cement powders were characterized using X-Ray Fluorescence (XRF), XRD and SEM techniques. The physical appearance of the cements is shown in Figure 3.2. The XRF analysis was conducted by CTL Group Laboratories and the results are presented in Fig. 3.3. Comparing the oxide compositions of the cements, it can be seen that while they contain similar quantities of CaO (in the range of 43-46%), their SiO_2 content varied from 51.5% for cement #1 to 43% for cement #4. The calcium silicate in cement #1 is least diluted with other oxides, whereas other cements contain substantial amounts of other oxides (Al_2O_3, Fe_2O_3, MgO, K_2O). The highest amount of these oxides can be found in cement #4. The loss on ignition (LOI) and the amount of total alkalis present in these cements were determined using XRF analysis and the results are given in Table 3.2. All cements showed similar values of LOI except cement #2 which had LOI as around twice as LOI values of other cements. The lowest alkali content was found in cement #1, and the highest one was determined in cement #3.

Figure 3.2. Physical appearance of the low-lime
calcium silicate cement powders
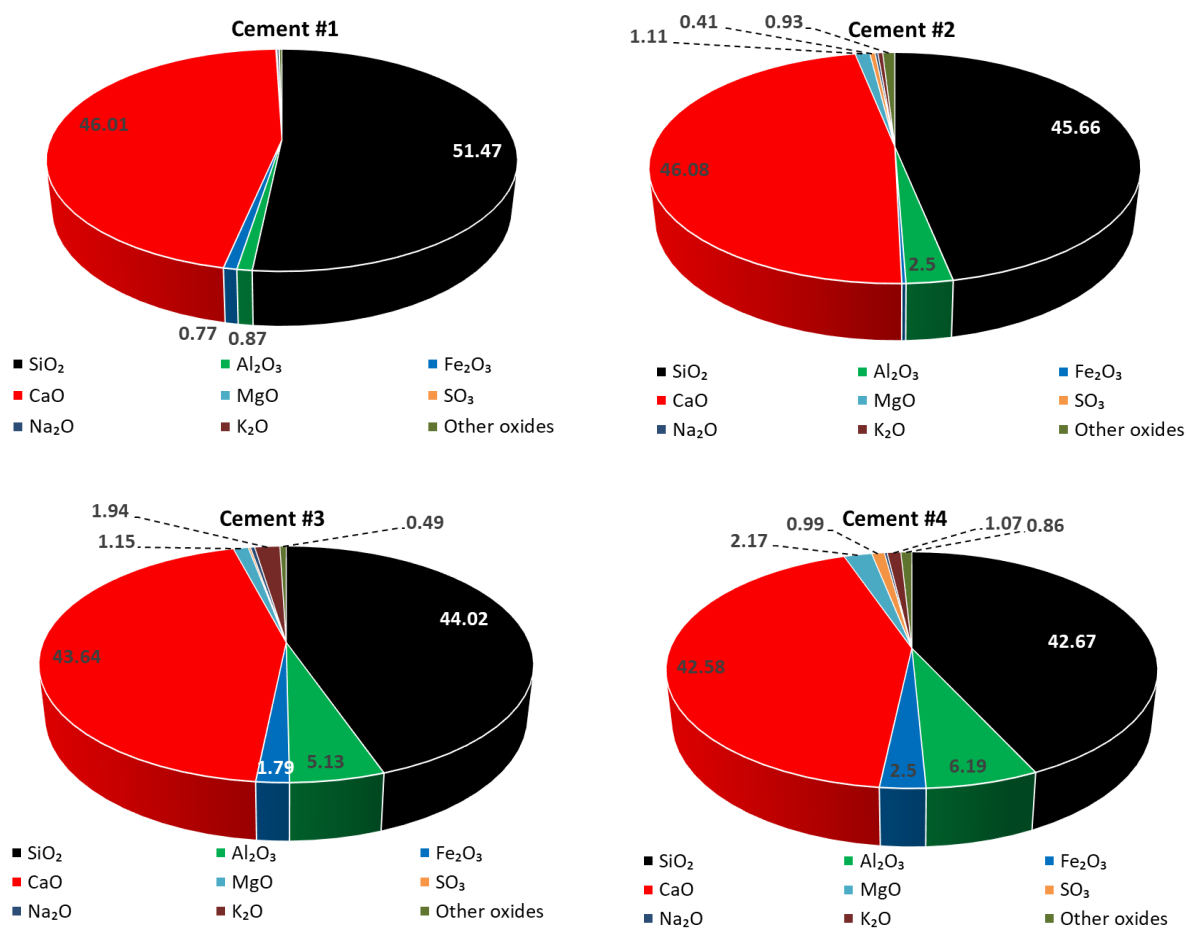
Figure 3.3. Oxide composition (%) of the cements

Table 3.2. LOI and the amount of total alkalis of the cements

	Cement #1	Cement #2	Cement #3	Cement #4
LOI, %	0.72	1.61	0.71	0.79
Tot.,alkalis, %	0.18	0.45	1.61	0.92

The XRD analysis show significant diversity of the cements (see Figure 3.4). Cement #1 consists of almost 100% of natural wollastonite while the cement #2 appears to be purely amorphous calcium silicate as indicated by the presence of a broad hump in two theta range ≈26-34°. Mineralogical composition of the cements #3 and #4 is almost the same and both cements contain represented minerals. The majority of the XRD pattern peaks in these two cements belong to larnite (β-$2CaO \cdot SiO_2$), pseudo-wollastonite ($CaO \cdot SiO_2$), rankinite ($3CaO \cdot 2SiO_2$), gehlenite ($2CaO \cdot Al_2O_3 \cdot SiO_2$), sanidine feldspar ($(K, Na)(AlSi)_4O_8$), quartz ($SiO_2$) and cristobalite ($SiO_2$). The difference between the cements #3 and #4 is the proportion of the minerals: cement #3 contains more larnite and rankinite than cement #4. In contrast, cement #4 contains more gehlenite and sanidine feldspar. The ratio of the calcium silicates to the remaining (inert) minerals appeared to be approximately 1.1 and 0.9 for cements #3 and #4 respectively. Moreover, the narrow shape of the peaks shown on the XRD pattern of cement #4 seems to indicate the presence of a well-developed crystalline phases, on the other hand, peaks present in cement #3 are broader and poorer defined.
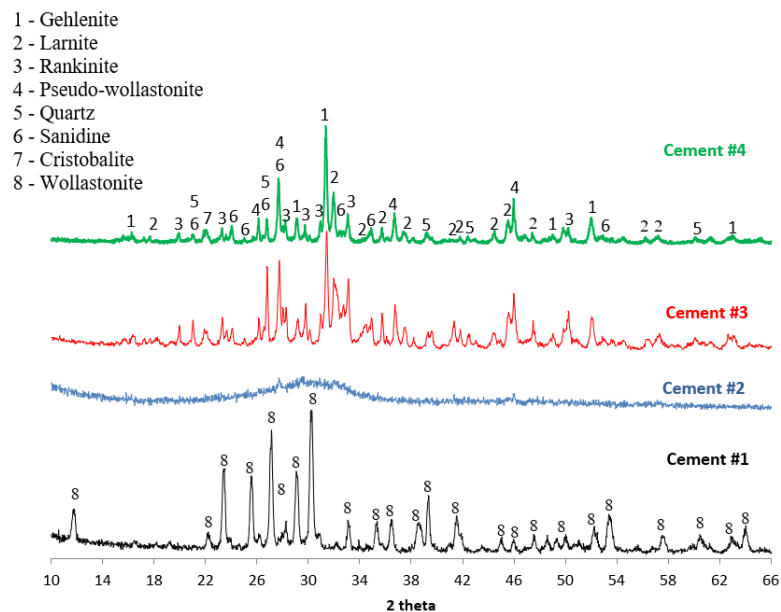
Figure 3.4. XRD patterns of the cements

The SEM imaging was used to further investigate the morphology of the grains of cements #1, #2, #3 and #4 cements. The micrographs of the cements are presented in Fig.3.5. The grains of cement #1, which is mainly natural wollastonite, appear as the needle-like crystals with the length of 2 – 60 μm. As it is showed in Fig. 3.5 (b), the particles of the cement #2 look glassy and are concavely shaped which is characteristic of amorphous structure. The morphology of the grains of both cements #3 and #4 resembles that of the grains of the OPC (Fig. 3.5 (c, d)). The angular grains vary in size and contain various crystalline components.

a)

b)

c)

d)
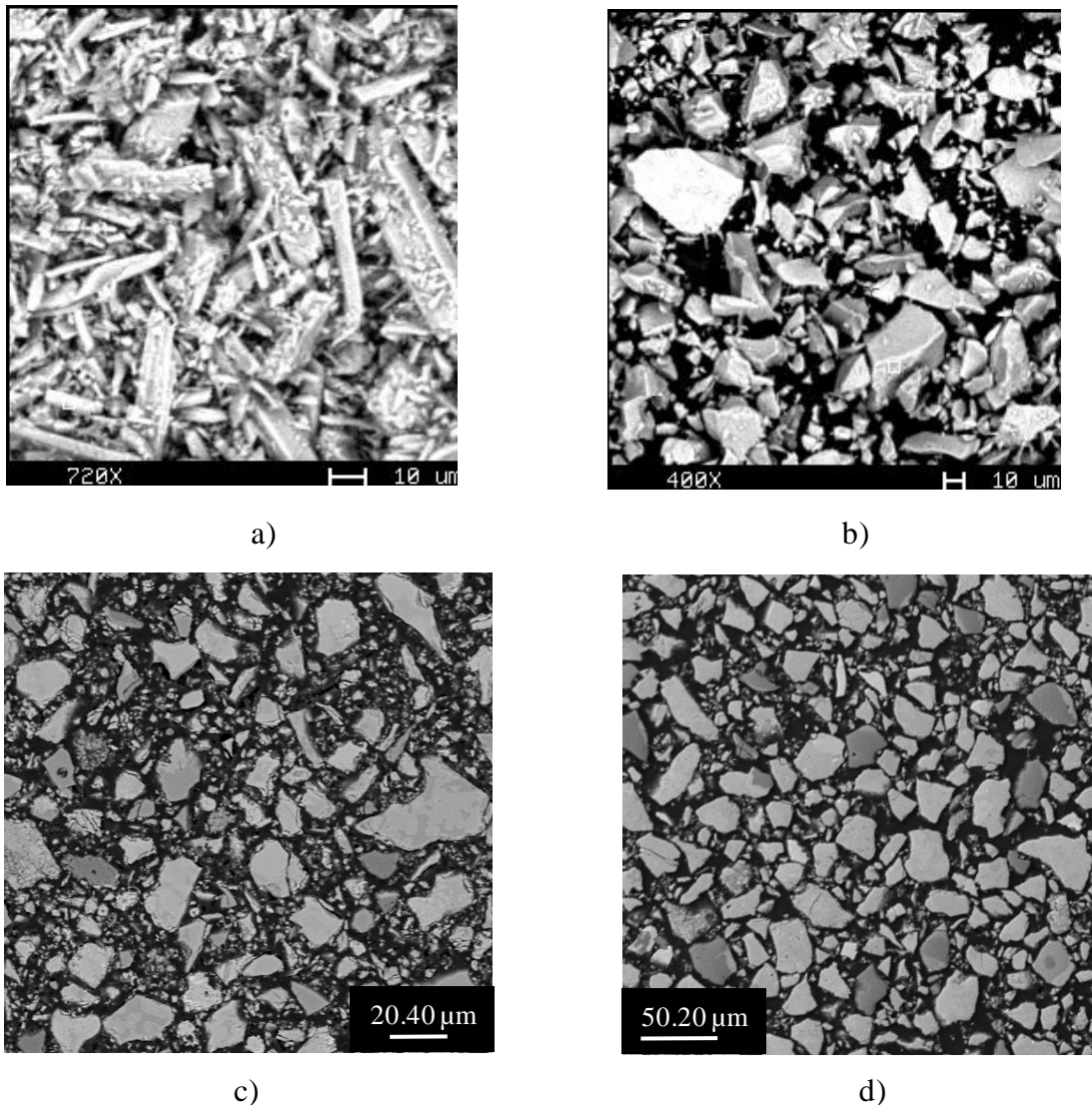
Figure 3.5. SEM micrographs (BSE mode) of the cements (a – cement #1, b – cement #2, c – cement #3, d – cement #4)

The data obtained from characterization of the cements used in this study was used to place them in ternary CaO – Al_2O_3 – SiO_2 phase diagram as in Figure 4.6. As can be seen, all cements are located within the small triangle with silica, larnite (belite) and gehlenite forming its vertices. The general composition of the three cements within this small triangle is marked by dashed oval.
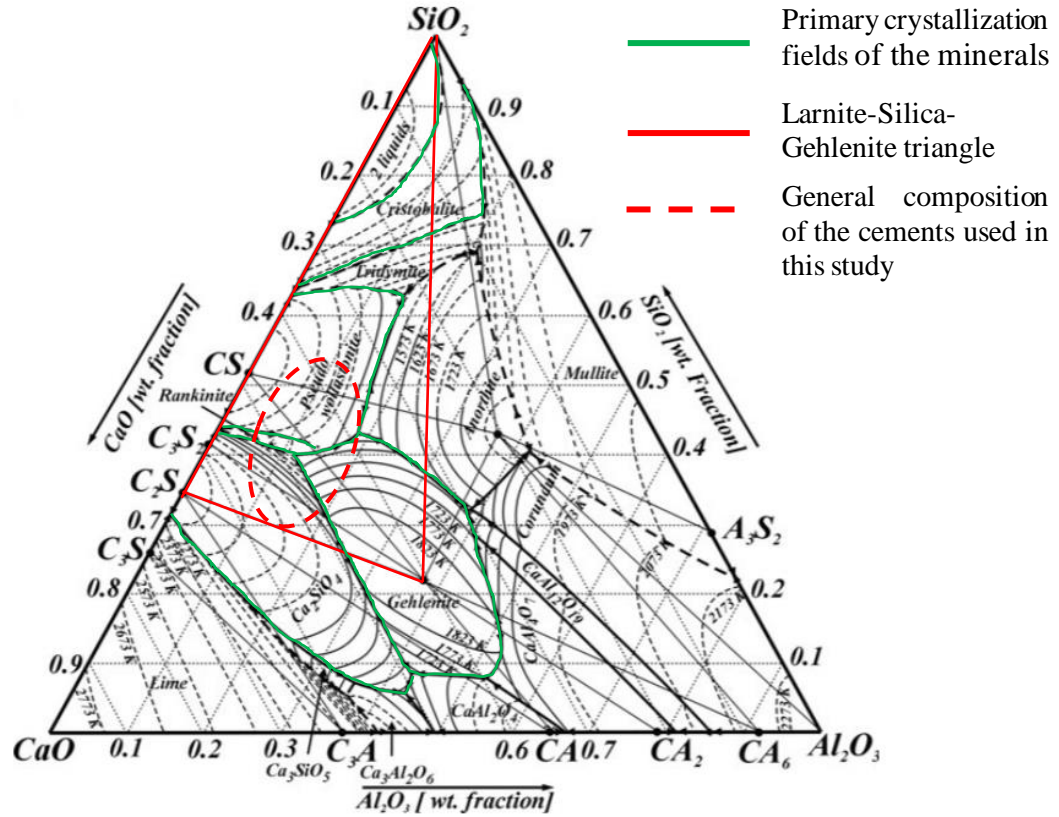
Figure 3.6. Ternary phase diagram of CaO-Al2O3-SiO2 system (adopted from Haccuria et al. (2016)) showing the general composition of cements used in this study

3.3.2   Characterization of carbonated pastes

Carbonated cement paste samples were prepared by hand mixing small amounts of cement powders with de-ionized water at water-to-cement ratio of 0.35. Once mixed, the pastes were placed in a thin (1.0 – 1.5 mm) layer in the. VWR sterile polystyrene Petri dishes with diameter of 60 mm and the height of 1.5 mm. Immediately after completion of casting, the paste-containing Petri dishes were placed in VWR Symphony 1.4A CO_2 incubator where they were carbonated for 5 days. The environmental conditions within the incubator were as following: temperature 23℃

90-100% relative humidity and 20% concentration of carbon dioxide. After completion of the carbonation, the paste samples were pulverized with mortar and pestle and stored sealed in glass vials before being used for testing.

Prior to being subjected to sulfate solutions exposure, the powdered carbonated paste samples were thoroughly characterized using thermal (TGA), XRD and FT-IR techniques. These non-exposed samples will from now on be referred as control samples.

TGA analysis results

The amount of calcium carbonates produced after carbonation was estimated by analyzing the weight loss in TGA thermograms in two temperature ranges: 650-800°C (see Fig. 3.7) and 450-630°C (see Fig. 3.8). The weight loss observed within temperature range 650-800°C is the result of decomposition of highly crystalline calcium carbonate phase – mainly calcite. On the other hand, weight losses observed within the lower temperature range are associated with decomposition of poorly crystalline forms of calcium carbonate, namely, vaterite. The quantitative examinations are shown in Table 3.3. These results show that the amount of calcite in cement #1 and cement #2 pastes appeared to be comparable: around 40-42 g/100 g of the paste sample. The portion of the calcite formed in cement#3 and cement #4 pastes were ~27 and ~32 g/g100 of the paste sample respectively. These lower values compared to cement #1 and #2 pastes is due to the dilution of the cements #3 and #4 by other inert minerals as previously described in 3.3.1. Analysis of the first derivative of the thermogram (DTGA) curves presented in Figure 3.8 shows the presence of the small hump in the temperature range 450-630°C. In addition to the main calcium carbonate (mainly calcite) decomposition peak, specifically, the plots for cement #2 and #4 pastes contain small and narrow peaks adjacent to the main peak. In contrast, the DTGA curve of the cement #3 paste contains well distinguishable broad peak. Compared with the results of these three cement pastes, the DTGA curve of the cement #1 paste does not seem to contain any noticeable hump other than main calcite peak. The areas of these the smaller peaks were considered when estimating the total amounts of calcium carbonates and the total amount of calcite.
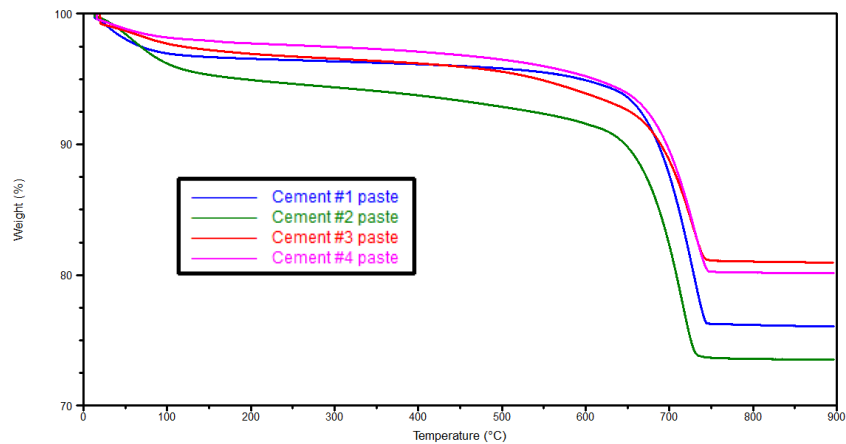
Figure 3.7. TGA thermograms of the reference paste samples
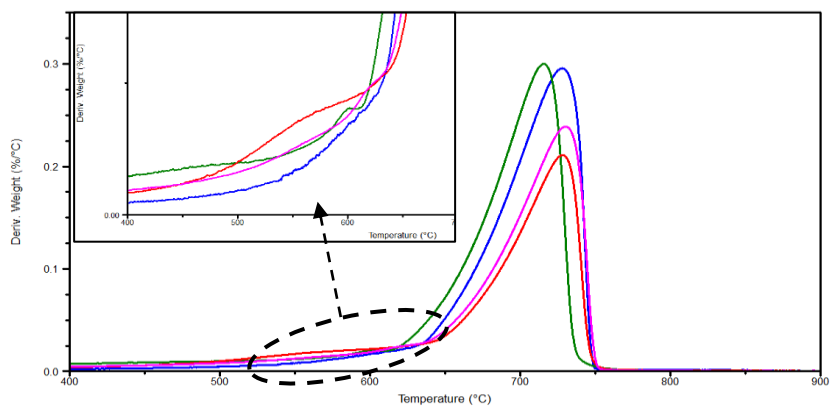
Figure 3.8 DTGA curves of the reference (i.e., non-exposed) paste samples: left upper corner image contains the magnified view of the hump in the temperature range 450-630°C

Table 3.3. Amounts of carbonates in the reference (i.e., non-exposed) carbonated paste specimens

Cement paste	Calcite/Total amount of carbonates, g/100 g of the paste sample	Presence of the hump	Hump range, °C
#1	41.5	No	-
#2	40.5/42	Yes	567-619
#3	27.2/34	Yes	450-633
#4	32.5/36	Yes	500-632

XRD analysis results

The XRD patterns of paste samples are presented in the Figures 3.9 and 3.10. It can be seen that all carbonated paste samples contain calcite. However, peaks of vaterite were also observed in the pastes made from cements #2, #3 and #4. The vaterite peaks are more distinguishable in the cement #3 and #4 paste samples, while the local magnification was needed to reveal the vaterite peaks in the XRD pattern of the cement #2 paste. Comparing the XRD patterns shown in Figure 3.4 with shown in Figures 3.9 and 3.10, it can be seen that carbonation process practically removed the peaks belonging to larnite and rankinite.

a)

b)
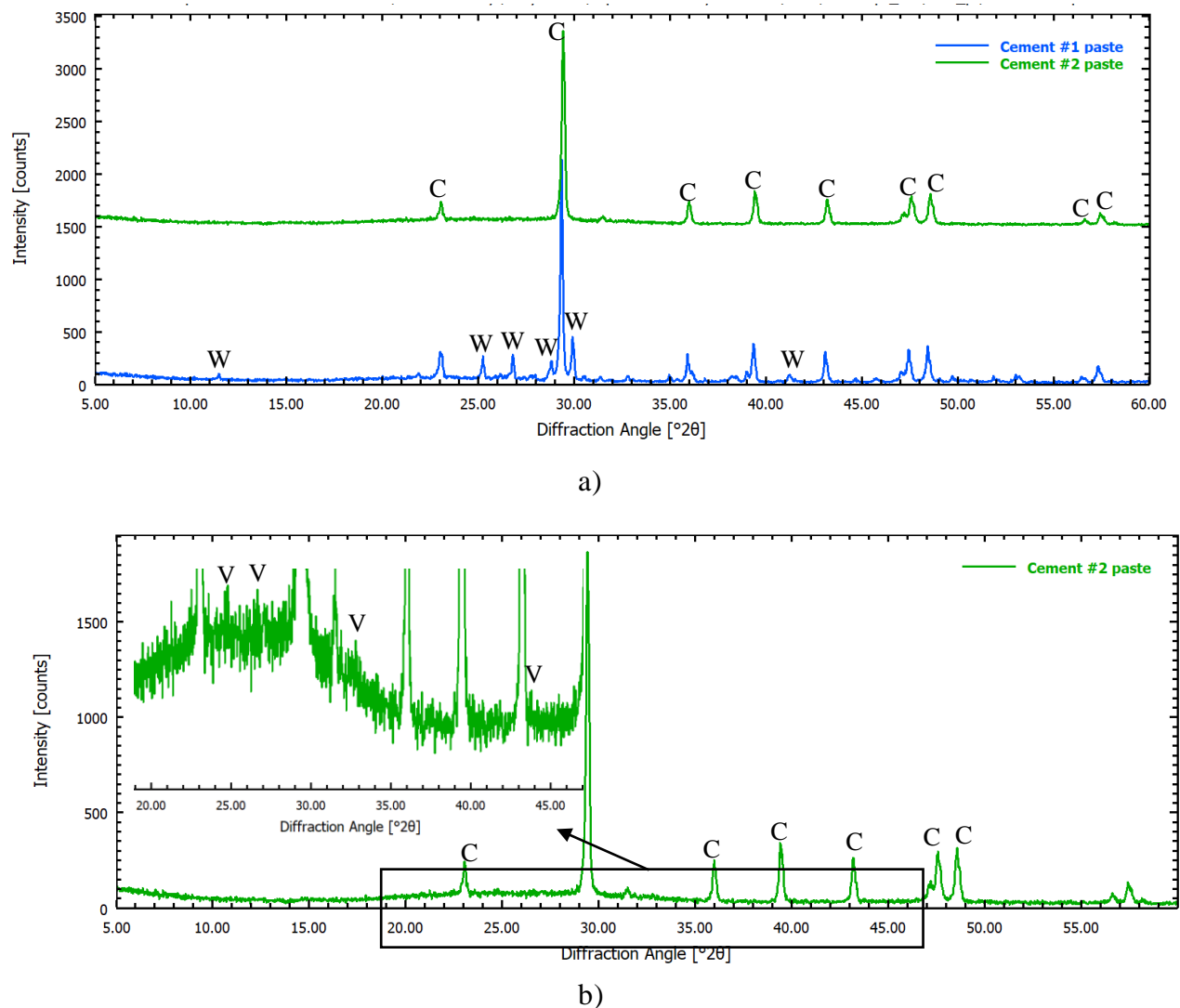
Figure 3.9. XRD patterns of carbonated cement #1 and #2 pastes: a) both cement pastes with all the main peaks labeled; b) XRD pattern of cement #2 paste with magnified peaks of vaterite (key: C - calcite, V - vaterite, W - wollastonite)
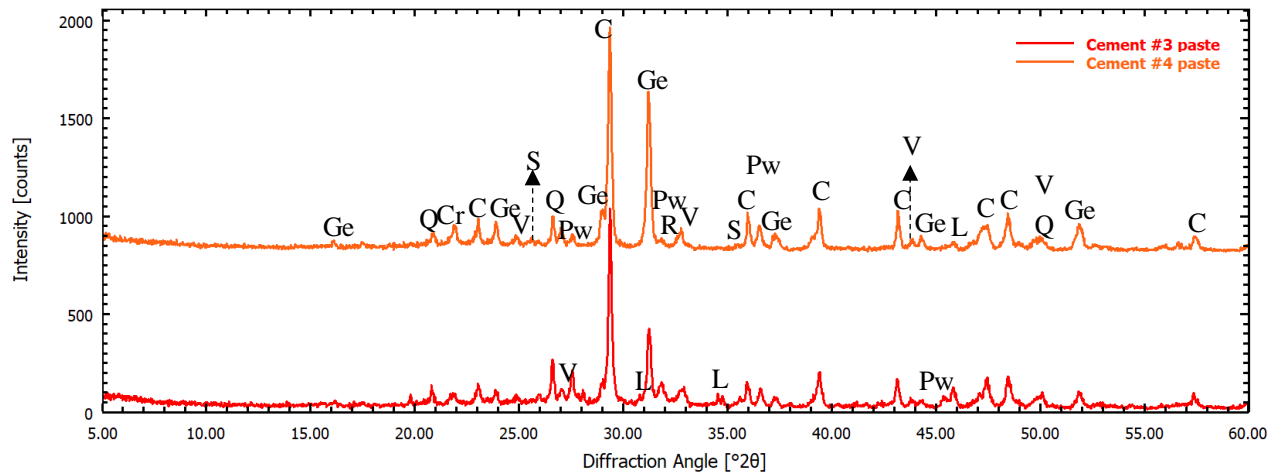
Figure 3.10. XRD patterns of carbonated cement #3 and #4 pastes (key: C – calcite, Cr – cristobalite, Ge – gehlenite, L – larnite, Pw – pseudo-wollastonite, Q – quartz, R – rankinite, S – sanidine, V – vaterite)

FT-IR analysis results

The FT-IR absorption spectra are shown in Figure 3.11. The bands with the peaks at around 1420, 874 and 712 cm^{-1} belong to calcite and are visible in spectra from all four pastes. Similarly, to TGA results, there are distinguishable differences in intensities and shapes of the bands. Namely, almost all calcite bands in the spectrum from cement #1 paste sample appear to be sharper and have higher intensity compared to those observed in spectra from other paste samples. As an example, the absorption band located at ~1420 cm^{-1} seems to be much broader in case of pastes from cement #3 and #4 than the same band observed for paste from cement #1. According to Milkey [46], who examined the FT-IR spectra of different feldspar minerals, the sharp and well-defined peaks indicate a well-developed crystalline structure of a mineral. Applying these observations to data presented in Figure 3.11, it can be inferred that the calcite formed in cement #1 paste is more likely crystalline than in other paste samples. Again, this observation correlates well with findings from the TGA results. Regarding other polymorphs of calcium carbonate, the aragonite spectrum is similar to one of calcite except for the presence of two doublets in 850-900 cm^{-1} and 670-714 cm^{-1} range [27, 31]. No such doublets were observed in any of the spectra shown in Figure 3.11. This observation confirms the results of XRD analysis. On the other hand, it was challenging to highlight the presence of the vaterite which was visible in XRD patterns of all pastes except the one produced from carbonated wollastonite. The FT-IR peaks characteristic of vaterite

(at ~1070 and 873 cm^{-1} [32, 37]) overlapped with those assigned to silica and calcite, respectively. The FT-IR curves did not contain a band located at ~745 cm^{-1} which is typically interpreted to represent absorption due to deformation of carbonate ion. However, the band was located at ~848 cm^{-1} which appeared as a shoulder on the calcite band (~874 cm^{-1}) in the spectra of cement #3 and #4 paste samples.

The strong broad band located between 1000-1300 cm^{-1} and a smaller one located at ~800 cm^{-1} more likely belong to amorphous silica [32, 3 and 34]. The former band, according to the published data [30, 27, 52, 46, 51], occurs due to Si-O stretching vibrations in all silicate structures. However, the shape and intensity of that band vary from sample to sample. At this point, it is worthwhile to highlight the importance of the FT-IR spectroscopy for this study, particularly with respect to the amorphous silica content of the CCS system. This is because neither the thermal analysis, nor the XRD techniques utilized in this work can provide sufficient indications of the presence of the amorphous silica gel and any changes it undergoes.

To further confirm the location of the amorphous silica bands, two reference materials: the meta-silicic acid (H_2SiO_3) and amorphous fumed silica also were examined using the FT-IR method. The results are shown in Figure 3.12. The curves of both reference specimens contain three different peaks. The first of these three peaks (the largest one) is located in the range at around 1000-1300 cm^{-1}, the second (smaller) peak is located in the range 760-860 cm^{-1} and the third (smallest) peak is located in the range of ~940-970 cm^{-1}. Furthermore, all three peaks in the case of fumed silica, are slightly shifted (for ~10-20 cm^{-1}) to the left. On top of that, the main largest band of the fumed silica seems to be steeper and narrower than that of the silicic acid. Launer (1952) points out that the Si-O band tends to shift towards the higher wavenumber values and becomes narrower as Si/O ratio increases. By comparing the spectra of these reference samples with the ones of carbonated CS paste samples, it can be inferred that all carbonated paste samples may contain traces of the silicic acid, especially in the case of carbonated wollastonite paste. For other three paste samples, the main silica band appears to be broader, less resolved and shifted to lower frequency ranges. As stated by Yu et al. (1999), in CSH-like gels (C/S≤1.2) the shift of the Si-O band in the direction of lower wavenumber is mainly associated with de-polymerization of silicate chains and the increase in the Ca/Si ratio. The researchers, who used the FT-IR technique to study clay mineralogy, mention factors that may influence the band shift. These may include elongation of the inter-atomic distances and subsequent weakening of the Si-O bond due to doping

with different cations and/or cation exchange [30, 27, 52, 46, 41]. In such cases, both the atomic mass and ionic radius of the elements involved are important. Based on these reported findings, one can conclude that the amorphous silica gel present in the carbonated pastes prepared from cements #2, 3 and 4 pastes are likely modified with calcium ions.
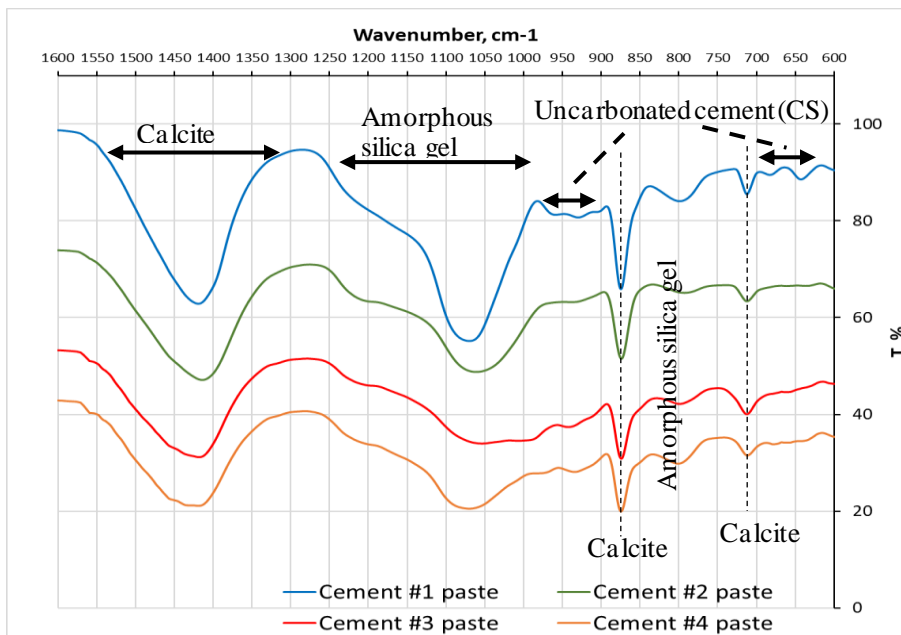
Figure 3.11. FT-IR spectra of the carbonated reference (i.e., not exposed to sulfate solutions) paste samples
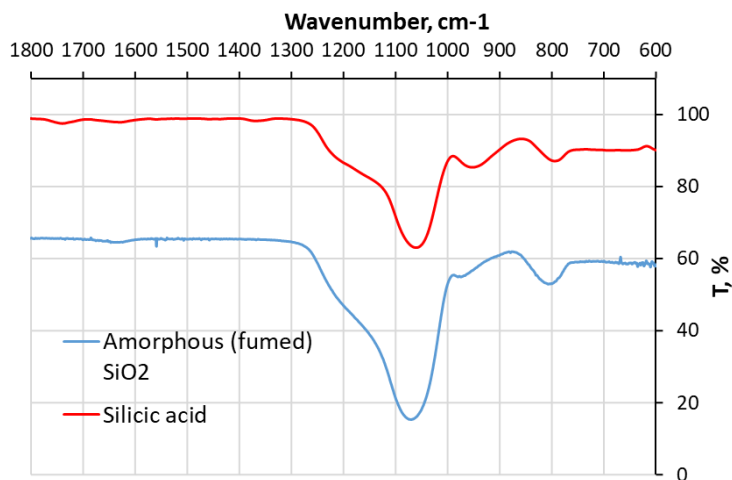
Figure 3.12. FT-IR spectra of reference (silica) samples

3.4 Methodology of the Sulfate Exposure Experiment

3.4.1 Experimental setup

In current study, three different types of sulfate solutions were used. The American Chemical Society (ACS) reagent grade anhydrous sodium sulfate, anhydrous magnesium sulfate and 18-hydrate aluminum sulfate chemicals were used to prepare 0.35M sulfate solutions. The pH values of the original sulfate solutions (i.e., before they came in contact with the paste powders) were in the range of 6-7 for sodium and magnesium sulfate solutions. On the other hand, the aluminum sulfate solution was rather acidic with pH level in between 3-4.

All four carbonated paste samples were pulverized, using mortar and pestle, sieved through #200 (75 μm) sieve and submerged in sulfate solutions using solid to liquid ratio of 1:4. The slurry samples were kept sealed in plastic centrifuge tubes with 50 mL capacity and agitated periodically twice a week by hand. Due to its acidic nature, the mixing of aluminum sulfate solution with paste powders resulted in release of CO_2 gas bubbles from the decomposition of calcium carbonates. For this reason, the tubes containing aluminum sulfate solution were sealed only after the bubbling of CO_2 has ceased. In addition to the sulfate solutions, paste powder samples were also submerged in de-ionized water. In total, 140 slurry samples – 4 sets (32 samples per each solution type) – were prepared and stored at room temperature (23±5°C). Ultimately, the exposure test was held for 120 days. At different time periods (0.5, 1, 5, 10, 20, 60, 90 and 120 days) of exposure 16 samples in total (4 different paste sample slurries per each solution type) were taken from the set for further analysis.

3.4.2 Post exposure analysis

After reaching the pre-designated period of exposure, the slurry samples were centrifuged and filtered using 0.2 μm cellulose acetate filter to separate solids from the soak solutions. The solids were then oven-dried at 35±5°C for three days, pulverized using mortar and pestle and stored in sealed glass vials with plastic cap. Afterwards, the powdered solids were subjected TGA, DSC, XRD and FT-IR analysis following the procedure described in section 3.2.

The filtered solutions were kept sealed in 15 mL plastic centrifuge tubes and stored in laboratory refrigerator at ~4-5°C, until they were removed for analysis. The chemical analyses, which included the ICP and IC tests, were conducted according to the procedures described in 3.2.

3.5   Results

3.5.1   Soak solution chemistry

The focus of the chemical analysis of the soak solutions was on the change (over time) in concentrations of the main ions present in the original sulfate solutions (i.e., Na^+, Mg^{2+}, Al^{3+} and SO_4^{2-}) as well as the dynamics of the leaching of calcium and silica species from the carbonated pastes prepared from the four low-lime calcium silicate cements exposed to various sulfate solutions and to the de-ionized water. The procedures described in section 3.2 were followed when preparing the samples and conducting the test.

De-ionized water soak solution

Figure 3.14 shows change in concentrations with time of Ca and Si species present in soak solutions of pastes exposed to deionized water for all 4 types of CCS paste matrices used in the study. Unlike to what was observed in case of hydrated OPC paste exposed to de-ionized water (see Fig. 3.13), graphs presented in Figure 3.13 show that the amount of leached silica (expressed as silicon species) is 2-3 times higher than that of calcium.
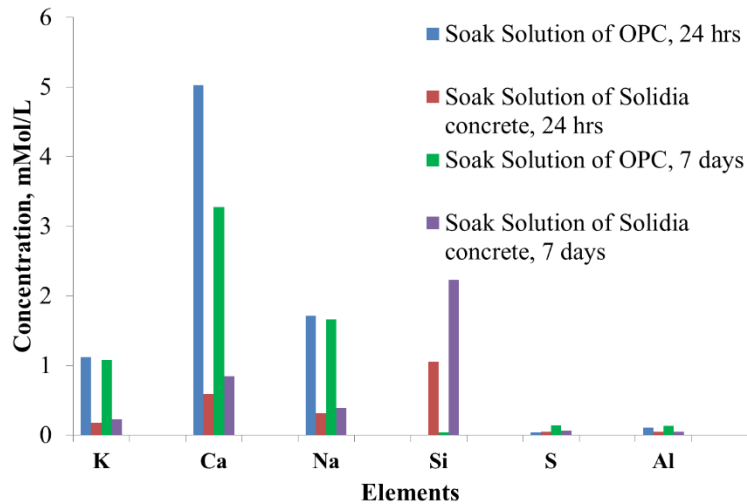
Figure 3.13. Concentration of the elements in the leachates of OPC and CCS concrete

Compared to other CCS pastes, the highest amount of calcium leached out from cement #3 paste (Fig. 3.14 (a)). This might be due to the presence of more soluble forms of calcium carbonate

polymorphs (e.g., vaterite), as found during the analysis of the XRD results (see section 3.3.2), or due to leaching from the particles of leftover larnite (β-C$_2$S) and from calcium-modified silica product of carbonation reaction. However, in all cases, the concentration of calcium stabilized after 5-10 days of contact with de-ionized water.

As shown in Fig. 3.14 (b), at end of the testing period the lowest amount of silica leached out from carbonated wollastonite paste (cement #1), whereas the highest concentrations of silica were observed in soak solutions that were in contact with cement #2 and cement #3 pastes. These results can be linked to the results of FT-IR analysis of the CCS pastes (see Fig. 3.11 of section 3.3.2) and demonstrate the variability of the structure of the amorphous silica gel among the four CCS pastes used in the study. More specifically, the more polymerized and less modified by calcium ions form of silica gel present in the matrix of carbonated wollastonite appears to be less soluble compared to ones which were described as poorly ordered, less polymerized and probably doped with calcium.

a)   b)
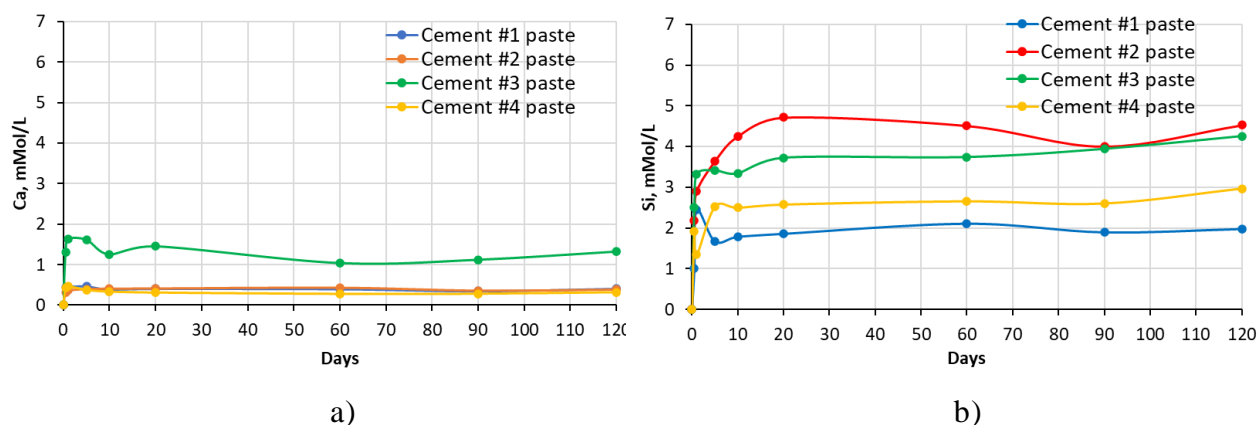
Figure 3.14. Change in concentration with time of: (a) Ca and (b) Si species present in soak solutions of pastes exposed to de-ionized water

Sulfate soak solutions

The chemical analysis of the sulfate soak solutions indicated that the sulfate-rich environment significantly influences the amount of calcium and silica ions leached out from the CCS matrices (see Fig. 3.15 – 3.18). As shown in the graphs presented in the above-mentioned Figures, all sulfate solutions triggered substantial increase (compared to deionized water soak solution) in the amount of calcium ions leached out from all four CCS matrices. Depending on the solution, the observed increases were in the range of 10-15 times. There is also a noticeable trend

of Ca ions concentration decay with time for all pastes exposed to aluminum sulfate, as well as cement #2 pastes exposed to sodium sulfate, and cements #3 and 4 pastes exposed to magnesium sulfate solution. This might be due to the consumption of calcium ions during precipitation of new compounds such as gypsum (see sections 3.5.2 and 3.5.3).

With respect to leaching of silica species, the effect of sulfate solutions, especially aluminum and magnesium sulfates, appears to be quite opposite to that observed for calcium species. As an example, for all four types of pastes the exposure to aluminum sulfate resulted in only minimal levels of silica in the soak solution, indicating that this sulfate solution stabilizes silica species present in the specimens. Similarly, it also appears that magnesium sulfate stabilized silica in all paste samples except that of the carbonated wollastonite paste (cement#1). However, the effect of sodium sulfate seems to be rather selective: it stabilized the leaching of silica compared to immersion in deionized water only for the cement #2 paste samples.

a)   b)
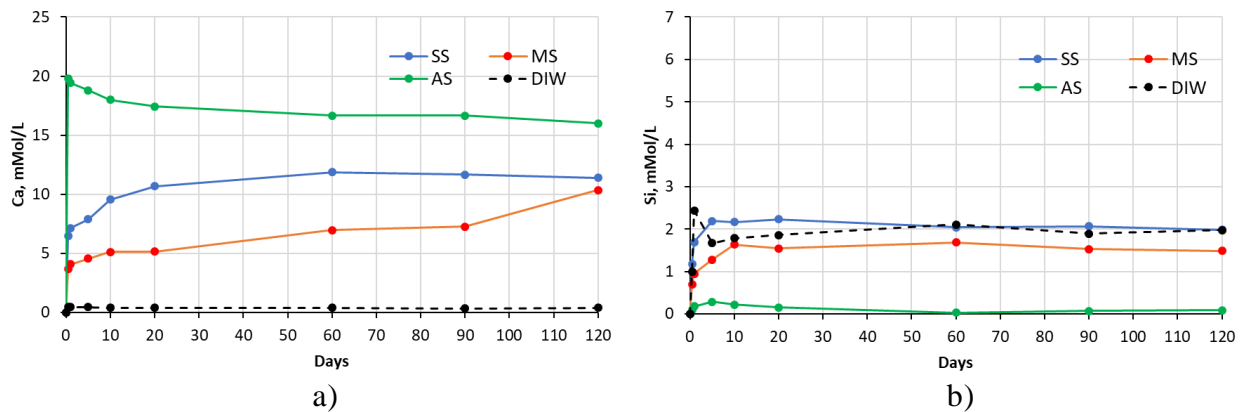
Figure 3.15. Changes in concentrations with time of: (a) Ca and (b) Si species present in sulfate soak solutions in contact with cement #1 paste specimens (key: SS – sodium sulfate, MS – magnesium sulfate, AS – aluminum sulfate, DIW – de-ionized water)
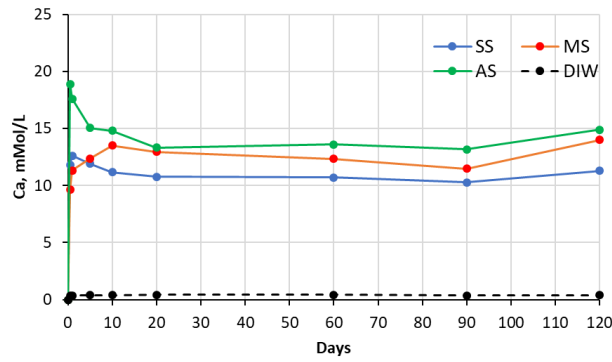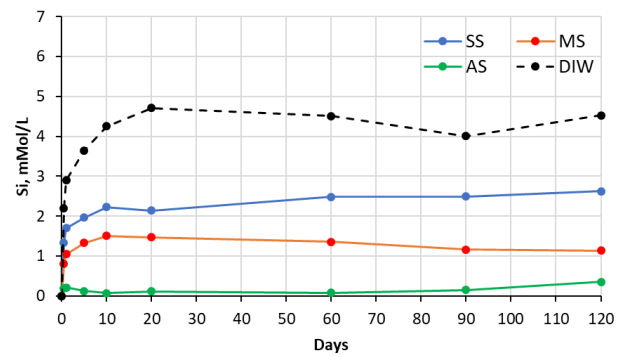
a)   b)

Figure 3.16. Changes in concentrations with time of: (a) Ca and (b) Si species present in sulfate soak solutions in contact with cement #2 paste specimens (key: SS – sodium sulfate, MS – magnesium sulfate, AS – aluminum sulfate, DIW – de-ionized water)
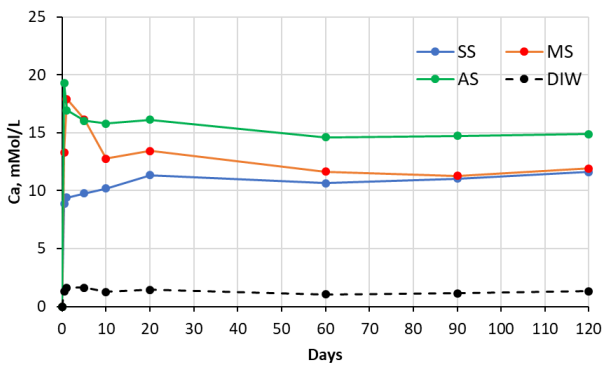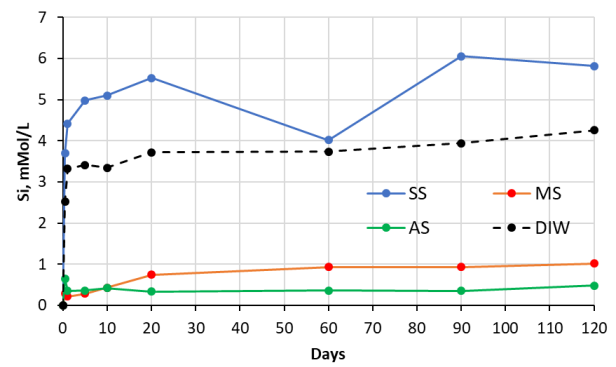
a)   b)

Figure 3.17. Changes in concentrations with time of: (a) Ca and (b) Si species present in sulfate soak solutions in contact with cement #3 paste specimens (key: SS – sodium sulfate, MS – magnesium sulfate, AS – aluminum sulfate, DIW – de-ionized water)

a)   b)
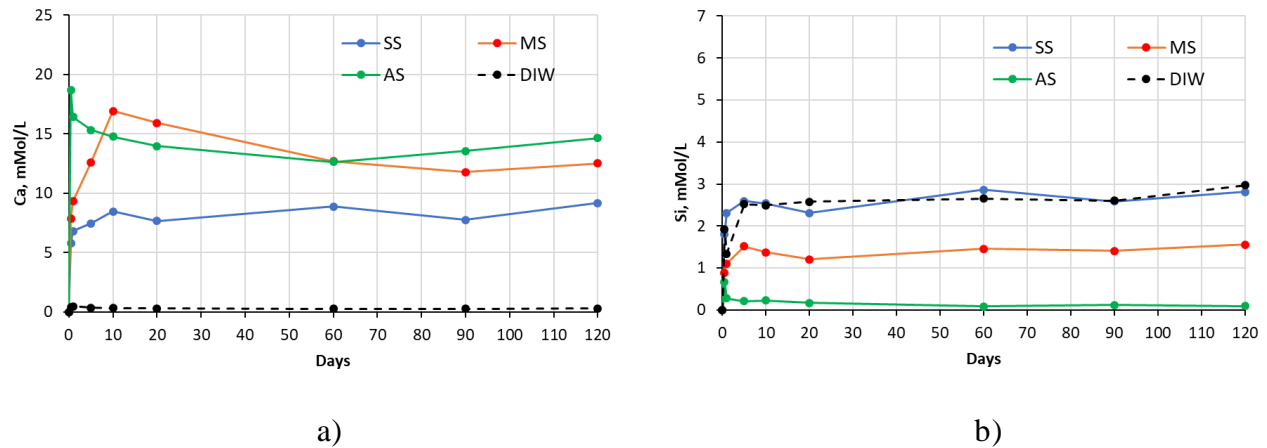
Figure 3.18. Changes in concentrations with time of: (a) Ca and (b) Si species present in sulfate soak solutions in contact with cement #4 paste specimens (key: SS – sodium sulfate, MS – magnesium sulfate, AS – aluminum sulfate, DIW – de-ionized water)

The change in concentrations (normalized with respect to the concentration at zero days) of sodium and magnesium ions over the entire test period is presented in Fig. 3.19. The concentrations of aluminum cation (and the associated sulfate anion) are not presented as they were negligibly small even after only one day of exposure. As shown in the graphs presented in Figure 3.19, concentrations of sodium ion remain essentially constant with the exception of a slight reduction in case of the cement #2 paste. In contrast, one can observe that over time the concentration of magnesium reduced as most as by ~68% for the cement #3 paste sample. In case of cement #2 and #4 paste samples, the reduction was about ~10%. The reduction in concentration of magnesium ions in soak solution in contact with cement #1 paste samples was very small (~2% detected only after 120 days of exposure).
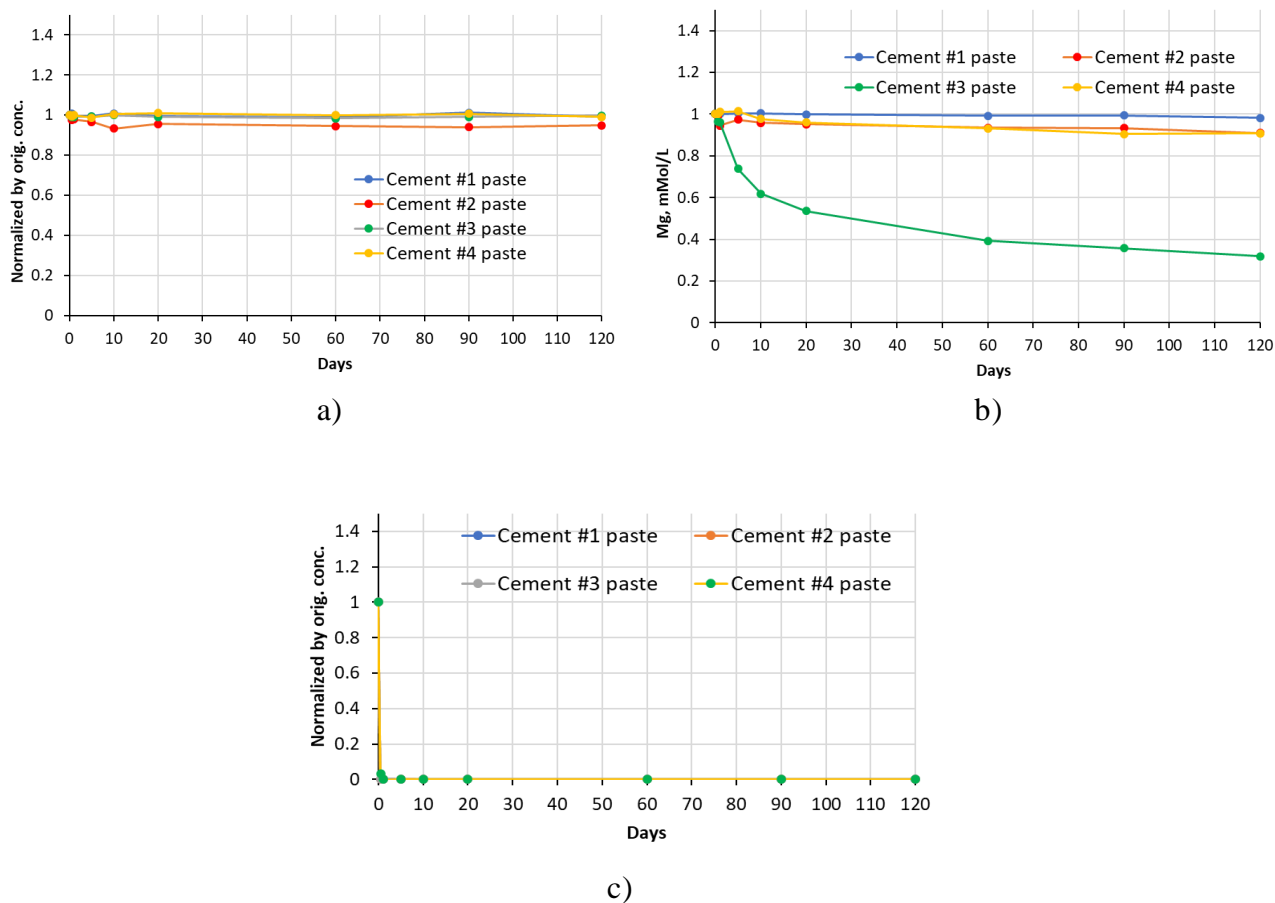
Figure 3.19. Normalized concentrations of Na$^+$ (a), Mg^{2+} (b) and Al^{3+} (c) ions in soak solutions of all cement paste samples

The plots of normalized changes in concentration of sulfate ions (for sodium, magnesium and aluminum sulfate solutions) for soak solutions in contact with all cement paste samples used in this study are presented in Fig. 3.20. The trends illustrated by the sulfate ion curves seem to be quite similar to those observed for the corresponding sodium, magnesium and aluminum cations.
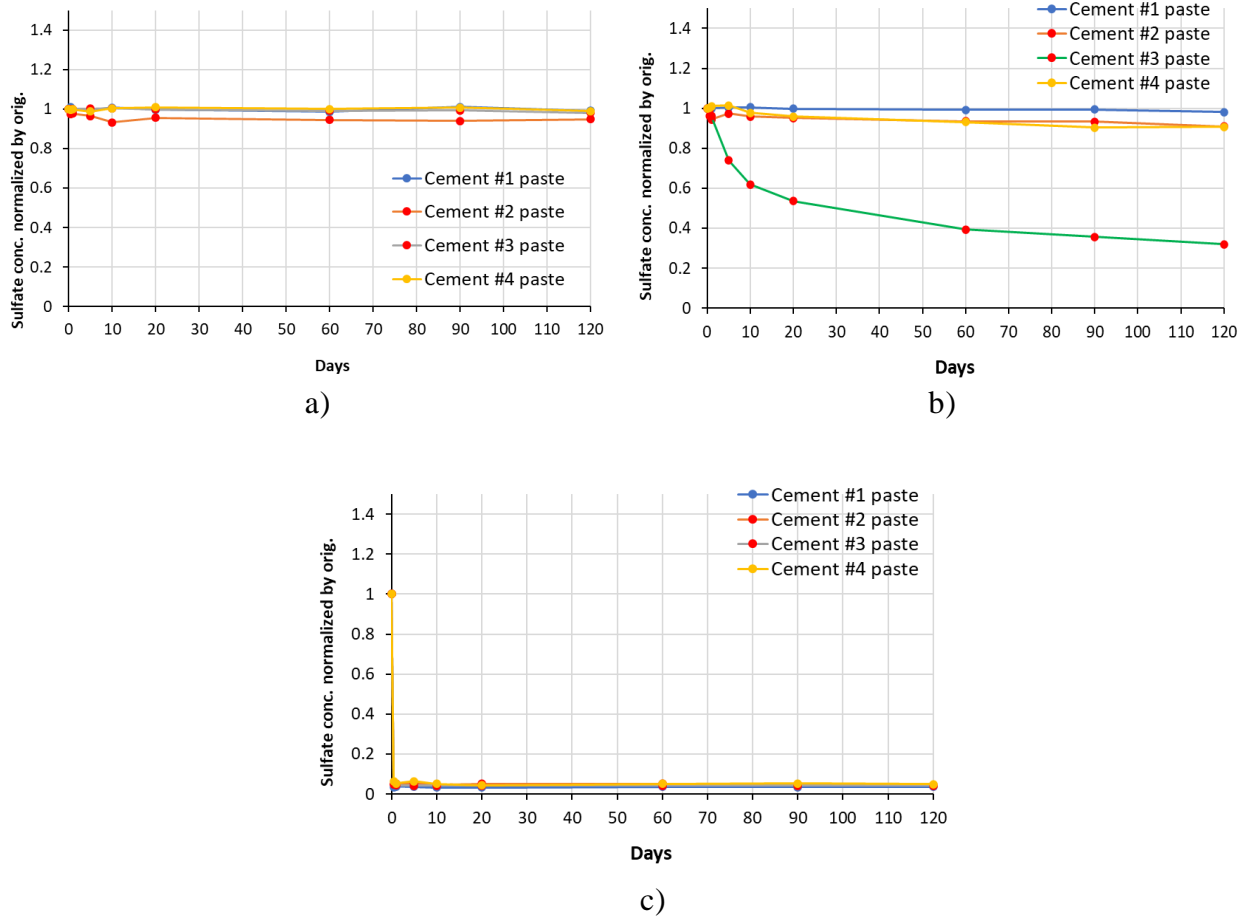
Figure 3.20. Change of sulfate concentration in sulfate soak solutions (a – sodium sulfate, b – magnesium sulfate, c – aluminum sulfate)

The pH level of the soak solutions by the end of the 120-day period achieved the following values:

- Sodium sulfate: 8-9 for cement #1, 2 and 4 paste samples; 10 for cement #3 paste sample.
- Magnesium sulfate: ~8 for all cement paste samples.
- Aluminum sulfate: ~7.5-7.8 for all cement paste samples.

The pH values of all soak solutions, including de-ionized water (reference) monitored during the whole 120-days period of test are plotted and presented in Fig. 3.21. The importance of the pH with respect to the stability of the sulfate bearing compounds formed during the exposure is discussed in section 3.5.2.
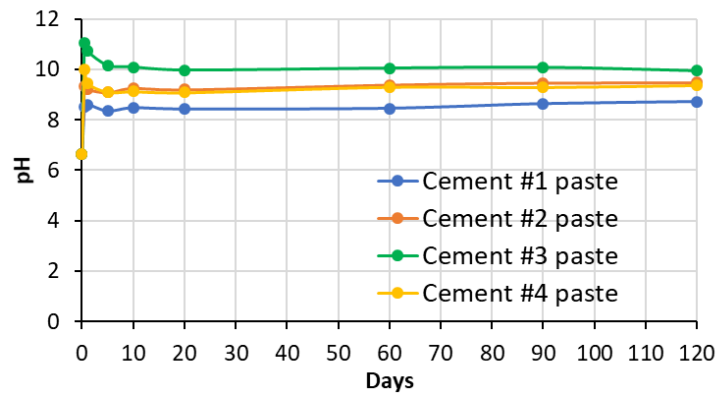
a)
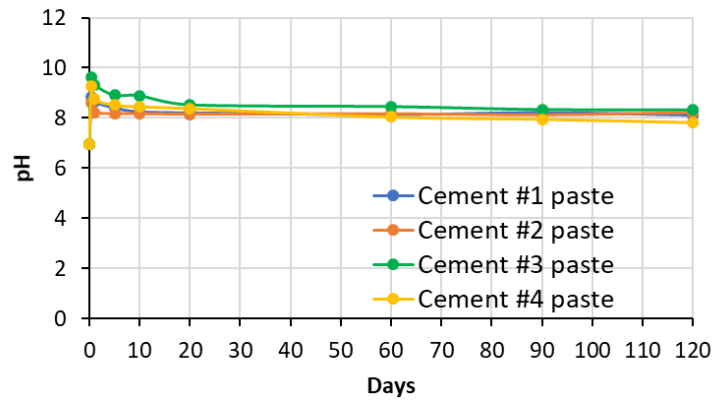
b)
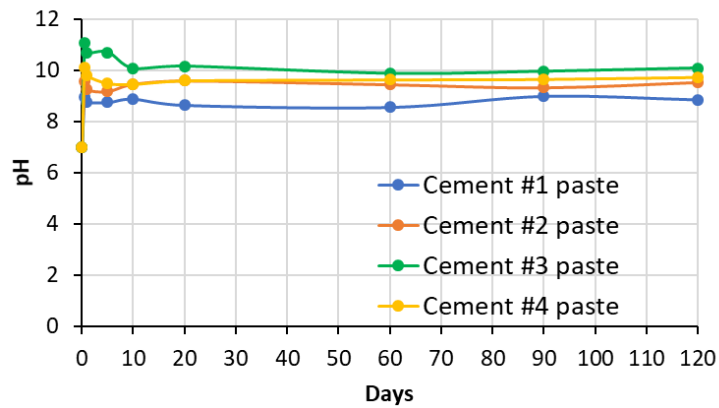
c)

Figure 3.21. pH values of the soak solutions: (a) – sodium sulfate, (b) – magnesium sulfate, (c) – aluminum sulfate, (d) – de-ionized water

Fig. 3.21 continued

d)
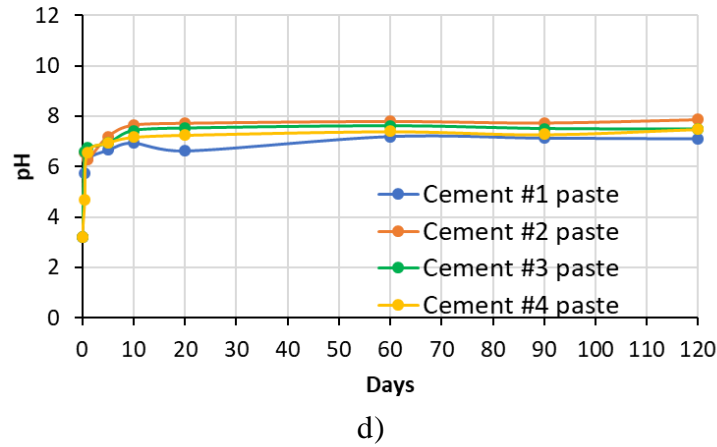
3.5.2 X-Ray diffraction results

Figures 3.22 to 3.25 present the XRD patterns obtained from, respectively, carbonated calcium-silicate paste samples #1 to #4. Each of these Figures contains four different patterns: one XRD pattern for the carbonated calcium-silicate paste that was not exposed to sulfate solutions (referred to as "control") and three XRD patterns obtained from the same paste after exposure to, respectively, sodium sulfate, magnesium sulfate and aluminum sulfate solutions. The analysis of these patterns indicates that the degree of alteration of the existing crystalline phases and the formation of the new crystalline phases depends on both, the type of the paste and the type of the sulfate solution. In general, the biggest change resulting from the exposure of the pastes to various sulfate solutions was formation of gypsum (mostly at the expense of calcite) in all pastes exposed to aluminum sulfate. In addition, formation of gypsum was also observed in pastes #2, #3 and #4 exposed to magnesium sulfate as well as paste #2 exposed to sodium sulfate.
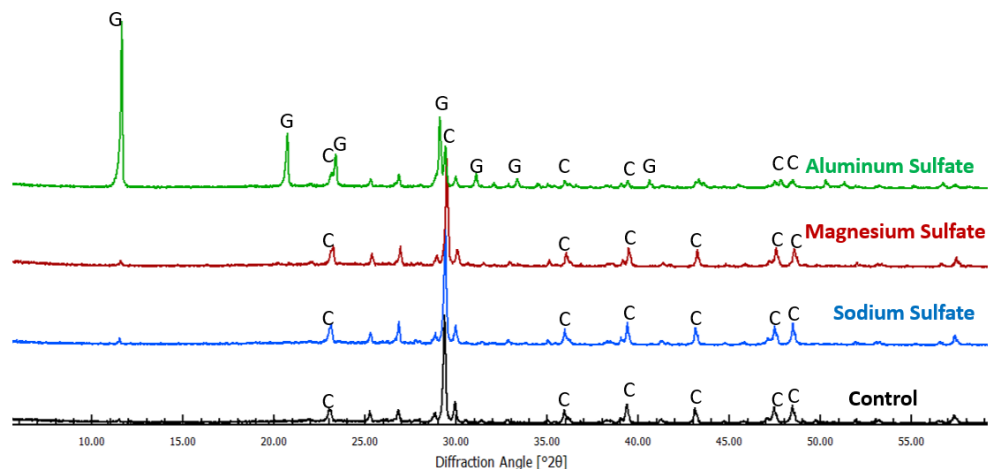
Figure 3.22. XRD patterns of the cement #1 paste samples after 120-days of exposure to sodium, magnesium and aluminum sulfate solutions (key: C – calcite, G – gypsum)
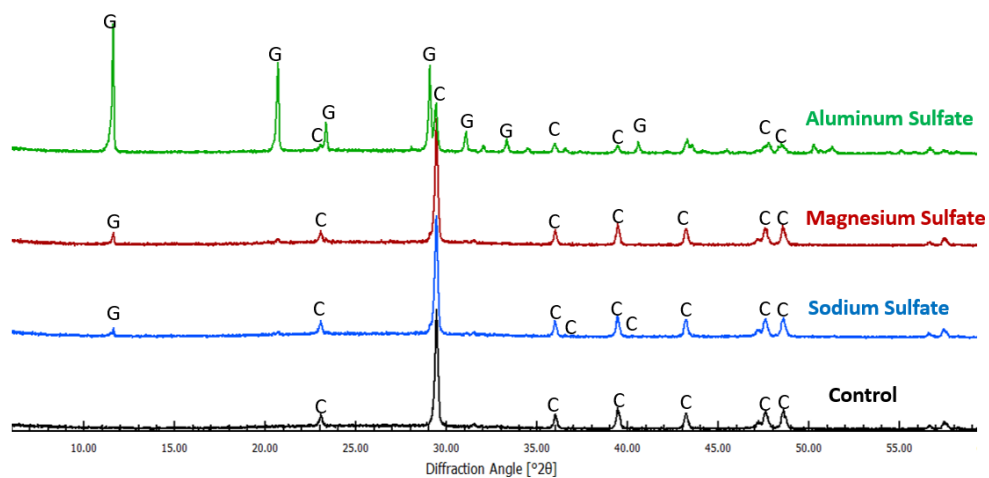
Figure 3.23. XRD patterns of the cement #2 paste samples after 120-days of exposure to sodium, magnesium and aluminum sulfate solutions (key: C – calcite, G – gypsum)
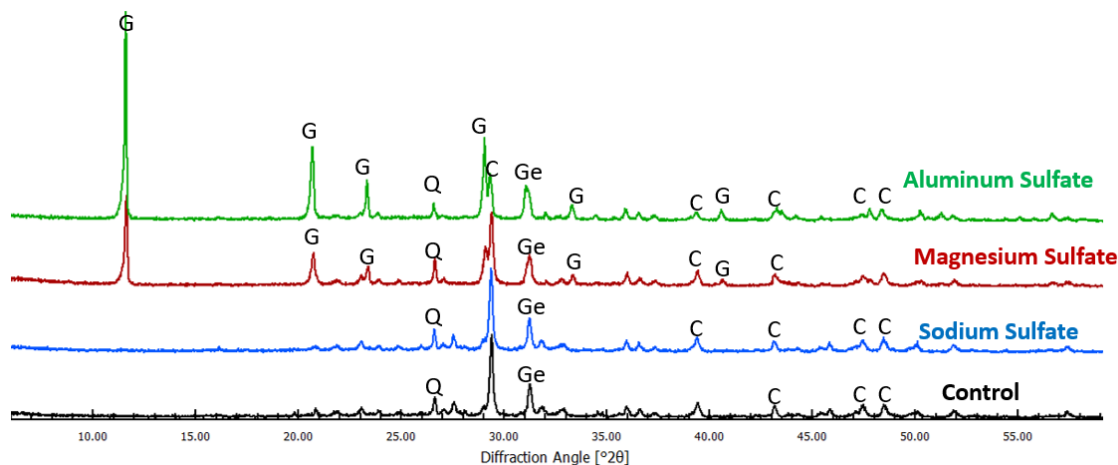
Figure 3.24. XRD patterns of the cement #3 paste samples after 120-days of exposure to sodium, magnesium and aluminum sulfate solutions key: C – calcite, G – gypsum, Ge – gehlenite, Q - quartz)
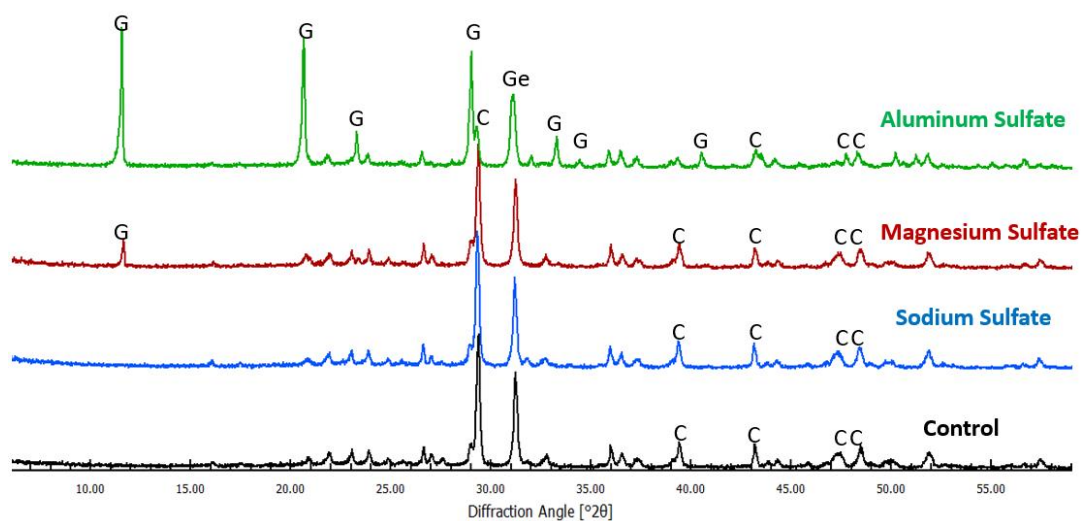
Figure 3.25. XRD patterns of the cement #4 paste samples after 120-days of exposure to sodium, magnesium and aluminum sulfate solutions (key: C – calcite, G – gypsum, Ge - gehlenite)

In an attempt to quantify the amounts of crystalline phases present in these pastes, their content of calcite (previously independently determined via TGA method) was utilized as an "internal" standard. Before attempting the phase quantification, the collected XRD data were subject to the Rietveld refinement procedure to more accurately determine their composition. The

combination of these two approaches allowed to calculate the amount of both, the crystalline and (by the difference) the amorphous components of the paste. The results of the phase quantification procedure for each type of cement paste are presented as cumulative diagrams in Fig. 3.26-3.29.

As shown in Figures 3.26(a) and 3.26(b), the carbonated wollastonite paste (cement #1) does not seem to have experienced any change in composition when exposed to either sodium or magnesium sulfate solutions. However, as can be seen from the graph in Fig.3.26(c), at the end of the 120 days long exposure period there is about 60% decrease in the amount of calcite and about 40% decrease in the amount of wollastonite when this paste was exposed to aluminum sulfate. Interestingly, during the first 20 days of exposure, the amount of amorphous phase declines, roughly at the same rate as that of calcite. This trend correlates well with the increase in the Si concentration values observed during the first 20 days of exposure in the aluminum sulfate soak solution (see Fig. 3.15 (b)). Past the first 20 days of exposure, the amount of amorphous phase starts to increase, and, at the end of 120 days it almost reaches the value recorded for the unexposed specimen (i.e. specimens at zero days of exposure). This increase in the amount of amorphous phase coincides with the decrease in the amount of wollastonite. In other words, it seems that upon the prolonged exposure it was the decomposition of wollastonite particles that resulted in the formation of additional amount of the amorphous phase.
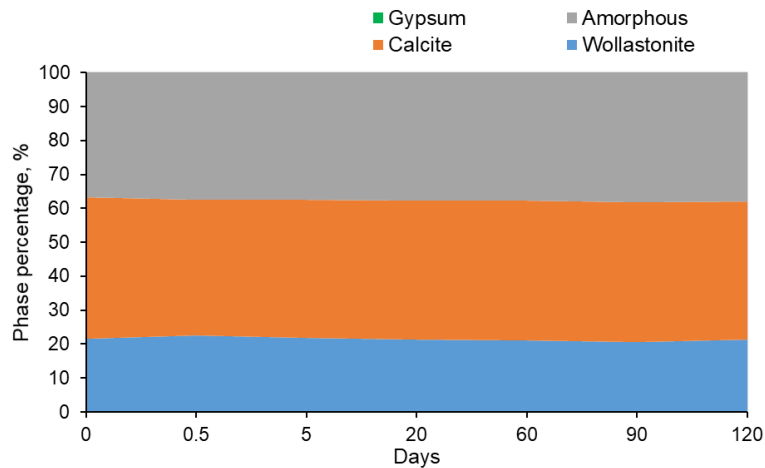
a) After exposer to sodium sulfate solution

Figure 3.26. The results of the QXRD analysis of paste samples from cement #1 (carbonated wollastonite) after sulfate exposure test

Fig. 3.26 continued
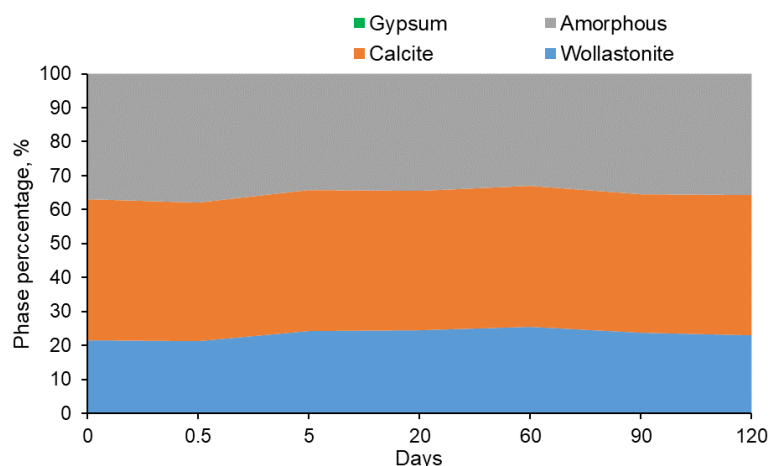
b) After exposure to magnesium sulfate solution

c)   After exposure to aluminum sulfate solution

The amount of gypsum seems to remain more-or-less constant after first half day of exposure and decreases only slightly by the end of the test. This agrees with the results of TGA experiment in Figure 3.32 which also shows the more or less constant amount of gypsum over the entire exposure period. It seems that the ratio of the components of the system in between the first half day and 20 days of exposure was kept more or less constant. Then after 60 days of the test, decrease of the wollastonite and gypsum, and increase of the amorphous phase and slight increase of calcite can be seen from the graph in Fig. 3.26 (c). Hypothetically, the carbonate ions (some portion of

which escaped during vigorous bubbling after contact of aluminum sulfate solution with paste powder) released to the aluminum soak solution may decompose the wollastonite mineral resulting in increase of amorphous phase and deposit of small amount of calcite. In addition to that, slight decrease of gypsum amount by the end of the test might be its decomposition due to the carbonate ion "attack".

Unlike cement #1 paste samples, the cement #2 paste samples were observed to undergo compositional changes upon exposure to all three types of sulfate solutions (see Fig. 3.27). In case of both sodium and magnesium sulfates, almost similar amount of gypsum appeared in the system.
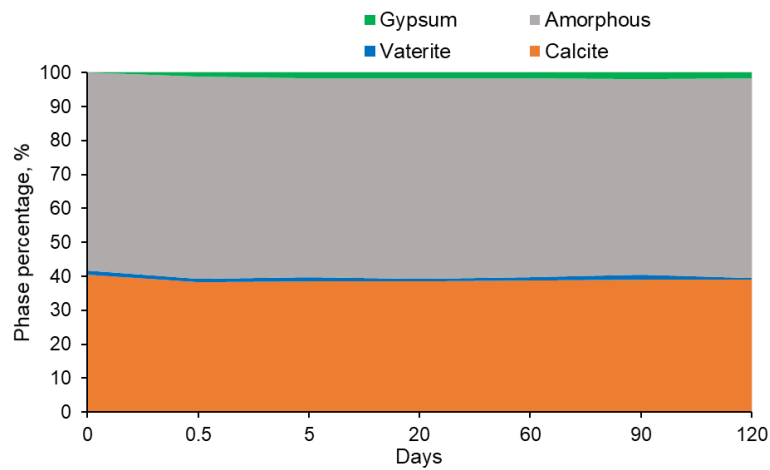
a) After exposure to sodium sulfate solution
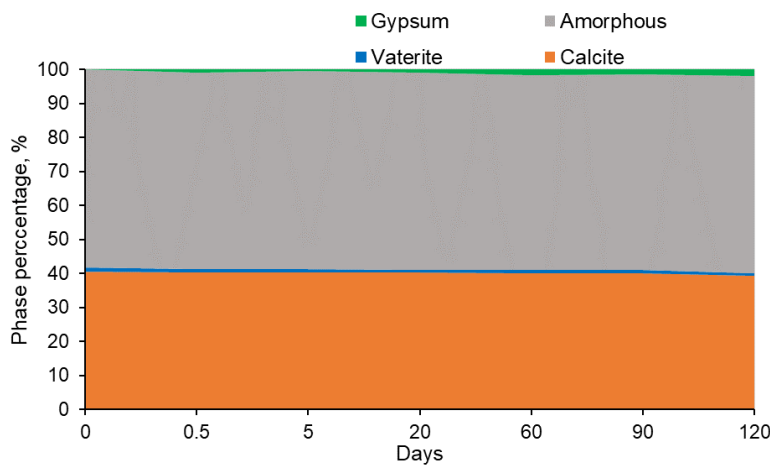
b) After exposure to magnesium sulfate solution

Figure 3.27. The results of QXRD analysis of paste samples from cement #2 after sulfate exposure test

Fig. 3.27 continued
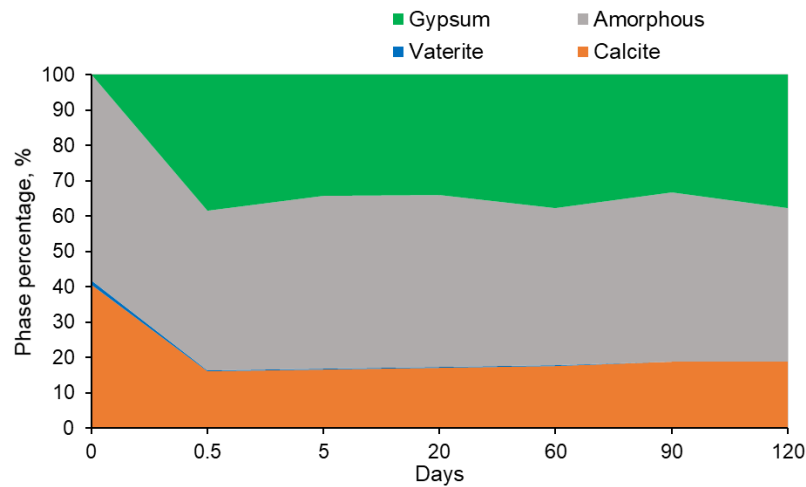
c) After exposure to aluminum sulfate solution

Regardless of the sulfate solution used, no noticeable change in the amount of the amorphous phase can be detected. Similar to cement #1 paste, there was a drastic compositional change in samples exposed to aluminum sulfate solution. First, the reduction of calcite amount and complete disappearance of vaterite took place. The amount of gypsum (formed almost immediately, i.e., within the first 0.5 days of exposure) seems to stay almost unchanged throughout the entire exposure period. Reduction trend can also be noticed in the amount of amorphous phase which can be explained by decomposition of uncarbonated cement (originally consisting of amorphous calcium silicate).

The results of quantitative XRD analysis of cement #3 paste samples are presented in Fig. 3.28. Again. no significant changes could be observed in the paste samples submerged in sodium sulfate solution (with the except ion of formation of almost negligibly small amount of gypsum), (see Fig. 3.28 (a)). Due to gypsum being present in such a small amount, it is hard to identify exactly which phase was involved in its formation. However, as it can be seen in Fig. 3.28 (b), the exposure to magnesium sulfate solution resulted in noticeable changes with respect to types and the amounts of the phases. First, the significant portion of the mass of the sample was occupied by gypsum, amount of which increased over the exposure period. In addition, the increase in the amount of the amorphous phase can be observed. All these increases seem to be counterbalanced by the decrease in the amounts of the calcium carbonates and reactive calcium silicates. Also, by

the end of the 120-day exposure period the slight reduction in the amount of gehlenite was also observed. Submersion of the cement #3 paste powder samples in aluminum sulfate solution resulted in the production of large amount of gypsum (~40-45%) shortly after the test started (approximately after a half day of exposure), decomposition of almost half of the amount of calcium carbonates and almost complete depletion of the reactive calcium silicates (see Fig. 3.28 (c)).
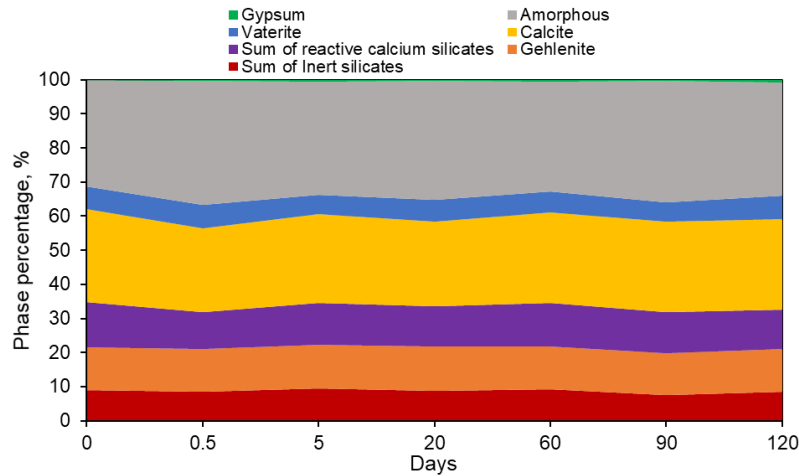
a) After exposure to sodium sulfate solution
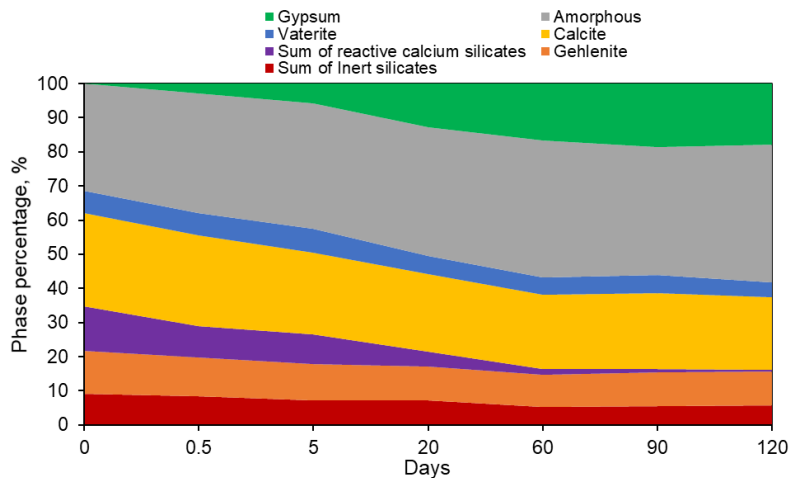
b) After exposure to magnesium sulfate solution

Figure 3.28. The results of QXRD analysis of paste samples from cement #3 after sulfate exposure test

Fig. 3.28 continued
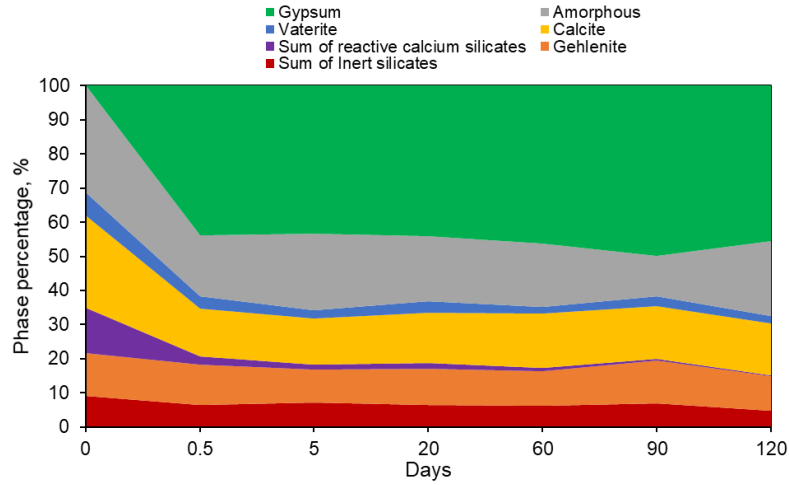
c) After exposure to aluminum sulfate solution

The QXRD results of the cement #4 paste samples after exposure to sodium sulfate solution did not reveal any significant changes in the amount or in the type of phases as illustrated in Fig. 3.29 (a). On the other hand, changes were observed in samples immersed in magnesium sulfate solution. Specifically, gypsum was observed to form, the amount increasing with the increase in the time of exposure. This was accompanied by the decrease in the of calcium carbonate phases and reactive calcium silicates (see Fig. 3.29, (b)). The trend of changes occurred in samples exposed to aluminum sulfate presented in Fig. 3.29 (c) looks similar to what was observed in case of cement #3 paste samples.
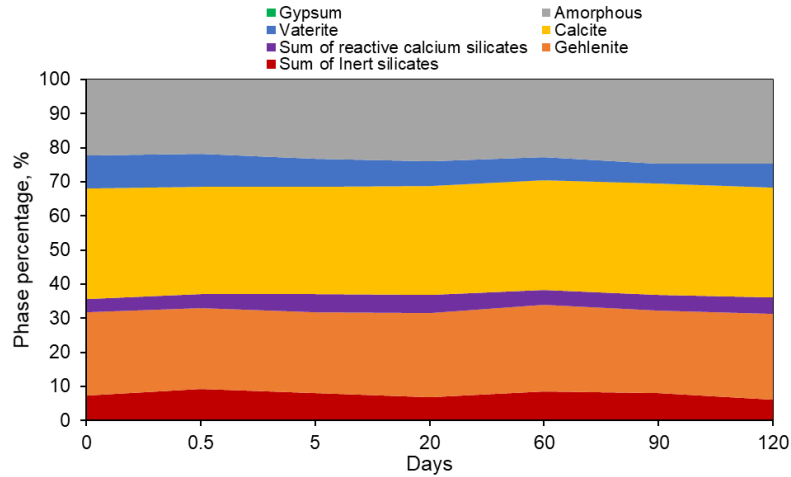
a) After exposure to sodium sulfate solution
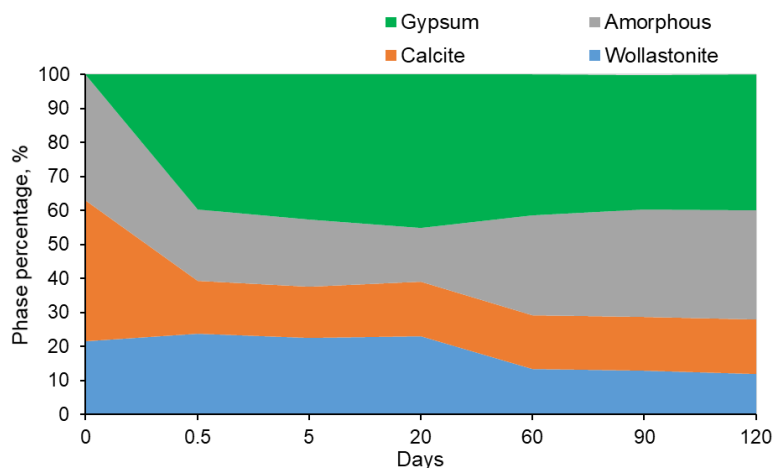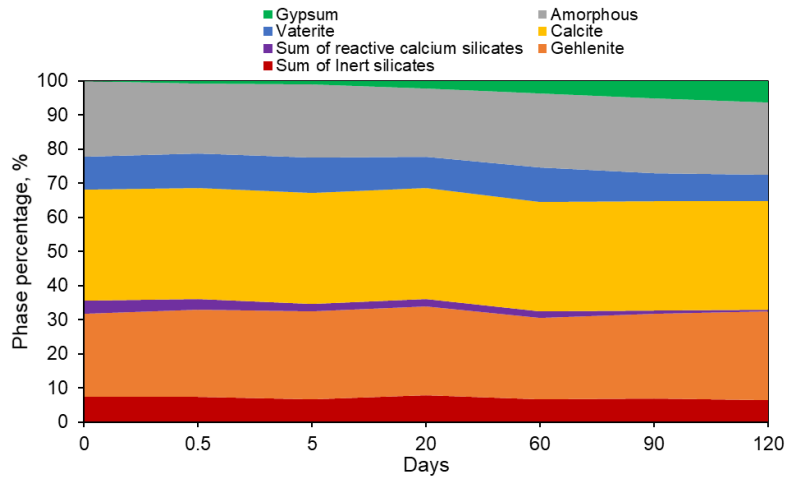

b) After exposure to magnesium sulfate solution
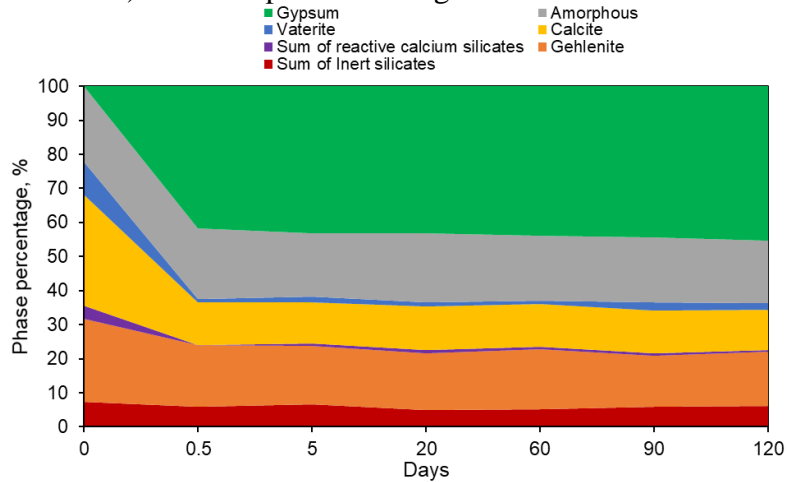
c) After exposure to aluminum sulfate solution

Figure 3.29. The results of QXRD analysis of paste samples from cement #4 after sulfate exposure test

3.5.3   Thermal analysis results

The purpose of the thermal analysis (TGA) of the paste samples after different periods of exposure was to quantify the change (if any) in the amount of calcium carbonate (mainly calcite) and gypsum formed during the exposure period. In order to avoid the overestimation of the quantities of gypsum formed (due to the continuous de-hydration of the amorphous silica gel in the temperature range of ~90- 150 °C), the methodology originally developed by Kim and Olek (2012) [36] for the estimation of the calcium hydroxide was implemented. The results of the quantitative evaluation of the gypsum formed during the exposure test are presented in the graphs shown in Fig. 3.30-3.32.

As it can be seen from these graphs, exposure to sodium sulfate solution at room temperature did not result in the formation of any significant amounts of gypsum compared to other sulfate solutions. Specifically, at the end of the exposure period only small amount (about 2.5 g of gypsum per 100 g of paste) was observed in cement #2 paste samples. In contrast, exposure to magnesium sulfate solution resulted in the formation of much more significant amounts of gypsum in all paste samples except in the case of carbonated wollastonite, i.e., cement # 1 samples (in this case only about 0.5 g/100 g of paste has formed). By the end of the 120-day expose period, ~24 g of gypsum per 100g of paste formed in cement #3 samples and ~4-6 g of gypsum per 100g of paste formed in cement #2 and #3 samples. In case of aluminum sulfate solution, about 30-32% (wt.) of gypsum formed in all paste samples within the first 12 hours of exposure. This was due to high acidity of the solution (pH≈3-4). Consequently, this resulted in the quick decomposition ("digestion") of the calcium carbonate phase, pH stabilizing at around 6-7, binding of released calcium ions by sulfate ions and precipitation of gypsum. That amount of gypsum remained more-or-less constant throughout the entire exposure period since the depletion of the sulfate ions occurred almost immediately (see Section 3.5.1).
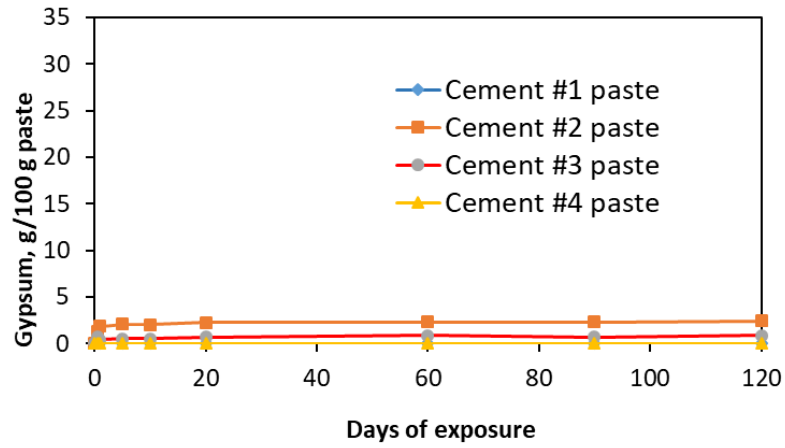
Figure 3.30. Amount of gypsum formed during exposure to sodium sulfate solution
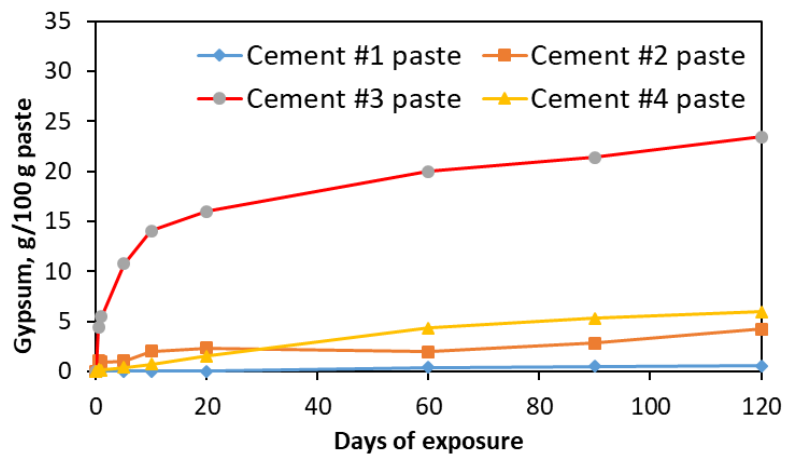
Figure 3.31. Amount of gypsum formed during exposure to magnesium sulfate solution
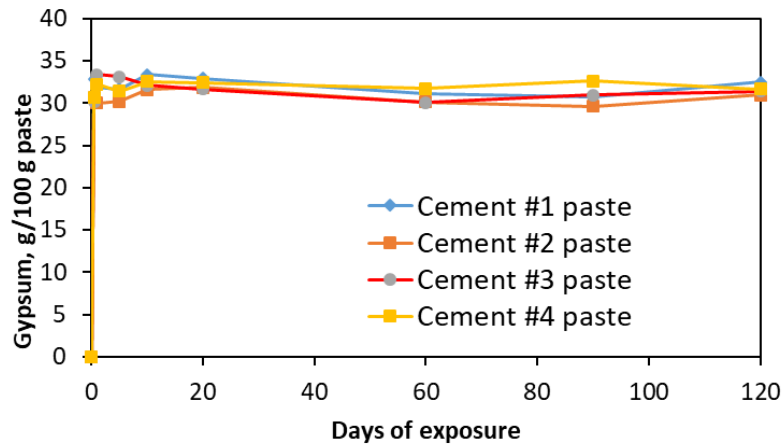
Figure 3.32. Amount of gypsum formed during exposure to
aluminum sulfate solution

The change in the amount of calcium carbonate (mainly calcite), normalized with respect to the amount of calcium carbonate present in carbonated pastes before the initiation of exposure to different sulfate solutions, is illustrated in the graphs presented in Fig. 3.33.

a)

b)
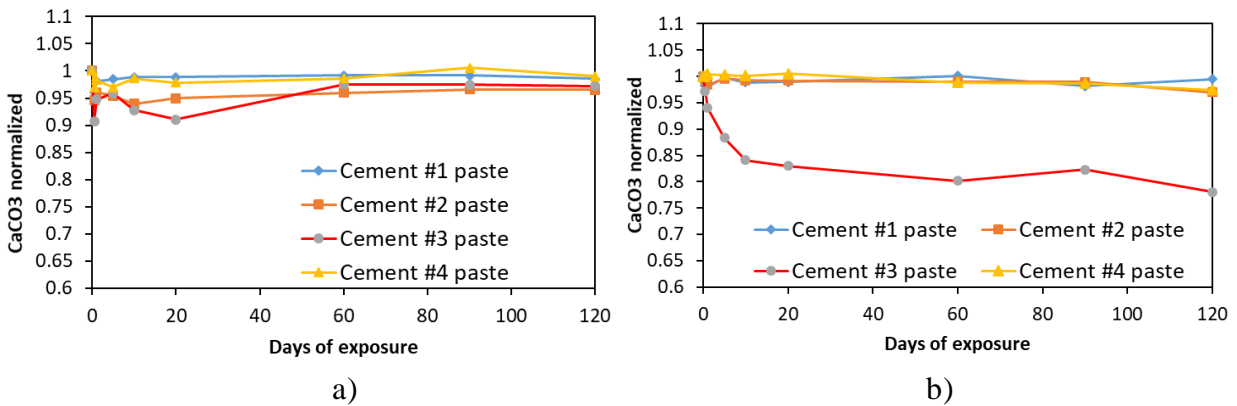
Figure 3.33. Change of calcium carbonate phase during exposure to a) sodium sulfate, b)
magnesium sulfate c) aluminum sulfate solution

Fig. 3.33 continued
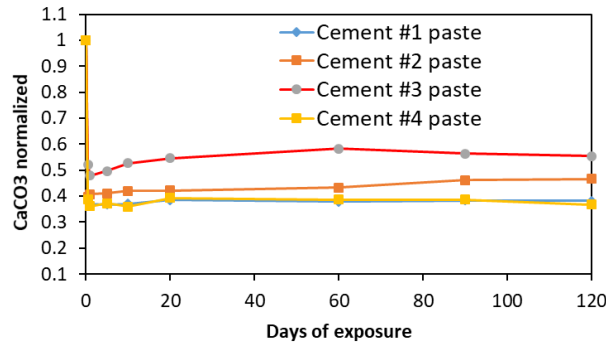
c)

Overall, the trends shown in Fig. 3.33 seem to be in certain correlation with the trends of gypsum, especially in case of cement #2-#4 paste samples submerged in magnesium sulfate: as the gypsum amount increases (Fig 3.33), the decrease of calcium carbonate (Fig. 3.31 (b)) can be observed. The total amount of gypsum formed after the exposure test was plotted in graph given Fig. 3.34. The exposure to sodium sulfate and magnesium sulfate solutions resulted in the highest amount of gypsum formed in cement #2 paste and cement #3 paste samples, respectively. Amount of gypsum formed in all paste samples subject to aluminum sulfate seems to be almost the same. By the end of the test, no gypsum was found in the cement #1 and #4 paste samples.
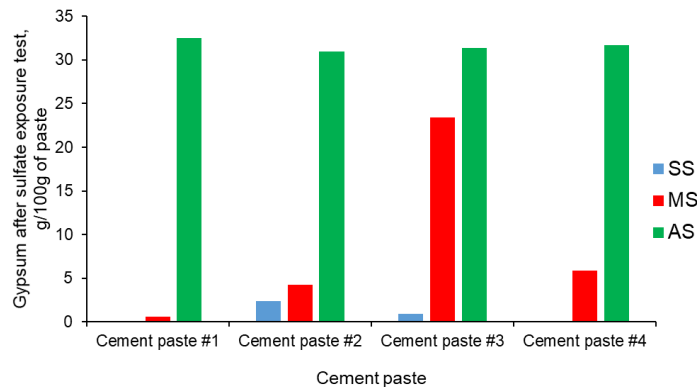
Figure 3.34. Amount of gypsum formed after the exposure test (key: SS – sodium sulfate, MS – magnesium sulfate, AS – aluminum sulfate)

To verify the assumption that all the calcium carbonate lost during the exposure to magnesium sulfate was consumed for the formation of gypsum, the comparison of stoichiometric amount of calcium carbonate needed for formation of gypsum and the amount of calcium carbonate

lost during the experiment was performed. For that the stoichiometric amount of needed calcium carbonate was calculated by using either reaction equation (3.3) or (3.5) (see section 3.6) and assuming that the molar ratio of gypsum/calcium carbonate was equal to 1.0. For that only the cement #2 and #3 paste results were available to use. The comparison was illustrated by plotting the correlation curves presented in Fig. 3.35. As it can be observed from the curves, to form the amount of gypsum during the sulfate exposure test almost twice as much as calcium carbonate lost during the experiment is needed. This infers that not all amount of gypsum was formed from the lost calcium carbonate, but also participation of some other calcium bearing phases may be needed.
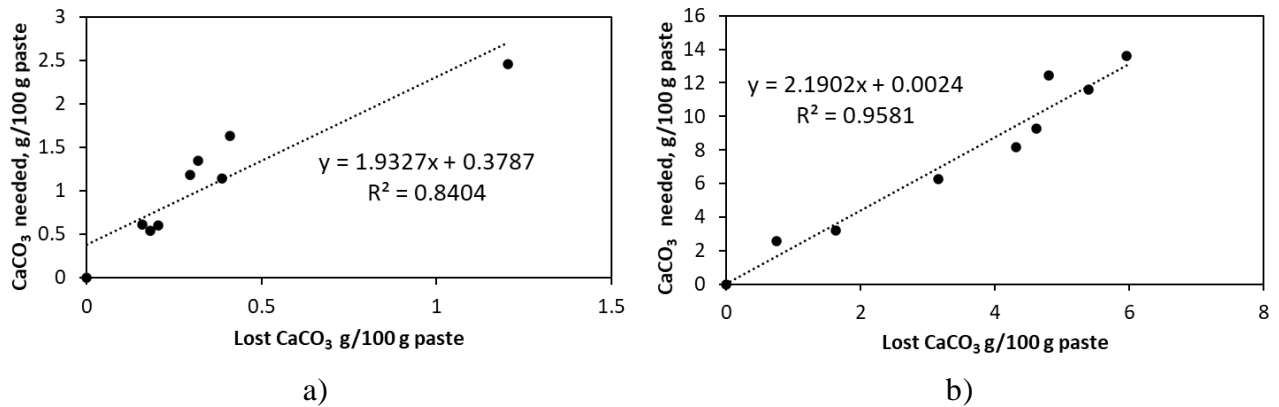
Figure 3.35. Correlation between lost and needed calcium carbonate amount: (a) – cement #2 paste, (b) – cement #3 paste

Another verification of the correlation of the experimental results with stoichiometry was performed for paste samples immersed in aluminum sulfate. As mentioned in section 3.5.1 (Fig. 3.19 (c) and Fig. 3.20), after about first half day of immersion in aluminum sulfate solution, the amount of sulfate ions was almost depleted together with aluminum ions in case of all paste samples which infers that the aluminum and sulfate ions are the rate controlling species. Therefore, the stoichiometric calculations were performed by implementing the amounts of calcium carbonate in the paste samples and sulfate ion concentration in aluminum sulfate solution determined by TGA and IC, respectively.

The depletion of sulfate ions at early periods of the test can be demonstrated by the stoichiometric calculations based on equation (3.4) from the section 3.6.3.

$$3CaCO_3 + Al_2(SO_4)_3 + 9H_2O \rightarrow 2Al(OH)_3 + 3(CaSO_4 \cdot 2H_2O) + 3CO_2\uparrow \qquad (3.4)$$
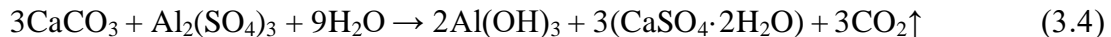
The concentration of the sulfate ions in original aluminum sulfate solution was determined by ICP analysis as 0.37 mol/L. Then if 3 g of paste powder was submerged in 20 mL of solution as per the experiment design, 0.37 mol/L x 0.02L x 96 g/mol = 0.71 g of sulfate ions become available for the reaction. Additionally, according to the estimation from the TGA analysis, 3 g of original paste powder (i.e., before it was exposed to sulfate solution) contained the calcium carbonate (calcite) in the range of 27.2 – 41.5% depending on the type of carbonated cement paste, i.e., 0.82-1.24 g of calcium carbonate. Now, since the molar ratio of the calcium carbonate and sulfate ions in the equation (3.4) is 1:1, then the following stoichiometric equation is valid:

$$X \qquad 0.71 \text{ g}$$
$$CaCO_3 \text{ (aq.)} + SO_4^{2-} + 2H_2O \leftrightarrow CaSO_4 \cdot 2H_2O + CO_3^{2-} \qquad (3.6)$$
$$100 \text{ g/mol} \quad 96 \text{ g/mol}$$
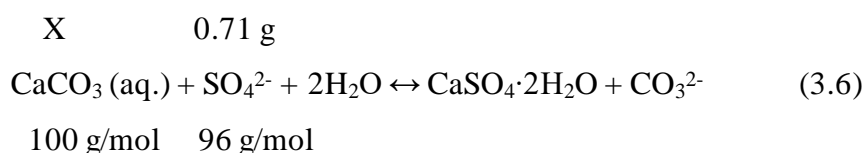
Here, X – amount of calcium carbonate in 3 g of paste powder. The value of moles is calculated as $\upsilon = X/M$ [mol], where M – molar mass of calcium carbonate. Then depending on the type of the cement paste, ~0.0082 – 0.0124 moles of calcium carbonate reacts with ~0.0074 moles of sulfate ions. This proportion clearly shows that the concentration of sulfate ions in the solution is the rate controlling parameter of the reaction.

These calculations reveal that, theoretically, $X = \frac{100 \times 0.71}{96} \approx 0.74$ g of calcium carbonate is needed to completely consume the available sulfate ions in the solution, which is around 60-90% of the total calcium carbonate amount in original paste powders. The summary of calculated values vs. measured ones (quantified by means of TGA analysis) is presented in Table 3.4 for all types of paste samples.

Table 3.4. Amount of consumed CaCO3 upon exposure to aluminum sulfate solution

Cement paste #	Consumed CaCO$_3$, %	
	Calculated	Measured
1	59.4	61.5
2	61	53.4
3	90.1	44.6
4	75.8	60.7

The comparison revealed one interesting point: except for carbonated wollastonite paste (cement paste #1), all others pastes lost smaller amounts of calcium carbonate than those predicted by calculations. This agrees with QXRD data interpretation (see section 3.5.2) where the decomposition of uncarbonated calcium silicates by $Al_2(SO_4)_3$ is claimed. As for the cement paste #1, lack of drastic difference between calculated and measured values also confirms the QXRD results showing that the uncarbonated wollastonite particles were decomposed by leftover carbonate ions and that gypsum was mainly formed by reaction of calcite reacted with aluminum sulfate.

3.5.4   Fourier Transform Infrared analysis results

The Fourier-Transform Infrared (FT-IR) spectra obtained from all four cement paste samples after 120 days of exposure to three types of sulfate solutions are presented in Fig. 3.36. As it can be seen from the graphs, exposure to magnesium and aluminum sulfates resulted in noticeable changes in the broad absorbance band for silica (in the range of 950-1250 cm^{-1}) Especially, the silica band of the cement #3 paste sample immersed in magnesium sulfate solution (see Fig. 3.36 (c)) appears to have shifted towards the higher wavenumber values (shorter wavelength) and contains two distinguishable peaks. As for aluminum sulfate solution, it seems affected the silica band and made it to shift its peak toward higher values of wavenumbers.
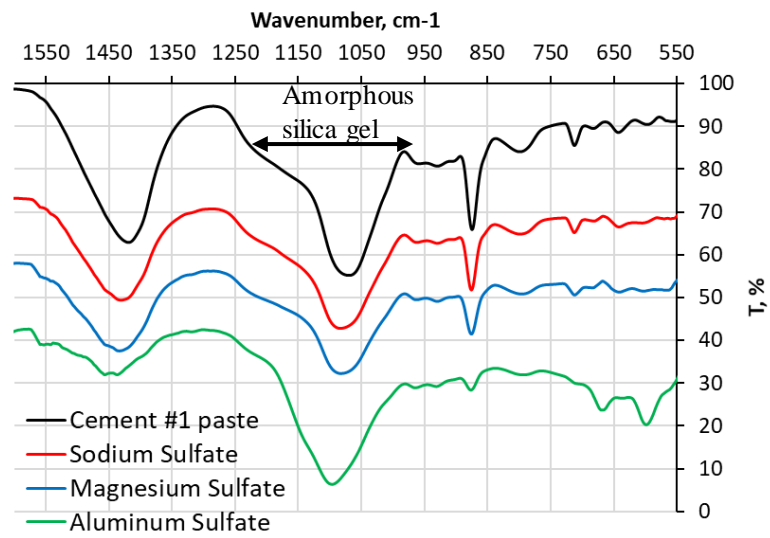
a)
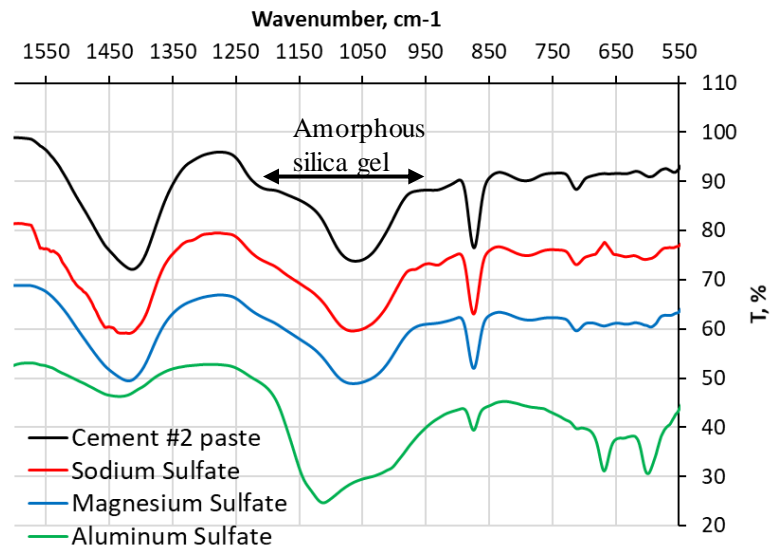
b)

Figure 3.36. FT-IR spectra of the paste samples after 120-day exposure to the sulfate solutions: (a) – cement #1 paste, (b) – cement #2, (c) – cement #3 and (d) – cement #4 paste samples. Key: SS – sodium sulfate, MS – magnesium sulfate, AS – aluminum sulfate

Fig. 3.36 continued
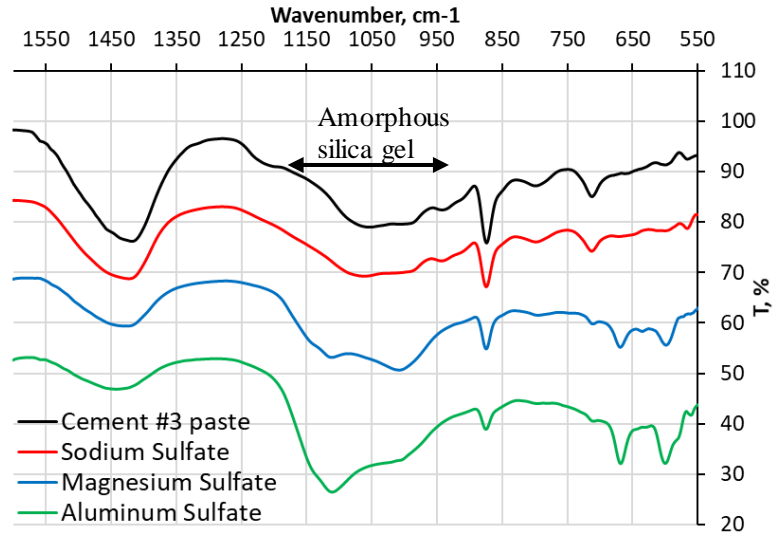
c)
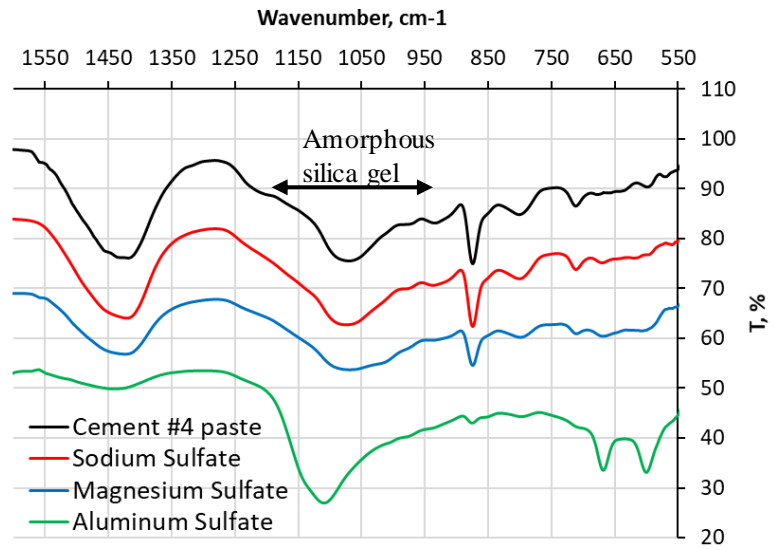
d)

3.6   Discussion

3.6.1   General features of the low-lime CCS systems exposed to sulfate solutions

The experimental results collected in the course of this work revealed several characteristics of the CCS systems exposed to sulfate solutions that are quite different from those observed in the OPC systems. First, the CSS matrix does not contain any reactive phases (e.g., calcium hydroxide or aluminates) as it consists mostly of barely soluble (and less reactive) calcium carbonate phases and amorphous silica. As the result, the low-lime CCS matrix is significantly less active towards sulfates compared to hydrated OPC system. This is reflected in the absence of ettringite deposits as well as in almost complete inertness towards sodium sulfate. In addition, it is necessary to mention that, compared to the hydrated OPC matrix, the CCS matrix is less alkaline, with highest pH values of the leachate being only ~10. The lower alkalinity of such systems substantially reduces the stability of the products of sulfate attack. Also, unlike the CSH gel present in the OPC systems, the hydrated silica gel present in the CCS matrix does not seem to suffer from the softening of the matrix and formation of magnesium silica hydrate (MSH).

Nevertheless, as it was revealed by the results obtained from various types of the CCS studied in this work, there are some peculiarities and nuances associated with specific types of calcium silicates which should be carefully considered when addressing the sulfate resistance of such systems. That issue is discussed in the next section of this document.

3.6.2   Effect of the type of the low-lime calcium silicate on the sulfate resistance of the CCS system

As demonstrated by the responses of all CCS pastes exposed to various sulfate solutions used in this work, different carbonated calcium silicates varied in their degree of resistance. While performing more in-depth analysis of these differences in response, it is important to distinguish between the effects of aluminum sulfate and the effects of two sulfates because of the acidic (pH~3-4) nature of the former solution. Specifically, when exposed to aluminum sulfate solution, the matrixes of all cement pastes showed signs of decomposition of calcium carbonate, significant amount of de-calcification of uncarbonated cement grains, reduction in the amount of leached silica, and formation of gypsum.

In case of other two sulfates, i.e., the sodium and magnesium ones, the level of sulfate resistance depended on the type of calcium silicate present in the binder and the composition of the carbonated phases formed from these silicates. In particular, matrixes resulting from carbonation of wollastonite appeared to be most resistant to both sodium and magnesium sulfates. This is likely because these matrixes contained mostly calcite, the most stable crystalline form of calcium carbonate, as well as relatively highly polymerized amorphous silica with relatively modest degree of modification by calcium ions [3].

As for the sodium sulfate, it appears that only cement #2 and #3 paste samples participated in the reaction as indicated by the observed formation of gypsum. Due to the presence of less stable calcium carbonate polymorphs (e.g., vaterite), and calcium modified silica gel with potentially highest Ca/Si ratio among all the paste samples used in this experiment, the cement #3 paste samples were found to be least resistant to sulfates. The above-mentioned factors were especially critical for pastes in contact with the magnesium sulfate. On the other hand, the samples made of cement #4, which contained less hydraulic calcium silicate (larnite) compared to cement #3 showed higher sulfate resistance.

3.6.3   Effect of the type of the sulfate solutions on the sulfate resistance of the CCS system

The dissolution of the components of the main binding matrix, calcium carbonate and amorphous silica, subjected to sulfate-rich medium was of primary interest during this study. However, one should not neglect the fact that noncarbonated cement particles might also contribute to calcium and silica leaching. Solubility of a mineral is influenced by several factors, including: the activity of an ion, the ionic strength of a solution, the ion-pairing constant (Evangelou, [17]) the pH level of the solution, and the temperature. According to previous reports [24], increasing the ionic strength of the solution (e.g., by adding an inert salt) can facilitate dissolution of otherwise barely soluble minerals.

The ionic strength of sulfate solutions is much higher than that of de-ionized water (which is considered to be close to zero) and can be estimated by using equation 3.1 (Adams [2], Harris [24]).

$$I = \frac{1}{2}\sum C_i \cdot Z_i^2 \qquad\qquad (3.1)$$

where C_i – concentration of an ion i, Z_i – charge magnitude of an ion i.

The calculated values of the ionic strength of the solutions used in the experiments are given in Table 3.5.

Table 3.5. Values of ionic strength of the sulfate solutions

Ion	C^*_i, mol/L	Z_i	$C_i \cdot Z_i^2$	I, mol/L
Sodium sulfate solution				
Na^+	0.679	1	0.679	1.055
SO_4^{2-}	0.358	2	1.430	
Magnesium sulfate solution				
Mg^{2+}	0.370	2	1.480	1.444
SO_4^{2-}	0.352	2	1.408	
Aluminum sulfate solution				
Al^{3+}	0.240	3	2.158	1.829
SO_4^{2-}	0.375	2	1.5	

*Note: The values of concentrations (Ci) used in calculations were obtained from the ICP and IC test results

As it can be seen from the results, the ionic strength of the sodium sulfate solution was the lowest and that of aluminum sulfate was the highest. These findings imply that that certain minerals. e.g., calcium carbonate may dissolve more easily in $MgSO_4$ and $Al_2(SO_4)_3$ solutions than in the Na_2SO_4 solution. An increase in the ionic strength of the solution intensifies the ionic atmosphere around the Ca^{2+} and CO_3^{2-} ions and results in reduction of their activity coefficients. However, the variation in general solubility of different polymorphs of calcium carbonate should be considered in the context of the characteristics of the solution.

Another factor influencing the solubility of minerals mentioned above is the ion-pairing ability of cations and anions of the sulfates present in the solution, as expressed by the ion-pairing constant (K). According to Evangelou [17], the decrease in the value of the ion-pairing constant increases the stability of the ion-ion pair. The values of the constants for some ion-pairs have been reported by Adams [2]. The equilibrium reaction which can potentially take place in sulfate soak solutions used in the present study, along with as well as their constants are given in Table 3.6.

Table 3.6. Ion-pairing constant values

Reaction equation	Ion-pairing constant (K)	Comments
Ions pairing with sulfate ion		
$NaSO_4^-$ (aq.) $\leftrightarrow Na^+ + SO_4^{2-}$	$2.4 \cdot 10^{-1}$	Most likely, magnesium and aluminum produce pairs with sulfates
$MgSO_4^0$ (aq.) $\leftrightarrow Mg^{2+} + SO_4^{2-}$	$5.88 \cdot 10^{-3}$	
$AlSO_4^+$ (aq.) $\leftrightarrow Al^{3+} + SO_4^{2-}$	$6.3 \cdot 10^{-4}$	
Ions pairing with carbonate ion		
$NaCO_3^-$ (aq.) $\leftrightarrow Na^+ + CO_3^{2-}$	$5.35 \cdot 10^{-2}$	It is more likely that $MgCO_3$ (aq.) will be present.
$MgCO_3^0$ (aq.) $\leftrightarrow Mg^{2+} + CO_3^{2-}$	$4 \cdot 10^{-4}$	
For Al^{3+}: N/A	N/A	

Comparing the ion-pairing constants, one may conclude that it is more likely to find aqueous magnesium sulfate and aluminum sulfate pairs, whereas Na^+ resides mostly "freely and independently". Here, it is also worthwhile to mention that Hasset and Jurinak (1971) [25] cited the work published by Akin and Lagerwerff (1965) who suggested that the presence of Mg^{2+} and SO_4^{2-} in the solution enhances the solubility of $CaCO_3$. Also, between Na^+ and Mg^{2+} ions, the carbonate ion seems to prefer pairing with Mg^{2+} by forming $MgCO_3$. This gives rise to the consideration of the possible chemical interaction between calcium carbonate and sulfates.

To evaluate the thermodynamic possibility of room temperature (296 K) chemical reactions between calcium and sulfate ions changes in the Gibbs free energy of various systems were evaluated as shown in equations 3.2-3.5:

$$CaCO_3 + Na_2SO_4 + 2H_2O \rightarrow Na_2CO_3 + CaSO_4 \cdot 2H_2O \tag{3.2}$$
$$\Delta G \approx 25 \text{ kJ}$$

$$CaCO_3 + MgSO_4 + 2H_2O \rightarrow MgCO_3 + CaSO_4 \cdot 2H_2O \tag{3.3}$$
$$\Delta G \approx -36 \text{ kJ}$$

$$3CaCO_3 + Al_2(SO_4)_3 + 9H_2O \rightarrow 2Al(OH)_3 + 3(CaSO_4 \cdot 2H_2O) + 3CO_2\uparrow \tag{3.4}$$
$$\Delta G \approx -307.2 \text{ kJ}$$
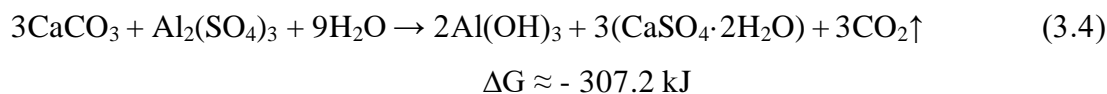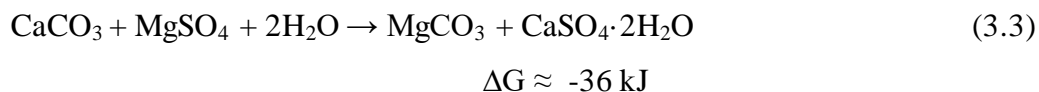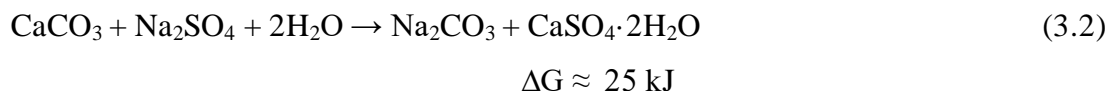
The values of the ΔG for the processes shown in equations 3.2 –3.4 imply that last two reactions are thermodynamically possible. These equations are, however, oversimplified since amorphous silica and/or calcium-modified silica most likely also participate in the reactions. This is indirectly confirmed by observed significant reduction in the amount of leached silica upon exposure to magnesium and aluminum sulfate solutions. In other words, unlike Na^+ ions, the Mg^{2+} and Al^{3+} ions, tend to stabilize the silica.

When the reaction involving magnesium sulfate (Equation 3.3) has been modified to include silica as an additional reactant (see Equation 3.5) the resulting value of ΔG changed form -36 kJ to -230 kJ. This indicates that thermodynamically the reaction shown in Equation 3.5 is more probable than the reactions shown in Equation 3.3.

$$CaCO_3 + MgSO_4 + SiO_2 + 3H_2O \rightarrow MgSiO_3 + CaSO_4 \cdot 2H_2O + CO_3^{2-} + 2H^+ \qquad (3.5)$$
$$\Delta G \approx -230 \text{ kJ}$$
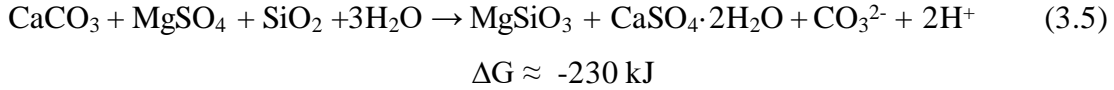
In addition to reacting with the components of the carbonated binding matrix of the CCS systems, the sulfate solutions (especially, $MgSO_4$ and $Al_2(SO_4)_3$) may cause de-calcification of the uncarbonated calcium silicate cement particles as it was evidenced in Chapter 2.

3.7   Conclusions

Overall, the main findings of this part of the study can be concluded as following:

- The type of cation of the sulfate solution matters: CCS showed higher resistance to Na_2SO_4 solution than to $MgSO_4$ due to the absence of reactive phases such as e.g. $Ca(OH)_2$ and/or calcium aluminates as in case of OPC.

- Nevertheless, interaction of some of the CCS samples with sodium sulfate resulted in the formation of gypsum (even though in negligible amount) which was not observed in the mortar expansion test during Phase I of the study.

- Less resistance to $MgSO_4$ was observed in CCS made of the cement containing more hydraulic calcium silicates. In this case, the hydrated silica gel might be extensively modified with Ca (even though it cannot be compared to Ca/Si ratio of CSH gel) which can participate in chemical reaction and contribute to the gypsum formation. Also, the consumption of magnesium ion and stabilization of silica indicate the interaction between hydrated silica gel and magnesium cation. Especially, this interaction might be due to cation exchange between calcium and magnesium ions. This emphasizes in its turn the importance of the calcium ions and silica during carbonation process and level of pureness of the hydrated silica gel in sulfate resistance.

- The CCS samples (carbonated wollastonite) containing more crystalline calcium carbonate polymorph (calcite) and more polymerized silica gel demonstrated better resistance to the sulfates.

4. PHASE III: LOW TEMPERATURE SULFATE EXPOSURE EXPERIMENTS PERFORMED ON DIFFERENT CCS PASTES

The results of the work were published in the proceedings of the 12th International Symposium of Brittle Matrix Composites (Warsaw, Poland, 2019).

Abstract

This paper summarizes the results of the experimental study involving low-temperature (5℃) exposure of carbonated, low-lime calcium silicate cements (CCSCs) pastes, to sodium sulfate and magnesium sulfate solutions. Individual pastes used in the study were prepared by mixing one of the three different types of low-lime calcium silicate cements with limited (w/c=0.3) amount of water and solidifying the resulting slurry by carbonation in the CO2 atmosphere. The cements used to prepare the pastes included the following materials: natural wollastonite (cement #1), amorphous calcium silicate (cement #2) and multi-mineral calcium silicate cement (cement #3-Solidia cement ™). The carbonated paste samples were powdered and mixed with each of the two types of sulfate solutions to form slurry with powder-to-solution ratio ~1:4 (by volume). The slurries were periodically agitated and stored for a period of 1.5 years at a temperature of 5±1℃. At the end of the exposure period, the slurries were centrifuged to separate the solids and the solutions. The resulting solutions were analyzed for the concentration of sulfates using ion chromatography (IC) technique. The solids separated during the centrifugation process were characterized by XRD, TGA, DSC and SEM techniques.

With respect to formation of reaction products, it was observed that, irrespective of the type of sulfate solution used, no new phases have formed in wollastonite pastes. Although none of the samples contained any thaumasite, well-developed peaks of gypsum were found in the XRD patterns of cement #2 and cement #3 pastes exposed to both sulfate solutions. The quantitative results of the TGA and DSC analyses indicated that the highest amount (~16-17 g/100g of paste) of gypsum formed in samples exposed to magnesium sulfate. Moreover, the same samples showed a net reduction (~5-6%) in the amount of $CaCO_3$. In addition, the IC analysis of magnesium sulfate solutions extracted from slurries in contact with cements #2 and #3 indicated significant (~80%) reduction in the concentration of sulfate ions, thus confirming the data obtained from the

analysis of solids. Finally, a close correlation was observed between the amount of sulfate ions consumed and the amounts of gypsum formed as determined by analysis of the DSC results.

4.1   Introduction

The aqueous carbonation of the low-lime (i.e., non-hydraulic) calcium silicates (CS), e.g., wollastonite ($CaSiO_3$), has been previously described (Bukowski and Berger [13], Huijgen et al. [28]) as involving the following three stages: a) leaching of calcium ions from the non-hydraulic phases (Eq. 1), b) dissolution of CO_2 in water and subsequent formation of carbonate ions (Eq. 2 and 3), and nucleation and growth of calcium carbonate (Eq. 4).

$$CaSiO_3(s) + 2H^+(aq) \rightarrow Ca^{2+}(aq) + H_2O(l) + SiO_2(s); \tag{1}$$
$$CO_2(g) + H_2O(l) \rightarrow H_2CO_3(aq) \rightarrow H^+(aq) + HCO_3^-(aq); \tag{2}$$
$$HCO_3^-(aq) + OH^-(aq) \rightarrow CO_3^{2-}(aq) + H_2O(l) \tag{3}$$
$$Ca^{2+}(aq) + CO_3^{2-}(aq) \rightarrow CaCO_3(s) \tag{4}$$
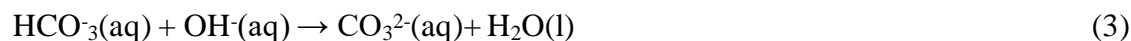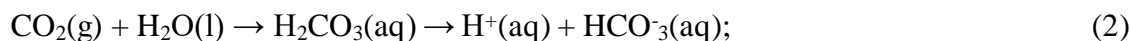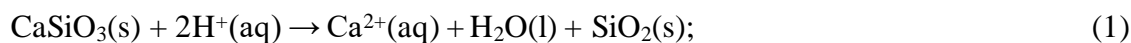
In previous research (Jain et al. [33]), the carbonated, low-lime calcium silicate cement (CCSC)-based systems were found to consist of calcium carbonate (main binding phase), amorphous silica (silica gel) and non-carbonated calcium silicate particles (remnants of the original cement grains). Further microstructural evaluation of the carbonated CSC-based paste using the ^{29}Si {^1H} CP-MAS NMR (Ashraf et al. [4]) also revealed the presence of poorly crystalline intermediate phases (Ca-modified silica gel). Similar phase (i.e., calcium-modified silica gel) was also found by Daval et al. [15] in the study of wollastonite carbonated at 90°C using high-resolution transmission electron microscopy.

While previous work (Jain et al. [33]) evaluated several durability properties of CCSC-based concrete (i.e., freeze-thaw resistance, scaling resistance, and sulfate resistance at room temperature), no data exists on sulfate resistance of such systems at low temperature. This study was undertaken to fill this gap by subjecting the CCSC pastes to sulfate solutions at 5°C in order to evaluate potential for formation of any new phases and chemical alteration of the existing components.

Although the studied systems contained all ions needed theoretically to form thaumasite (e.g., carbonate, sulfate, silicate and calcium – Gemrich et al. [20], Bensted and Varma [10]), practical

89

possibility of formation of this phase was rather doubtful. This was due, among others, such issues as an absence of calcium hydroxide (deemed to be necessary by Bellmann and Stark [9]), or aluminate phases to form ettringite which could serve as a precursor to formation of thaumasite (Kohler et al. [38]). However, one should keep in mind that these previous studies were performed on the ordinary Portland cement (OPC) systems and it is therefore difficult to generalize and apply the resulting findings to the low-calcium, non-hydraulic materials used in this study.

4.2   Materials and Methods

4.2.1   Materials

In this study, three different types of low-lime calcium silicate-based cements were used. Comparing the oxide composition of these cements (shown in Table 4.1) it can be seen while they contained similar quantities of CaO, their SiO_2 content varied from ~51.5% for cement #1 to 44% for cement #3. Cement #3 also contained the highest amounts of alkalis, as well as that of iron and aluminum oxides. The phase compositions of the cements were significantly different, as illustrated by the X-ray diffraction (XRD) patterns shown in Fig. 4.1. Specifically, cement #1 consisted of 100% of natural wollastonite, cement #2 was composed of completely amorphous calcium silicate, whereas cement #3 contained several reactive (rankinite, pseudo-wollastonite and larnite/belite) and non-reactive (melilite, quartz and feldspar) phases.

Table 4.1. Oxide composition of the cements by XRF analysis

Cement	Oxides, wt. %									
	CaO	SiO_2	Fe_2O_3	Al_2O_3	MgO	SO_3	Na_2O	K_2O	LOI	Tot. alkalis
#1	46.01	51.47	0.77	0.87	0.08	0.01	0.16	0.04	0.72	0.18
#2	46.08	45.66	0.22	2.50	1.11	0.41	0.21	0.37	1.61	0.45
#3	43.64	44.3	1.79	5.13	1.15	0.16	0.33	1.94	0.71	1.61
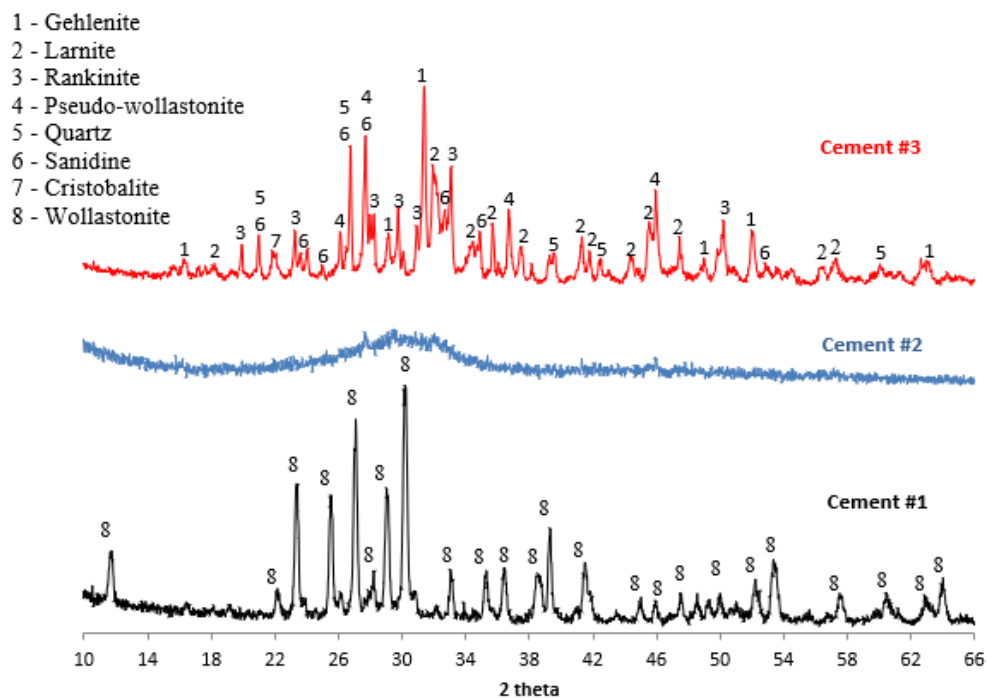
Figure 4.1. XRD diffractograms of the cements used in the study
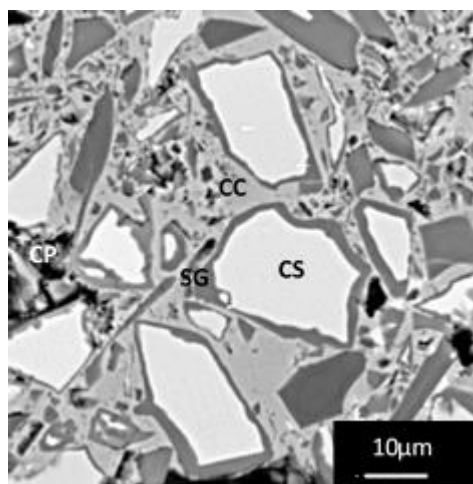
Figure 4.2. SEM micrograph of the carbonated paste made of cement #2 (CS – calcium silicate, CC – calcium carbonate, SG – silica gel, CP – capillary pore)

The American Chemical Society (ACS) reagent grade anhydrous sodium sulfate and magnesium sulfate chemicals were used for preparing 0.35M sulfate solutions used in the experiments.

The paste samples used in the study were extracted from the 5x5x5 cm carbonated cube specimens. The cube specimens were prepared by Solidia Technologies Inc. by carbonating the cement-water paste (w/c=0.3) for 24 hours at 65°C and 60-65% RH in high purity CO_2 environment at the pressure of 1 atm. By and large, the microstructure of these carbonated calcium silicate systems consisted of calcium carbonate, hydrated silica gel, unreacted cement grains and micro-/nano-pores (see Figure 4.2). Calcium carbonate phases (calcite, vaterite and aragonite) are the main space-filling and binding components. In addition, as mentioned earlier, the microstructure may also contain an "intermediate phase" composed of calcium modified silica gel (Ashraf and Olek [4], Daval et al. [15]). The layer of hydrated silica gel tends to deposit around the contours of un-carbonated grains of cement.

4.2.2 Methods

Paste samples were pulverized with mortar and pestle and submerged in sulfate solutions with solid to liquid ratio of 1:4. In total, six slurry samples were prepared. They were sealed in centrifuge tubes and stored in environmental chamber (at T = 5±1° C) for 1.5 years. The centrifuge tubes were agitated periodically every week by hand.

After termination of 1.5-year long exposure, the slurries were centrifuged and filtered using 0.2 µm cellulose acetate filter to separate solids from the soak solutions. The solids were triple washed with de-ionized water and oven-dried at 35±5°C for three days.

The X-ray diffraction (XRD), thermogravimetric analysis (TGA) and the differential scanning calorimetry (DSC) analysis were performed on powders which were prepared by pulverizing the solid particles with agate mortar and pestle until they passed No. 200 (75µm) sieve. For the XRD analysis the powder was mounted in the aluminum holder and scanned in the 2θ range of 5-60° (Siemens D500 diffractometer, CuK_α radiation, 50 kV at 30 mA, scanning rate of 0.02° 2θ/sec.). The resulting diffractograms were analyzed using Jade 9 software.

The TGA analysis was performed in nitrogen gas atmosphere (the flow rate of 50 mL/min) by heating powders in the TA Instruments Q50 Thermogravimetric analyzer up to a temperature 900°C at the rate of 10°C/min. The DSC analysis of the samples was performed using TA Instruments Q2010 apparatus by heating powder up to 600°C at the rate of 10°C/min in open aluminum pan.

The samples for scanning electron microscopy (SEM) analysis were prepared by mounting

the solids on the metal holder with adhesive carbon tape and coating them with palladium (Pd). The SEM imaging was performed using ASPEX Personal SEM equipped with energy dispersive X-Ray (EDX) analyzer operating at 15 keV.

The sulfate content of the soak solutions was determined using ion chromatography (IC) technique (DIONEX ICS-900).

4.3   Results and Discussion

4.3.1   Physical appearance of the samples

By the end of the exposure period some changes in the conditions of the samples were visible even to the naked eye. Specifically, an increase in the volume of the solid part was observed.in case of slurry samples made from cements #2 and #3 pastes submerged in magnesium sulfate solutions (e.g., Fig. 4.3(a)). Moreover, large crystals were observed to form in the sample of cement #2 soaked in magnesium sulfate solutions. These crystals were visible in both, the solid part of the sample and as the suspension in the solution (see Figure 4.3(b)). In contrast, no such changes were observed in slurries made of cement #1 paste, irrespective of the type of sulfate solution used during the experiment.

a)   b)
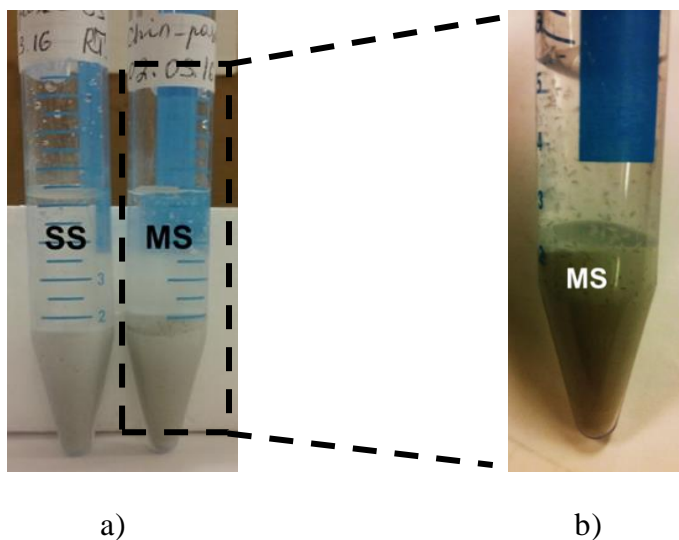
Figure 4.3. (a) Appearance of the powder slurries after the exposure to both sulfate solutions made of cement #2, and (b) suspension of crystals in the solution. (key: SS – sodium sulfate, MS – magnesium sulfate)

4.3.2 X-Ray diffraction results

Figures 4.4 –4. 6 show the XRD patterns of the cement paste powder samples before and after the exposure to sulfates. For all samples, neither thaumasite nor ettringite peaks were found. The diffractograms of the carbonated wollastonite paste samples showed no change other than slight decrease of the calcite peaks after exposure to the magnesium sulfate solution.

In case of other two cement paste samples (i.e., those made of cements #2 and #3), one of the main noticeable changes is appearance of the gypsum peaks. Especially, gypsum occurred very strongly in samples exposed to magnesium sulfate, whereas only small traces of it can be found in samples submerged in sodium sulfate.
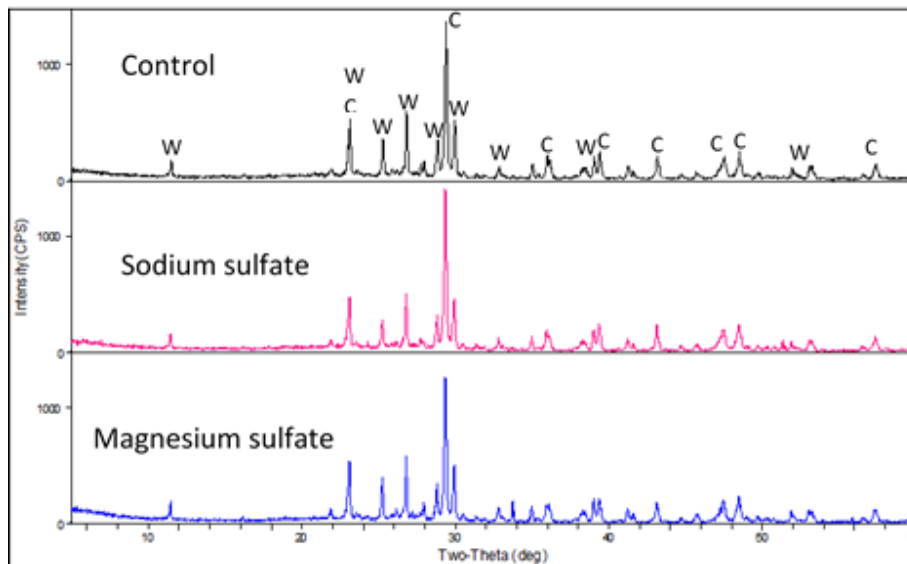
Figure 4.4. X-ray diffractograms of paste samples made of cement #1 before (control) and after exposure to sulfate solutions (key: C – calcite, W – wollastonite)
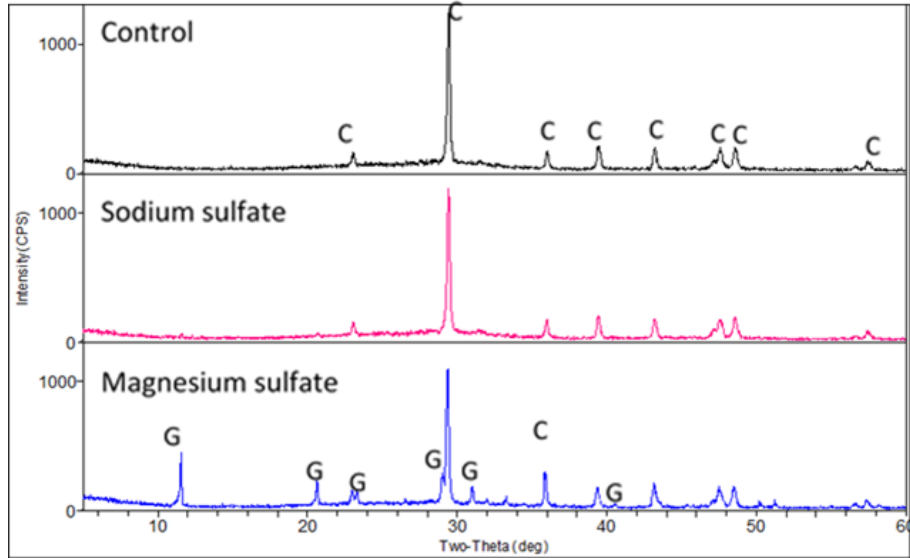
Figure 4.5. X-ray diffractograms of paste samples made of cement #2 before (control) and after exposure to sulfate solutions (key: C – calcite, G – gypsum)
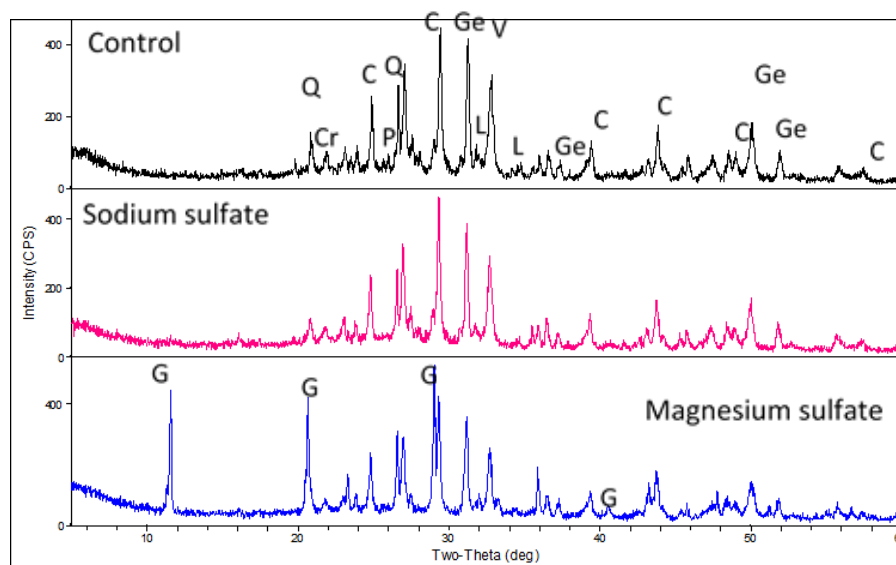
Figure 4.6. X-ray diffractograms of paste samples made of cement #3 before (control) and after exposure to sulfate solutions (key: C – calcite, Cr – cristobalite, G – gypsum, Ge – gehlenite, L – larnite, P – pseudo-wollastonite, Q – quartz, R – rankinite, S – sanidine, V – vaterite)

4.3.3 Results of thermal analysis

The amount of calcium carbonate ($CaCO_3$) phase present in the pastes before and after exposure to sulfate solutions was estimated from the results of the TGA analysis in the temperature region of 600°C to 850°C (corresponding to decomposition of calcite). The results of this analysis (normalized with respect to 100 grams of sample) are shown in Figure 4.7. It can be seen that the amount of $CaCO_3$ in carbonated wollastonite paste (cement #1) essentially did not change as the result of exposure to either of the two sulfate solutions. The effect of exposure to sodium sulfate on the amount of $CaCO_3$ in specimens from two other cements (i.e., cement #2 and #3) appears to be negligible as well. However, the results indicate that specimens made of cements #2 and #3 exposed to magnesium sulfate solution lost around 5-6% of calcium carbonate phase.
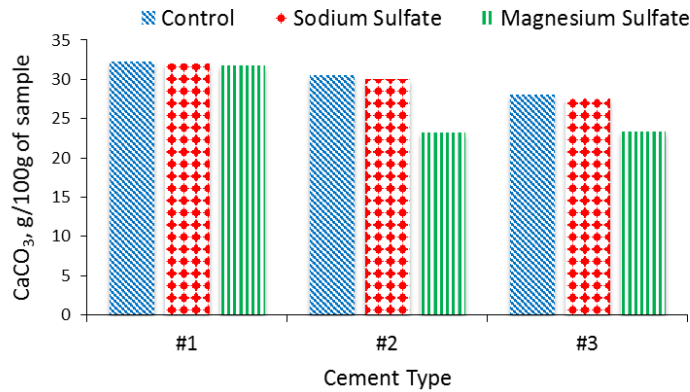
Figure 4.7. Amount of calcium carbonate phase present in paste
specimens before and after the sulfate solutions exposure test

Analysis of the derivative of the weight loss curves (DTG) revealed some additional information indicating mostly changes in the morphology (crystallinity) of the $CaCO_3$ (calcite). To this end, the DTG curves of the control (i.e., non-exposed) and sulfate-exposed specimens were combined in a single plot for the temperature range of 500° - 900°C, which corresponds to the range of decomposition of calcium carbonate (see Figures 4.8(a), 4.8(b) and 4.8(c)).

96
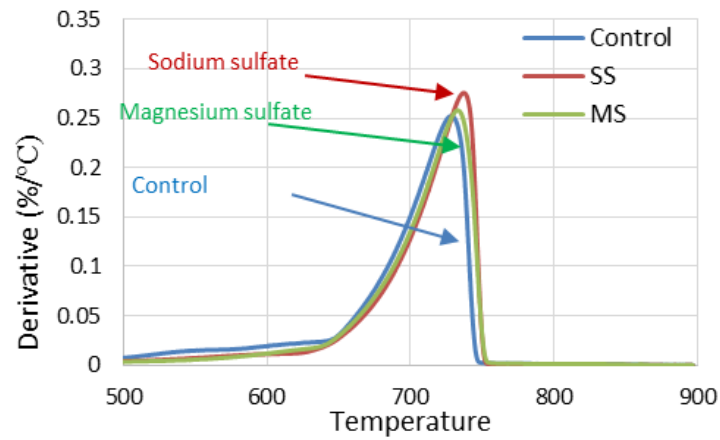
a) Cement #1 paste
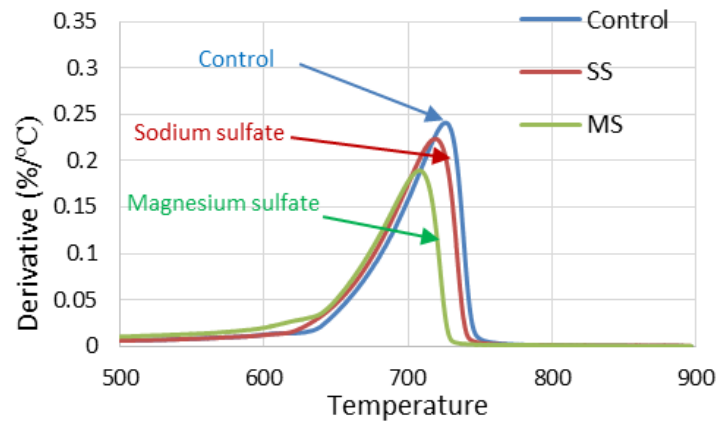
b) Cement #2 paste
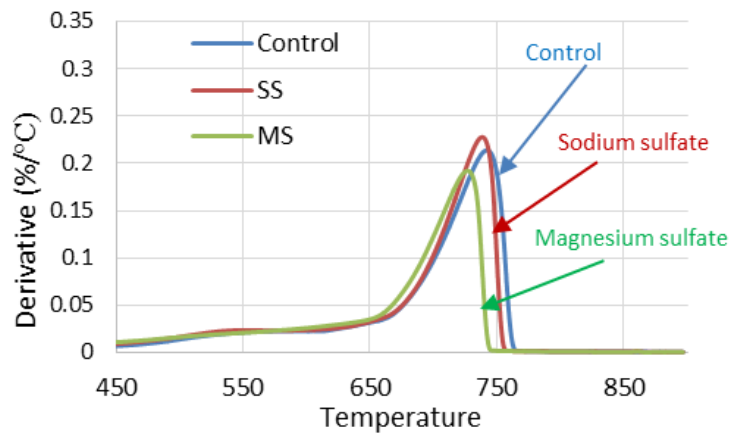
c) Cement #3 paste

Figure 4.8. DTG curves of control and sulfate-exposed paste samples (SS – sodium sulfate solution, MS – magnesium sulfate solution)

For the carbonated wollastonite paste samples, the DTG curves of sulfate-exposed specimens are slightly (~5°C) shifted to the right (i.e., toward higher temperature) of the DTG curve for the control specimen. This shift may indicate slight increase in the crystallinity of the calcite.

However, a completely opposite trend can be observed for sulfate-exposed paste specimens from cement #2. In this case, as seen from Figure 4.8(b), the DTG curves of specimens exposed to sulfates are shifted to the left (i.e., toward lower temperature) with respect to DTG curve of control specimen. The observed shift is about 10°C-12°C for specimen exposed to magnesium sulfate solution and about 3°C-5°C for the one exposed to sodium sulfate solution. This implies that for this particular cement both sulfate solutions (but especially the magnesium sulfate) attack the calcium carbonate phase and decrease the degree of its crystallinity. The behavior of specimens made from cement #3 (Figure 4.8(c)) is very similar to that of specimens made form cement #2.

Figure 4.9 shows the results of the DSC tests for all specimens exposed to both types of sulfate solutions. The curves for specimens from carbonated wollastonite (cement #1) are smooth over the entire range of test temperatures (25°C - 600°C) indicating lack of formation of new phases during the exposure to sulfate solutions. On the other hand, specimens made from cements #2 and #3 show well-defined gypsum peaks.
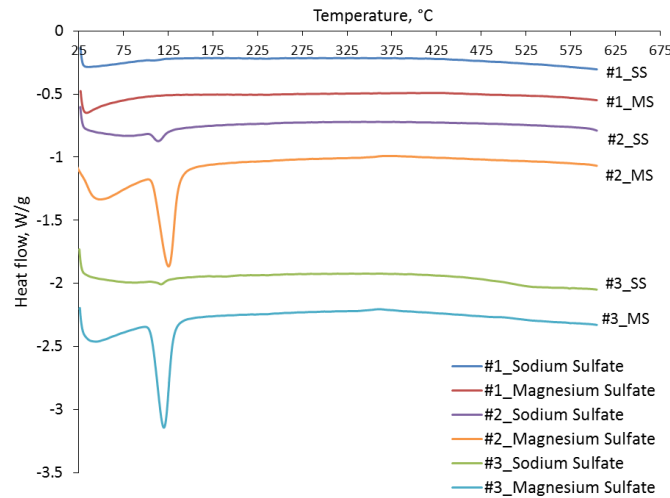
Figure 4.9. DSC curves of specimens exposed to sulfate solutions

The amount of gypsum formed was quantified using the calibration equation shown below:

$$Wt._{Gypsum}, \% = \frac{Q + 1.793}{5.91} \qquad (5)$$

where Q –heat of dehydration of gypsum (area under the peak), J/g. The calibration equation (5) was developed by analyzing a set of reference mixtures of pure gypsum and fired kaolinite with varied gypsum concentration.

The amount of gypsum determined in each sample exposed to sulfate solutions is presented in Figure 4.10. As can be seen, no gypsum formed in specimens from cement #1 (wollastonite) and only small amounts (less than 2 g/100 g of paste) formed in specimens from cements #2 and #3 exposed to sodium sulfate solutions. The highest amount of gypsum, around 16-17 g/100 g of paste sample, formed in samples soaked in magnesium sulfate solution.
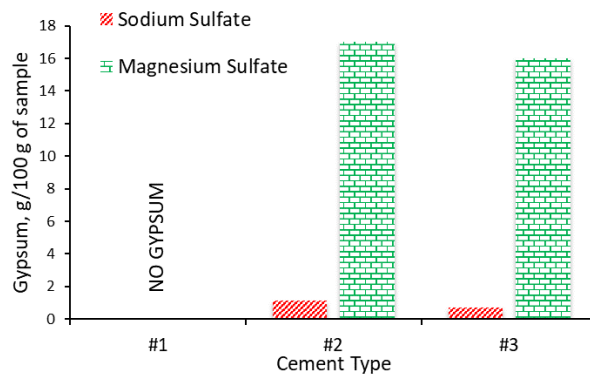
Figure 4.10. Amount of gypsum formed in pastes from various cements during the sulfate exposure

4.3.4   Ion Chromatography analysis results

Figure 4.11 shows concentrations of sulfate ions present in soak solutions at the end of the exposure period (normalized with respect to the concentration of sulfates in the original solutions). As it can be seen, concentrations of sulfates in solutions in contact with pastes from cement #1 (wollastonite) remained essentially the same as those found in the original solution, irrespective of the type of sulfate used. For pastes from cements #2 and #3, only very small (around 2-4%) reduction in sulfate concentrations was observed in sodium sulfate solutions. In contrast, for the same cements, a very significant (about 84-87%) reduction in sulfate concentrations was observed in magnesium sulfate solutions.
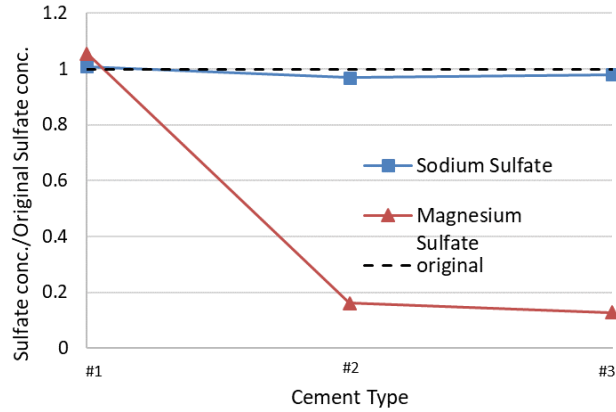
Figure 4.11. Normalized concentrations of sulfate ions in soak
solutions in contact with pastes from different cements

4.3.5 Results of SEM analysis

The scanning electron microscopy (SEM) examination of the microstructure of specimens after the completion of the low temperature exposure regime revealed that while specimens prepared from cement #1 (wollastonite) did not contain any gypsum deposits, such deposits were found in specimens made from cements #2 and #3. Furthermore, for a given type of cement, the morphology of the gypsum crystals was a function of the sulfate solution used during the experiment. As an example, the crystal of gypsum formed in paste made from cement #2 exposed to sodium sulfate solution (Figure 4.12(a)) has irregular shape and does not appear to be fully developed, suggesting that it likely precipitated at a faster rate and (possibly) near the end of the exposure period. However, gypsum that precipitated in the same type of paste while exposed to magnesium sulfate appears as large, very well-developed crystal with sharp edges (Figure 4.12(b)). That morphology implies continuous, slow precipitation that likely occurred over prolonged exposure period. The longest dimension of these gypsum crystals was in the range of 1-2 mm in pasted from Cement #2 and in the range 30-50 microns in pastes from cement #3.
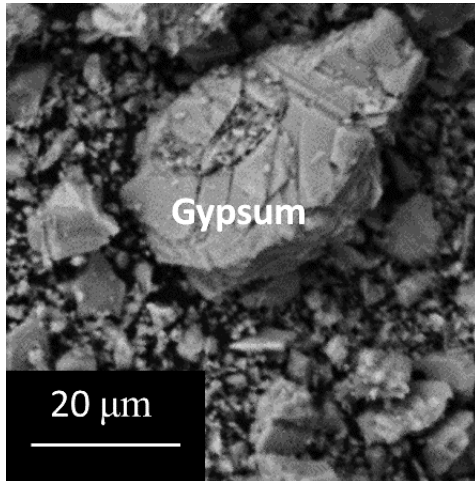
a) Cement #2 paste sample exposed to sodium sulfate solution
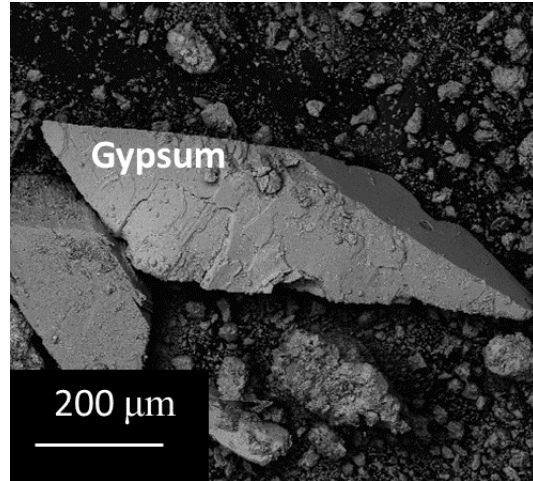
b) Cement #2 paste sample exposed to magnesium sulfate solution

Figure 4.12. SEM micrographs of the gypsum crystals formed after the sulfate exposure

In addition, SEM-EDX analysis also revealed that magnesium ions got incorporated in the structure of the hydrated silica gel in case of both, cement #2 and #3 paste (see Figure 4.13).
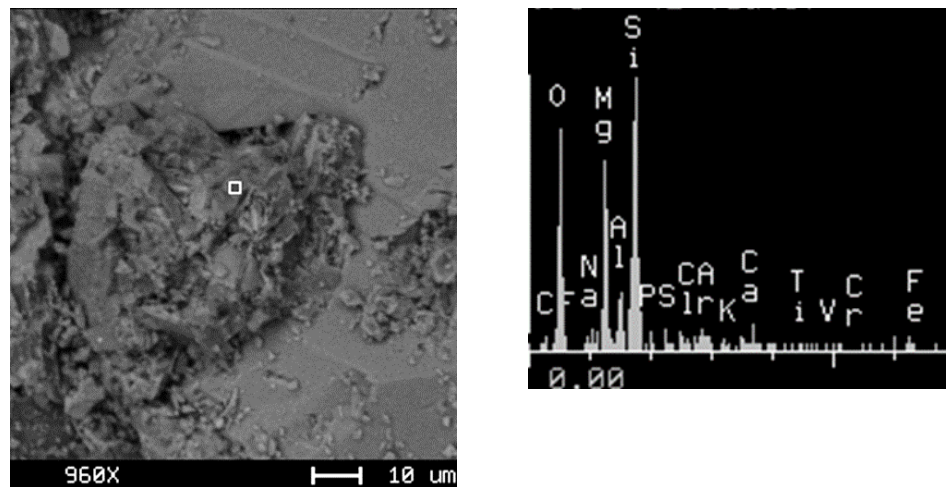
Figure 4.13. EDX spectrum of magnesium-bearing silica gel in the paste specimens from cement #2 exposed to magnesium sulfate solution

4.4   Discussion

The low-temperature sulfate exposure tests did not result in formation of thaumasite in any of the three carbonated calcium (CCSC) silicate pastes used in this study. This is despite the fact that, as mentioned earlier, the studied systems contained all of the ingredients (i.e., calcium, carbonate, silica and sulfate species) necessary for the formation of this phase. This confirms that fact that (as already mentioned in the "Introduction" section of this paper) having all ingredients present is not sufficient to form that phase if other conditions are not fulfilled as well.

From the studies by other researchers (Gremrich et al, [20] and Macphee and Barnett [45]), it is known that the thaumasite sulfate attack (TSA) affects mainly CSH gel in the presence of carbonates and sulfates and long-time exposure to low temperatures. The binding phase in low lime, CCSC systems is calcium carbonate with amorphous (and calcium depleted) layer of silica coating the non-carbonated cement particles. This layer of silica can mainly attract and hold cations. Although in some cases there exists an intermediate phase – so called calcium-modified silica gel – the amount of calcium in this phase is too low for coordinating (and fixing) of sulfate ions in gel structure. Since none of the cements used in the current study contained reactive aluminates, the formation of ettringite, potential precursor for formation of thaumasite, was also not possible. Therefore, instead of thaumasite, the formation of gypsum was observed. It should be added that gypsum is the only sulfate-bearing phase stable at pH levels lower than 10-11 which were the typical pH ranges observed this study.

The pastes made of three CCSCs used in this study all showed different levels of sulfate resistance. The carbonated wollastonite (cement #1) paste appeared to be the most resistant among all the pastes studied. Unlike in the case of pastes prepared from two other cements (i.e., cement #2 and #3), the carbonated wollastonite paste contained mainly calcite, which is highly crystalline polymorph of calcium carbonate phase. There are number of studies in environmental, agricultural and geochemical areas focused on utilizing wollastonite as acid neutralizing agent and suppressing hazardous effect of acid contaminated substances [Fernandes et al. [18], Lacroix et al. [40]). The use of this mineral in such applications is based on the fact that after the initial rapid release of calcium cations into solution, further leaching of calcium (and protonation) progresses very slowly resulting in local(surface) buffering effect. This local buffering effect, i.e., locally stable alkalinity level, might result in stable concentration of carbonate ions which can facilitate the precipitation of highly crystalline and pure calcium carbonate phases during carbonation. Moreover, atomistic

modelling of surface leaching phenomena on wollastonite particles also indicates that leaching of silica happens at relatively slow rates (Kundu et al. [39], Weissbart and Rimstidt [53]). The leaching experiment results (neither included here nor reported elsewhere) collected by the current authors also showed that the amount of silica leached from carbonated wollastonite paste was the lowest compared to the amount of silica leached from other two CCSC pastes.

It seems that the type and amount of highly crystalline $CaCO_3$ phases (mainly calcite) and the amount of leachable silica are the main factors distinguishing carbonated wollastonite paste from other two CCSC pastes used in the study. Based on that, one can therefore assume that the presence of less crystalline $CaCO_3$ polymorphs along with more mobile amorphous silica phases, are among the factors controlling the vulnerability of the carbonated CS system to sulfate attack. This has been confirmed by another experimental work conducted by the authors that involved exposing pure phases to sulfate solutions (the results are neither included here nor reported elsewhere) indicated that amorphous silica plays a role of a specific "catalyst" of the chemical reaction between $CaCO_3$ and sulfates. The specificity of this "catalyst" manifests itself in the fact that it fixes sulfate cations (especially, magnesium).

Based on all post-exposure characterization results, carbonated cement #2 and cement #3 pastes behaved almost identically during this study. Specifically, both of these pastes demonstrated chemical activity towards sulfate solutions, and both produced gypsum as a sulfate-bearing product. In addition, in both cases, Mg ions were found within the structure of the amorphous silica gel.

Based on the above discussion, it can be concluded that the presence of a less crystalline form of $CaCO_3$ (i.e., vaterite, amorphous calcium carbonate), leachable amorphous silica gel, and/or Ca-modified silica gel can be considered a "weakness" of these two carbonated systems. The slight difference in the amount of gypsum formed can be explained by recalling the fact that cement #2 consisted of almost purely amorphous CS, whereas the content of CS in cement #3 was lower due to the presence of other, non-reactive phases.

The dissociation of gypsum reaction represented by equation (6) was used to verify if all sulfate ions lost from the soak solutions were consumed in the process of gypsum formation.

$$\overset{\mathbf{a}}{CaSO_4 \cdot 2H_2O} \leftrightarrow Ca^{2+} + \overset{\mathbf{x}}{SO_4^{2-}} + 2H_2O \tag{6}$$

172 g/mole   96 g/mole

For example, about 17 g/100 g of gypsum formed in cement #2 paste during the 1.5 years exposure to magnesium sulfate solution. This required approximately 0.095g/1g of sulfate ions. Evaluation of the initial (actual) concentration of magnesium sulfate solution using ion chromatography (IC) technique revealed the presence of ~0.11g of sulfate ions per 1 g of the paste sample. This means that ~86% of sulfate ions were consumed to form gypsum. At the same time, the IC analysis of the magnesium sulfate soak solution after the test indicated ~85% decrease in sulfate ions. These data demonstrate that there were no other sulfate consuming reactions.

The study also indicated that, in case of cements #2 and #3, the type of sulfate cation is important with respect to sulfate resistance. Specifically, exposure of pastes from cements #2 and #3 to magnesium sulfate produced significantly higher amounts of well-developed gypsum crystals than in the case of exposure to sodium sulfate solution. On top of that, magnesium ion migrated into amorphous silica gel structure. In contrast, for both of these pastes, exposure to Na_2SO_4 solution resulted in formation of small amounts of finer, and not well-developed crystals of gypsum. Also, no ingress of sodium cation into the solid mass was observed.

The chemical reaction between the sulfates and calcium carbonate phases of the CCSC pastes resulting in formation of gypsum can be represented by equations (7) and (8).

$$CaCO_3 + Na_2SO_4 + 2H_2O \rightarrow Na_2CO_3 + CaSO_4 \cdot 2H_2O \tag{7}$$

$$CaCO_3 + MgSO_4 + 2H_2O \rightarrow MgCO_3 + CaSO_4 \cdot 2H_2O \tag{8}$$
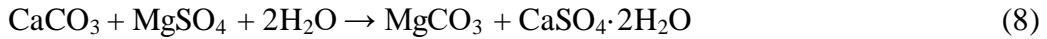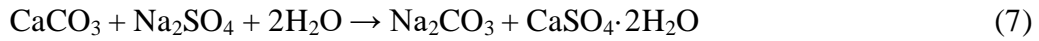
The possibility of these reactions taking place can be simply checked by determination of Gibbs free energy change at 5°C (278K) using equation (9).

$$\Delta G = \Delta H - T\Delta S = [\Sigma \Delta H_{prod} - \Sigma \Delta H_{react}] - T[\Sigma S_{prod} - \Sigma S_{react}] \tag{9}$$

All the thermodynamic values of the reaction components were taken from online open source [16]. As the calculations showed, the values of ΔG are $\Delta G_{(7)} \approx 24$ kJ and $\Delta G_{(8)} \approx -52.3$ kJ for reactions (7) and (8) respectively. These values imply that only reaction (8) can possibly happen spontaneously. Therefore, the gypsum found in samples exposed to Na_2SO_4 solution must have been produced as a result of sulfates reacting with some other phases present in cement #2 and

cement #3 paste specimens. One of the possible candidates may be the amorphous Ca-modified silica gel.

Also, comparison of Na^+ and Mg^{2+} ions reveals that magnesium ion has a negative entropy ($\approx$-138 J/mol*K vs. $\approx$59 J/mol*K for sodium ion) and smaller ionic radius (0.078 nm vs. 0.098 nm). As such, it may be more prone to participate in cation-exchange processes and in binding with other anionic groups/complexes. On the other hand, in addition to the fact that Na^+ ion is much more "free and independent" in the solution, its ionic radius is close to that of Ca^{2+} ion (0.1 nm). With respect to charge balance, two Na^+ ions should substitute one Ca^{2+} ion.

Returning to the equation (8), it is worthwhile to note that practically no magnesium carbonate was found in the solids by the end of the test, indicating that the real chemical reaction likely proceeds via different (and probably rather complex) path involving silica species from the gel.

4.5   Conclusions

The focus of this paper was on evaluating low-temperature sulfate resistance of carbonated pastes made from, low-calcium silica cements (CSCs). The study involved 1.5 years of exposure of three different pastes to solutions of sodium and magnesium sulfates at the temperature of ~5°C.

Despite low temperature exposure and the presence of all ions necessary to formation of thaumasite, no such phase was observed in any of the CCSC systems used in the study. This, in turns, confirms the validity of assumptions regarding the importance of the presence of reactive aluminates, ettringite, calcium hydroxide and high-calcium C-S-H gel to formation of thaumasite as none of these components were present in the CCSC pastes used in this study. Nevertheless, the post-exposure characterization of the paste solids and soaking sulfate solutions helped to reveal some peculiarities of carbonated CSC-based systems utilized in this study. The following points briefly highlight the main findings:

1)   Higher content of highly crystalline calcium carbonate phases and low-leachability silica increases the low-temperature sulfate resistance.

2)   The low-temperature reactions between carbonated CCSC pastes produces gypsum as the main sulfate-bearing reaction product.

3)   The type of cation present in the sulfate solution had significant influence on the amount of gypsum formed in the two of the three (i.e., based on the cement #2 and

cement #3) pastes, with magnesium sulfate resulting in much greater amounts of gypsum that that recorded for sodium sulfate. Also, ingress of magnesium ions into silica gel structure was observed. That was not the case for sodium ions.

4)   During exposure to magnesium sulfate, the amount of calcium carbonate decreased indicating that it was likely consumed in the process of gypsum formation. However, there were also indications that apart from calcium carbonate polymorphs, poorly crystalline and/or amorphous, calcium modified silica phases might have also contributed to gypsum formation.

Good agreement between the amounts of sulfates incorporated in gypsum and the amounts of sulfates lost from the soak solutions strongly implies that gypsum was the only sulfate-bearing product formed during the exposure test.

5. GENERAL CONCLUSIONS

In general, the outcomes of all three phases of the research work in mutual agreement. Moreover, the results of the Phase II study helped to check the hypotheses formulated in Phase I of the study. Here is the list of hypotheses with verification decisions:

- *The sulfate resistance of the CCS depends on the type of sulfates. They are likely to be susceptible to magnesium sulfate ($MgSO_4$) attack, but not sodium sulfate.* **True. Failed to reject.**

- *Chemical interactions between magnesium sulfate and CCS results in decalcification of the matrix and formation of gypsum.* **True. Failed to reject.**

- *Mainly, the relatively inertness of CCS to sodium sulfate is due to the absence of calcium hydroxide in the matrix of CCS.* **Partially true.**

- *Unlike in case of hydrated OPC, the gypsum formed in CCS matrix does not seem to turn into the internal source of sulfates to initiate the secondary sulfate attack (ettringite formation).* **True. Failed to reject.**

- *CCS with highly ordered crystalline (more stable) calcium carbonate phases are supposed to be more sulfate resistant.* **True. Failed to reject.**

Also, in Phase III, it was shown that in spite of the availability of the necessary species, thaumasite sulfate attack is less likely to happen in CCS matrix exposed to sulfates at low temperature.

6. POSSIBLE DIRECTIONS OF FUTURE RESEARCH STUDIES

Even though both study areas: carbonation – mineral sequestration of carbon dioxide – and sulfate resistance are considered to be as one of the widely investigated ones all over the world, still there is "a plenty of room" for this tandem. Here are the some of the possible directions which may deserve an attention for future fundamental research:

1) *In situ* study of the different low-lime calcium silicates during carbonation in order to understand more comprehensively if the carbonation routes are different. This may help to better explain why one carbonated calcium silicates are more sulfate resistant than others.

2) Study of the possibilities of the optimization of the carbonation regimes to achieve better sulfate resistance of the vulnerable CCS matrices.

3) Is there ITZ in CCS system? Does the paste – aggregate interface locally differ chemically?

REFERENCES

1. ACI 201.2R-16 Guide to Durable Concrete, ACI Committee 201.

2. Adams F., "Ionic Concentration and Activities in Soil Solutions", Soil Soc. Amer. Proc., 35 (1971), pp. 420-426.

3. Ashraf W. and Olek J., "Carbonation Behavior of Hydraulic and Non-hydraulic Calcium Silicates: Potential of Utilizing Low-Lime Calcium Silicates in Cement-based Materials" J. Mater. Sci, 51 (2016), pp. 6173-6191.

4. Ashraf, W., Olek, J., Jain, J. (2017) Microscopic features of non-hydraulic calcium silicate cement paste and mortar. Cement and Concrete Research, 100, 361-372.

5. ASTM Standard Designation C1012-13, Standard Test Method for Length Change of Hydraulic-cement Mortars Exposed to a Sulfate Solution, ASTM, PA, 2013

6. ASTM Standard Designation C109-12, Standard Method for Compressive Strength of Hydraulic Cement Mortars (using 2-in. [50 mm] Cube Specimens), ASTM, PA, 2013.

7. ASTM Standard Designation C778-17 Standard Specification for Standard Sand, ASTM, PA, 2017

8. Bakharev. T., "Durability of Geopolymer Materials in Sodium and Magnesium Sulfate Solutions", *Cement and Concrete Research,* 35 (2005), pp. 1233-1246.

9. Bellmann F., Stark J. (2008) The role of calcium hydroxide in the formation of thaumasite. Cement and Concrete Research, 38, 1154 – 1161.

10. Bensted, J., Varma, S.P. (1974) Studies of Thaumasite - Part II. Silicates Industries 39(1), 11-19.

11. Bonen. D and Cohen. M.D., "Magnesium Sulfate Attack on Portland Cement Paste – I. Microstructural Analysis", *Cement and Concrete Research",* 22 (1992), pp. 169-180.

12. Bonen. D and Cohen. M.D., "Magnesium Sulfate Attack on Portland Cement Paste – II. Chemical and Mineralogical Analysis", *Cement and Concrete Research,* 22 (1992), pp. 707-718.

13. Bukowski J. M. and Berger R. L., "Reactivity and Development of CO_2 Activated Non-Hydraulic Calcium Silicates," *Cement and Concrete Research*, 9 (1979) pp. 57-68.

14. Bukowski, J.M., Berger, R.L. (1979) Reactivity and strength development of CO_2 activated non-hydraulic calcium silicates. Cement and Concrete Research, 9, 57–68.

15. Daval, D., Martinez, I., Guigner, J-M., Hellmann, R., Corvisier, J., Findling, N., Dominici, C., Goffé, B., Guyot, F. (2009) Mechanism of wollastonite carbonation deduced from micro- to nanometer length scale observations. American Mineralogist, 94, 1707-1726.

16. Duda. A., "Aspects of Sulfate Resistance of Steelwork Slag Cements", *Cement and Concrete Research*, 17 (1987), pp. 373-384.

17. Evangelou V.P., "Pyrite Oxidation and Its Control", CRC Press, 1995.

18. Fernandez–Caliani J.C., Barba-Brioso C., Perez-Lopez R. (2008) Long-term interaction of wollastonite with acid mine water and effects on arsenic and metal removal. Applied Geochemistry, 23, 1288-1298.

19. Fiori, C., Vandini, M., Prati, S. and Chiavari, G. "Vaterite in the Mortars of a Mosaic in the Saint Peter Basiloca, Vatican (Rome)", *Journal of Cultural Heritage,* 10 (2009), pp.248-257.

20. Gemrich J., Jiroušková, K., Kulísek K. (2015) Synthesis of pure thaumasite, Applied Mechanics and Materials, 723, 456 – 459.

21. Goto S., Suenaga K., Kado T. and Fukuhara M., "Calcium silicate carbonation products", J. *Am. Ceram. Soc*. 78 (1995) 2867–2872.

22. H.F.W. Taylor, Cement Chemistry, 2nd ed., Thomas Telford Publishing, 1997

23. Hakkuria E., Crivit. T., Hayes P.C., Jak E., "Selected Phase Equilibria Studies in the Al_2O_3–CaO–SiO_2 System". *J. Am. Ceram. Soc*., 99 (2016) pp. 691-704

24. Harris D.C., "Quantitative Chemical Analysis", 6th edition, W.H. Freeman and Company, New York, 2003.

25. Hasset J.J. and Jurinak J.J., "Effect of Mg^{2+} ion on the Solubility of Solid Carbonates", Soil Soc. Amer. Proc., 35 (1971), pp. 403-406.

26. http://www.drjez.com/uco/ChemTools/Standard%20Thermodynamic%20Values.pdf (accessed May, 2019).

27. Huang C.K. and Kerr P.F., "IR Study of Carbonate Minerals". The American Mineralogist, 45 (1960), pp. 311 -324.

28. Huijgen, W. J.J. and Comans, R. N. J. "Carbon Dioxide Sequestration: Literature Review Update 2003 – 2004". *Report ECN-C-05-022*. Energy Research Center of Netherlands, 2005

29. Huijgen, W.J.J., Witkamp, G.J. and Comans, Rob N.J. (2006) Mechanisms of aqueous wollastonite carbonation as a possible CO_2 sequestration. Process. Chemical Engineering Science, (61), 4242-4251.

30. Hunt J.M, Wisherd M.P. and Bonham L.C., "IR Absorption Spectra of Minerals and Other Inorganic Compounds". Analytical Chemistry, 22 (1950), 12, pp1478-1497.

31. Hunt J.M. and Turner D.S., "Determination of Mineral Constituents of Rocks by IR", Analytical Chemistry, 25 (1953), 8, pp.1169-1174.

32. Ihli J., Wong W., Noel E., Kim Y.,Christenson H.K., Duer M., Meldrum F., "Dehydration and Crystallization of Amorphous Calcium Carbonate in Solution and Air", *Nature Communications*, 5 (2014), pp. 2-10.

33. Jain, J.A., Seth, A., DeCristofaro, N. (2019) Environmental impact and durability of carbonated calcium silicate concrete. Proceedings of the Institution of Civil Engineers – Construction Materials 172(4), 179–191.

34. Kalousek G.L. and Roy R., "Crystal chemistry of Hydrous Calcium Silicates: II. Characterization of Interlayer Water", J. Amer. Cer. Soc., 40 (1957), 7, pp. 236-239.

35. Kielland J.K., "Individual Activity Coefficients of Ions in Aqueous Solution", J. Amer. Cer. Soc., (1937), pp. 1675-1678.

36. Kim T. and Olek J., "Effects of Sample Preparation and Interpretation of Thermogravimetric Curves on Calcium Hydroxide in Hydrated Pastes and Mortars", Transportation Research Record, 2290 (2012), pp. 10-18.

37. Kirboga, S. and Oner, M., "Investigation of Calcium Carbonate Precipitation in the Presence of Carboxymethyl Inulin", *CrystEngComm,* 15 (2013), pp. 3678-3686.

38. Köhler S., Heinz D., Urbonas L. (2006) Effect of ettringite on thaumasite formation. Cement and Concrete Research, 36, 697 – 706.

39. Kundu, T.K., Hanumantha Rao K., Parker., S.C. (2003) Atomistic simulation of the surface structure of wollastonite and adsorption phenomena relevant to flotation. International Journal of Mineral processing, 72, 111-127.

40. Lacroix E., Brovelli A., Barry D.A., and Holliger C. (2014) Use of silicate minerals for ph control during reductive dichlorination of chloroethens in batch cultures of different microbial consortia, Applied and Environmental Microbiology, 80, 3858-3867.

41. Launer P.J., "Regularities in the IR Absorption Spectra of Silicate Minerals", Amer. Mineralogist, 42 (1957), pp. 764-784.

42. Loewenthal R.E. and Marais G.v.R., "Carbonate Chemistry of Aqueous Systems: Theory and Application", AnnArbor Sciences, 1976.

43. Lowenstam, H. A. and Abbot, D. P., "Vaterite: A Mineralization Product of the Hard Tissues of a Marine Organism (Ascidiacea)", *Science,* 188 (1975), pp. 363-365.

44. Ma, Y. and Feng, Q., "A Crucial Process: Organic Matrix and magnesium Ion Control of Amorphous Calcium Carbonate Crystallization on β-Chitin Film", *CrystEngComm,* 17 (2015), pp. 32-39.

45. Macphee D.E., Barnett S.J. (2004) Solution properties in the ettringite – thaumasite solid solution series. Cement and Concrete Research, 34, 1591 – 1598.

46. Milkey R., "IR Spectra of Some Tectosilicates", The American Mineralogist, 45 (1960), pp. 990-1007.

47. Popescu, M.-A., Isopescu, R., Matei, C., Fagarasan, G. and Plesu, V., "Thermal Decomposition of Calcium Carbonate Polymorphs Precipitated in the Presence of Ammonia and Alkylamines", *Advanced Powder Technology,* 25 (2014), pp. 500-507.

48. Robie R.A. and Hemingway B. S. and Fisher J., "Thermodynamic Properties of Minerals and Related Substances at 298.15 K and 1 Bar Pressure and at Higher Temperature", U.S. Geological Survey Bulletin, 1452, Washington, 1979.

49. Santhanam, M., Cohen, M. D. and Olek, J., "Mechanism of Sulfate Attack: A Fresh Look Part 1: Summary of Experimental Results", *Cement and Concrete Research,* 32 (2002), pp. 915-921

50. Słomka-Słupik. B, Podwórny. J and Łukowiec D., "Corrosion of blastfurnace slag paste in aqueous solution of $(NH_4)_2SO_4$", *Cement Wapno Beton,* 6 (2016), pp. 379-388.

51. Stubican V. and Roy R., "IR Spectra of Layer-Structure Silicates", J. Amer. Cer. Soc., 44 (1961), 12, pp.625-627.

52. Tettenhorst R., "Cation Migration in montmorillonite". The American Mineralogist, 47 (1962), pp. 769-773.

53. Weissbart, E.J, Rimstidt, J.D. (2000) Wollastonite: Incongruent dissolution and leached layer formation. Geochimica et Cosmochimica Acta, 64(23), 4007-4016.

54. Young J. F., Berger R. L. and Breese J., "Accelerated Curing of Compacted Calcium Silicate Mortars on Exposure to CO_2", *J. Am. Ceram. Soc.*, 57 (1974) pp. 394-397.

55. Yu, Kirkpatrick et al., "Structure of CSH: FTIR", J. Amer. Cer. Soc., 82 (1999), 3, pp. 742-748.